1 **RESEARCH ARTICLE**

2

3 **dsRNA-induced immunity targets plasmodesmata and is suppressed by**

4 **viral movement proteins**

5

6 **Caiping Huang[a], Ana Rocio Sede[a], Laura Elvira-González[a], Yan Yan[b], Miguel**

7 **Rodriguez[b], Jerome Mutterer[a], Emmanuel Boutant[a,c], Libo Shan[b], and Manfred**

8 **Heinlein[a,d]**

9 [a]Institut de biologie moléculaire des plantes, CNRS, Université de Strasbourg, 67000 Strasbourg,

10 France

11 [b]Department of Biochemistry and Biophysics, College of Agriculture and Life Sciences, Texas A&M

12 University, College Station, TX 77843, USA

13 [c]Current address: UMR 7021, CNRS, Laboratoire de Bioimagerie et Pathologies, Université de

14 Strasbourg, Faculté de Pharmacie, 67400 Illkirch, France

15 [d]Correspondending Author: heinlein@unistra.fr

16

17 **Short title:** dsRNA-induced PTI restricts virus movement

18 **One-sentence summary:** dsRNA-induced antiviral PTI targets plasmodesmata for callose deposition
19 and is suppressed by virus-encoded movement proteins.
20
25
26 **Abstract**
27 Emerging evidence indicates that in addition to the well-recognized antiviral RNA silencing, dsRNA
28 elicits responses of pattern-triggered immunity (PTI), likely contributing plant resistance against virus
29 infections. However, compared to bacterial and fungal elicitor-mediated PTI, the mode-of-action and
30 signaling pathway of dsRNA-induced defense remain poorly characterized. Here, using multi-color *in
31 vivo* imaging by GFP mobility, staining of callose and plasmodesmal marker lines, we show that
32 dsRNA-induced PTI restricts the progression of virus infection by triggering callose deposition at
33 plasmodesmata, thereby likely limiting the macromolecular transport through these cell-to-cell
34 communication channels. The plasma membrane-resident kinase module of SERK1 and BIK1/PBL1,
35 plasmodesmata-localized proteins PDLP1/2/3 and calmodulin-like CML41, and Ca^{2+} signals are
36 involved in the dsRNA-induced signaling leading to callose deposition at plasmodesmata and antiviral
37 defense. In addition, unlike classical bacterial elicitor flagellin, dsRNA does not trigger detectable
38 reactive oxygen species (ROS) burst, further substantiating a partially shared immune signaling
39 framework with distinct features triggered by different microbial patterns. Likely as a counteract
40 strategy, viral movement proteins from different viruses suppress the dsRNA-induced host response
41 leading to callose deposition to achieve infection. Thus, our data support the new model of how plant
42 immune signaling constrains the virus movement by inducing callose deposition at plasmodesmata
43 and how viruses counteract this layer of immunity.
44

45   **Keywords:** double-stranded RNA, pattern-triggered immunity, plant virus, plasmodesmata

46

47   **IN A NUTSHELL**

48   **Background:** Plants use different defense mechanisms pathogens. The major mechanism that plants

49   use for defense against viruses is known as RNA silencing. This mechanism is triggered by the

50   presence of viral double-stranded (ds)RNA and uses small RNAs to inhibit viral replication by

51   targeting the viral genome for degradation. Recently, it was found that dsRNA elicits antiviral defense

52   also through a protein-mediated mechanism known as pattern-triggered immunity (PTI). However, the

53   underlying mechanism of antiviral PTI and how viruses overcome this plant defense mechanism to

54   cause infection is unknown.

55   **Question:** In this study we asked how dsRNA-induced PTI acts to inhibit virus infection and whether

56   we can identify components of the PTI signaling pathway. Moreover, we wanted to know how viruses

57   overcome this plant host defense response in order to cause infection.

58   **Findings:** We demonstrate that dsRNA-induced PTI targets plasmodesmata (PD), the intercellular

59   communication conduits in plant cell walls that viruses use to spread infection from cell to cell. By

60   inducing the deposition of callose, dsRNA-induced PTI reduces PD permeability, thus restricting

61   virus movement. We identified PTI signaling components required for dsRNA-induced PD callose

62   deposition and delineate a PTI pathway showing important difference to PTI pathways triggered by

63   microbial elicitors. Moreover, viral movement proteins (MPs) suppress the dsRNA-induced callose

64   deposition response at PD. This leads to a new model of how plant immune signaling constrains virus

65   movement and how viruses counteract this layer of immunity.

66   **Next steps:** This study calls upon the identification of the PTI dsRNA receptor and the mechanisms

67   of PTI signaling (involving identified components such as SERK1, BIK1, calcium channels, CML41,

68   PDLP1/2/3) and PTI suppression by MPs, and how dsRNA-induced PTI and RNA silencing are

69   controlled during the spread of infection.

70

71   **Introduction**

72   The virome of plants is dominated by RNA viruses (Dolja et al., 2020) and several of these cause

73   devastating diseases in cultivated plants leading to global crop losses (Jones and Naidu, 2019; Jones,

74   2021). To infect plants, RNA viruses engage in complex interactions with compatible plant hosts. In

75   cells at the spreading infection front, RNA viruses associate with cellular membranes and replicate

76   their genome through double-stranded RNA (dsRNA) intermediates. Moreover, they use their

77   movement proteins (MP) to interact with membrane-associated transport processes in order to achieve

78   the movement of replicated genome copies through cell wall nanochannels called plasmodesmata

79   (PD) in order to infect new cells (Heinlein, 2015). Importantly, sensing of viral dsRNA by the host

80   triggers defense responses against infection, which viruses must be able to control in order to

81   propagate.

82

83   The most important antiviral host response in plants is RNA silencing (Ding and Voinnet, 2007). It

84   involves host DICER-LIKE enzymes that inhibit viral replication by cleaving the viral dsRNA

85   replication intermediate into small interfering RNAs (siRNAs). These viral siRNAs can associate with

86   ARGONAUTE proteins in RNA-induced silencing complexes (RISCs) to further guide the sequence-

87   specific degradation and translational suppression of viral RNA. To control this antiviral response and

88   to enhance their replication, viruses have evolved specific effector proteins that interfere with the

89   RNA silencing pathway at distinct steps (Csorba et al., 2015). More recent research has shown that in

90   addition to the antiviral RNA silencing response, RNA virus infection also activates pattern-triggered

91   immunity (PTI) (Kørner et al., 2013), whereby dsRNA acts as an important elicitor (Niehl et al.,

92   2016). Unlike RNA silencing, PTI is triggered by specific recognition of conserved microbe- or

93   pathogen-associated molecular patterns (MAMPs or PAMPs) by pathogen-recognition receptors

94   (PRRs) and the induction of defense signaling (DeFalco and Zipfel, 2021). Importantly, dsRNA-

95   induced PTI is independent of dsRNA sequence. Thus, PTI is activated by viral dsRNA but also as

96   well by non-viral dsRNA, for example GFP dsRNA or the synthetic dsRNA analog polyinosinic-

97   polycytidilic acid [poly(I:C)] (Niehl et al., 2016), a well-known ligand of the dsRNA-perceiving

98   TLR3-receptor in animals (Alexopoulou et al., 2001). Similar to virus replication, treatment of

99   *Arabidopsis thaliana* plants with poly(I:C) elicits antiviral defense along with activating typical PTI

100   responses, such as mitogen-activated protein kinase (MPK), ethylene production, seedling root growth

101   inhibition, and marker gene expression (Kørner et al., 2013; Niehl et al., 2016). Poly(I:C)-triggered

102   ethylene production and antiviral defense were shown to depend on the co-receptor kinase SOMATIC

103   EMBRYOGENESIS RECEPTOR-LIKE KINASE 1 (SERK1) (Niehl et al., 2016) but neither other

104   components of the signaling pathway nor the mechanism by which PTI restricts virus infection are

105   known. Here, we demonstrate that unlike RNA silencing, which controls viral RNA accumulation,

106   dsRNA-induced PTI acts on PD to restrict virus movement. New components of the PTI signaling

107   mechanism to PD are identified and shown to be critical for limiting virus infection and symptom

108   formation. Moreover, the observations indicate that the cell-to-cell propagation of virus infection is

109   linked to the ability of the viral MP to suppress the dsRNA-induced defense response leading to PD

110   closure. Taken together, the results draw a central role of PTI signaling and suppression in

111   determining the ability of viruses to spread infection between cells in susceptible plants.

112

113   **Results**

114

115   **dsRNA causes inhibition of virus movement in *N. benthamiana***

116   To discover how dsRNA-induced PTI inhibits RNA virus infection, we visualized the effect of

117   poly(I:C) treatment on local infections of *Nicotiana benthamiana* plants using tobacco mosaic virus

118   tagged with green fluorescent protein (TMV-GFP). The TMV-GFP infection sites were lower in

119   number and smaller at 7 days post inoculation (dpi) in plants treated with poly(I:C) or with a bacterial

120   PTI elicitor derived from flagellin (flg22) than in control plants treated with water (**Figure 1, A** and

121   **B,** and **Figure S1**). The treatments did not cause a significant change in GFP fluorescence intensity,

122   an indicative for viral replication and accumulation (**Figure 1A**) indicating that they may not exert a

123   significant bulk effect on viral RNA accumulation in infected cells. To test this further, we measured

124   the accumulation of viral RNA in leaves agroinfiltrated for expression a cell-autonomous, MP-

125   deficient TMV replicon (TMVΔMΔC-GFP). As is shown in **Figure 1C**, pre-treatment of the leaves

126   with poly(I:C) did not elicit a significant effect on TMVΔMΔC-GFP viral accumulation through a

127   time-course of infection at 1, 3, and 5 days post infection (dpi) compared to leaves treated with water.

128   Therefore, the reduced size and number of infection sites in poly(I:C)-treated leaves suggested that the

129   poly(I:C)-triggered immunity may be linked to the reduced cell-to-cell movement of the virus.

130

131   **dsRNA triggers callose deposition at PD along with the activation of typical PTI responses in *N.***

132   ***benthamiana***

133   Because virus intercellular movement occurs through PD (Heinlein, 2015) we hypothesized that

134   dsRNA inhibits virus movement by causing PD closure. A major mechanism restricting the

135   conductivity of PD for the transport of macromolecules involves the deposition of callose (β-1,3-

136   glucan) in the cell wall region surrounding the PD channel (Wu et al., 2018). Consistently, treatment

137   of *N. benthamiana* plants with poly(I:C), flg22, or water, and quantification of PD-associated callose

138   by *in vivo* aniline blue staining (Huang et al., 2022) revealed that both poly(I:C) and flg22 trigger

139   increased levels of PD-associated callose in a concentration-dependent manner (**Figure 1, D** and **E**).

140   A similar induction of callose at PD is also seen upon treatment of *N. benthamiana* plants with Phi6

141   dsRNA (Niehl et al., 2018) (**Figure 1F**), which dismisses the possibility that poly(I:C) induced callose

142   deposition through an unspecific effect. In agreement with poly(I:C)-induced callose deposition at

143   PD, poly(I:C)-treated tissues showed reduced PD permeability as determined by a GFP mobility

144   assay. In this assay, isolated individual cells of *N. benthamiana* leaves were transformed for the

145   expression of cytoplasmic GFP together with red fluorescent protein tagged with a nuclear

146   localization signal (NLS-RFP) as a red fluorescent cell-autonomous marker. Whereas more than 97%

147   of the observed GFP-expressing cells showed GFP mobility into one or two adjacent cell layers in

148   control (water)-treated tissues, this mobility was reduced to 31% in the presence of poly(I:C) (**Figure**

149   **1, G - I**). Moreover, as previously noted in Arabidopsis (Niehl et al., 2016), poly(I:C) triggered a

150   moderate MPK activation and the level of activation is significantly weaker than the activation

151   observed with flg22 (**Figure 1J**). Poly(I:C)-treated leaves also exhibited the induction of *N.*

152   *benthamiana* defense-related genes, such as genes encoding BOTRYTIS INDUCED KINASE1

153   (BIK1), PATHOGENESIS-RELATED PROTEIN 2 (PR2), NADPH/RESPIRATORY BURST

154   OXIDASE PROTEIN B (RBOHB) and ENHANCED DISEASE SUSCEPTIBILITY 1 (EDS1),

155 whereas the gene for BRASSINOSTEROID INSENSITIVE 1 (BRI1) was down-regulated
156 (**Figure 1K**).
157
158 **Poly(I:C)-induced PD callose deposition in Arabidopsis requires PTI signaling components but**
159 **is independent of ROS and MPK**
160 To determine how dsRNA elicits the deposition of callose at PD, we turned our attention to
161 Arabidopsis. As noted previously (Niehl et al., 2016) the treatment of *A. thaliana* Col-0 plants with
162 poly(I:C) causes a significant induction in some PTI-related gene expression, including *SERK1*
163 (**Figure 2A**), whereby the induction of *PR5* was found to be SERK1-dependent (**Figure 2B**).
164 Moreover, the same treatment as well as the treatment with 50 ng/µl phi6 dsRNA increased the PD-
165 associated callose levels as seen before in *N. benthamiana* (**Figure 2, C and D**). The induced callose
166 depositions are exactly localized to PD as shown in transgenic *A. thaliana* Col-0 plants expressing PD
167 markers PLASMODESMATA CALLOSE BINDING 1 fused to the red fluorescent protein
168 mCHERRY (mCherry-PDCB1) or the Plasmodesmata-localized β-1,3 glucanase 2 fused to the yellow
169 fluorescent protein mCitrine (PdBG2-mCitrine) (Benitez-Alfonso et al., 2013) (**Figure 2, E** and **F**).
170 Interestingly, dsRNA-induced callose deposition was strongly inhibited in *bik1 pbl1* plants (**Figure**
171 **2G**), which are deficient in the receptor-like cytoplasmic kinase (RLCK) BIK1 and its homolog
172 PBS1-LIKE KINASE1 (PBL1). The BIK1 receptor-like cytoplasmic kinase (RLCK) module is an
173 important component of PTI signaling that integrates signals from multiple pathogen-recognition
174 receptors (PRRs), as shown by its direct interaction with the PRR proteins FLAGELLIN SENSITIVE
175 2 (FLS2), EF-TU RECEPTOR (EFR), PEPTIDE RECEPTOR (PEPR)1 and PEPR2, and CHITIN
176 ELICITOR RECEPTOR KINASE 1 (CERK1) (Lu et al., 2010; Zhang et al., 2010; Liu et al., 2013),
177 and its ability to phosphorylate and activate downstream targets, such as the NADPH Oxidase
178 RESPIRATORY BURST OXIDASE HOMOLOG D (RBOHD) (Kadota et al., 2014). BIK1 and
179 PBL1 have additive effects; unlike the single mutants, the *bik1 pbl1* double mutant was shown to
180 strongly inhibit PAMP-induced defense responses (Zhang et al., 2010). In addition, *bik1 pbl1* plants
181 are also deficient in poly(I:C)-induced MPK activation and seedling root growth inhibition as
182 compared to Col-0 wild type (WT) plants (**Figure 2, H and I**).
183 Perception of flg22 by the FLS2 and BAK1 (BRASSINOSTEROID INSENSITIVE1 (BRI1)-
184 ASSOCIATED RECEPTOR KINASE1) co-receptor complex induces rapid phosphorylation of BIK1,
185 evidenced by a protein mobility shift in immunoblotting analysis (Lu et al., 2010; Zhang et al., 2010).
186 To determine if BIK1 is phosphorylated in the presence of poly(I:C), Arabidopsis WT Col-0
187 protoplasts expressing HA epitope-tagged BIK1 were treated with poly(I:C) for 20 minutes.
188 Subsequent Western blot analysis with anti HA-antibody revealed that similar to flg22 treatment,
189 poly(I:C) treatment induces a mobility shift of BIK1-HA proteins (**Figure 3A**). BIK1 phosphorylation
190 was confirmed by the absence of this mobility shift in the presence of calf intestine phosphatase (CIP)
191 (**Figure 3, A and B**) or the protein kinase inhibitor K-252a (**Figure 3B**). Taken together, the data

192 suggest the involvement of BIK1/PBL1 in dsRNA-triggered immunity mediating the callose
193 deposition at the PD.

194 Previously, we showed that *serk1-1* mutants show the reduced levels of poly(I:C)-induced
195 ethylene production and antiviral protection [Niehl, 2016 #6670]. We further investigated the
196 involvement of SERK1 in poly(I:C)-induced BIK1 phosphorylation. As is shown in **Figure 3C**, the
197 level of poly(I:C)-induced BIK1 phosphorylation was increased upon SERK1 overexpression in WT
198 Col-0 plants and decreased in the *serk1-1* mutant. Importantly, the poly(I:C)-induced PD callose
199 deposition was drastically reduced in *serk1-1* mutants compared to WT Col-0 plants (**Figure 3D** and
200 **E**). Whereas the median PD callose level increased by 48% in WT col-0 plants upon poly(I:C)
201 treatment, only a minor increase in the median PD callose level was observed in the *serk1* mutant.
202 Thus, the data indicate that SERK1 contributes to poly(I:C)-induced BIK1 phosphorylation and may
203 function genetically upstream of BIK1.

204 To investigate the poly(I:C)-induced signaling pathway downstream of BIK1, we examined the
205 production of reactive oxygen species (ROS) by a luminescence assay. ROS play important roles in
206 plant development and stress responses (Mittler, 2017) and are also produced during infections with
207 fungal and bacterial pathogens (Castro et al., 2021). ROS accumulate also upon perception of the
208 fungal and bacterial elicitors chitin and flagellin (flg22) (Nuhse et al., 2007; Cheval et al., 2020) and
209 have been linked to local and systemic signaling, including calcium signaling, and the deposition of
210 callose at PD (Faulkner et al., 2013; Cheval et al., 2020). Notably, neither the treatment of
211 Arabidopsis Col-0 plants (**Figure 4A**) nor the treatment of *N. benthamiana* plants (**Figure 4B**) with
212 poly(I:C) led to the production of ROS. By contrast, strong responses were recorded in both plant
213 species upon treatment with the flg22 elicitor. In addition, *rbohd* and *rbohf* mutants deficient for the
214 major ROS-producing NADPH oxidases RESPIRATORY BURST OXIDASE HOMOLOG D
215 (RBOHD) and RBOHF (Castro et al., 2021) responded like WT Col-0 plants to the presence of
216 poly(I:C) in showing induced callose deposition at PD (**Figure 4C**). Thus, unlike for chitin and
217 flagellin (flg22), the induction of PD callose deposition by poly(I:C) is likely independent of ROS.
218 Moreover, *mpk3* and *mpk6* single mutants that are deficient for the mitogen activated protein kinases
219 (MPK) 3 and 6, respectively, as well as the *mpk3 amiRmpk6* mutants (an *mpk3* mutant in which
220 *MPK6* is silenced by an artificial miRNA) (Li et al., 2014) showed increased levels of callose at PD
221 upon poly(I:C) treatment similar to WT plants (**Figure 4D**). Considering the relatively weak
222 activation of MPKs by poly(I:C) treatment (**Figure 1J** and **Figure 2H**), it is possible that the MPK3/6
223 module may not play a major role in dsRNA-induced callose deposition. Alternatively, it is also
224 possible that additional yet non-identified MPKs may be involved in this process.

225 To further investigate the signaling pathway induced by dsRNA, additional mutants were tested.
226 We started with Arabidopsis mutants deficient in the PD-localized proteins (PDLPs), which are a
227 family of eight proteins that dynamically regulate PD (Thomas et al., 2008). PDLP5 plays a non-
228 redundant role in intercellular systemic acquired resistance (SAR) signaling (Lim et al., 2016) and in

229   mediating salicylic acid (SA)-induced PD closure, a process required for resistance against the
230   bacterial pathogen *P. syringae* (Lee et al., 2011; Wang et al., 2013). However, *pdlp5* mutant plants
231   showed strong callose deposition at PD upon poly(I:C) treatment (**Figure 4E**), indicating that dsRNA-
232   induced callose deposition is independent of PDLP5 and of a potential SA response mediated by this
233   protein. Next, we tested a PDLP1, PDLP2 and PDLP3, which play redundant roles in callose
234   deposition at PD (Thomas et al., 2008), in callose deposition within haustoria formed in response to
235   infection by mildew fungus (Caillaud et al., 2014), and also as binding receptors for tubule-forming
236   viruses (Amari et al., 2010). Whereas *pdlp1 pdlp2* (*pdlp1,2*) and *pdlp1 pdlp3* (*pdlp1,3*) double
237   mutants showed a normal poly(I:C)-induced callose deposition, *pdlp1 pdlp2 pdlp3* (*pdlp1,2,3*) triple
238   mutant plants were unable to significantly increase PD-associated callose levels in response to
239   poly(I:C) (**Figure 4E**). This observation suggests the involvement of PDLP1, PDLP2 and PDLP3 in
240   dsRNA-triggered immunity and in mediating the callose deposition at the PD.

241

242   In further screening of other mutants for dsRNA sensitivity, we found that poly(I:C)-induced callose
243   deposition at PD also depends on the Ca^{2+}-binding, PD-localized CALMODULIN-LIKE protein 41
244   (CML41). This protein was shown to mediate rapid callose deposition at PD associated with a
245   decreased PD permeability following flg22 treatment (Xu et al., 2017). Plants of *CML41*
246   overexpressing transgenic lines (*CML41-OEX-2* and *CML41-OEX-12*) (Xu et al., 2017) showed
247   increased PD-associated callose levels upon poly(I:C) treatment similar to WT Col-0 plants (**Figure
248   4F**). In contrast, transgenic plant lines in which *CML41* is downregulated by an artificial miRNA
249   (*CML41-amiRNA-1* and *CML41-amiRNA-4*) (Xu et al., 2017) showed a seven- to eight-fold lower
250   ability to respond to this treatment as compared to WT Col-0 (**Figure 4F**). The reduction in the
251   response to poly(I:C) of *CML41-amiRNA* plants correlates with the reduced level of *CML41*
252   expression in these lines (Xu et al., 2017) (**Figure 4G**). Consistent with the role of CML41 in the
253   callose deposition response to poly(I:C), the permeability of PD was previously shown to be sensitive
254   to cytosolic Ca^{2+} concentrations (Tucker and Boss, 1996; Holdaway-Clarke et al., 2000). To test the
255   role of Ca^{2+} in dsRNA-triggered innate immunity, we treated plants with poly(I:C) together with
256   EGTA, a Ca^{2+}-chelating molecule. The level of callose induced at PD after dsRNA treatment was
257   reduced in the presence of EGTA in a concentration-dependent manner (**Figure 4H**), indicating a role
258   of Ca^{2+} in poly(I:C)-triggered PD regulation. Together, these results suggest a role for CML41 and
259   Ca^{2+} in the poly(I:C)-induced defense response at PD. The observation that the poly(I:C)-induced
260   callose levels were not significantly increased by *CML41* overexpression may be due to that the
261   endogenous level of *CML41* expression in WT plants is sufficient for the full activity of the PD-
262   localized CML41 proteins. However, the level of expression in WT plants is critical as a reduction in
263   *CML41* levels strongly affected PD callose levels.

264

265   **BIK1/PBL1 and CML41 are essential for dsRNA-induced antiviral resistance**

266 Previously, we showed that poly(I:C) co-treatment during virus inoculation protects Arabidopsis
267 plants against infection by oilseed rape mosaic virus (ORMV) and that efficient protection depends on
268 SERK1 (Niehl et al., 2016). As we demonstrate here, SERK1 plays an essential role in the poly(I:C)-
269 induced callose deposition at PD, implying a role of PD closure in dsRNA-induced antiviral
270 resistance. To further test the significance of PD callose deposition of BIK1/PBL1 and CML41 in
271 dsRNA-induced antiviral resistance, we inoculated poly(I:C)-treated and non-treated *bik1 pbl1* and
272 *CML41 amiRNA-1* plants with ORMV. Whereas poly(I:C) treatment prevented symptoms at 28 dpi
273 and resulted in a strongly reduced virus titer in WT Col-0 plants, *bik1 pbl1* and *CML41 amiRNA-1*
274 plants showed severe virus-infected symptoms and accumulated high virus levels in poly(I:C)-treated
275 plants similar to those plants without poly(I:C) treatment upon ORMV infection (**Figure 5, A** and **B**).
276 Ablation of virus-inoculated leaves from plants at different times after inoculation showed that the
277 time required for the virus to exit the inoculated leaf and to cause systemic infection was three days in
278 WT plants. By contrast, this time was reduced to 24 hours in *bik1 pbl1* mutants and *CMLl41-amiRNA-*
279 *1* plants (**Figure 5, C** and **D**). These findings show that dsRNA-induced antiviral PTI occurs at the
280 level of virus movement. Consistent with this PTI effect on virus movement, the experiments reveal a
281 dsRNA-induced signaling pathway that requires SERK1, BIK1/PBL1, CML41, Ca^{2+} and PDLP1/2/3
282 for callose deposition at PD. This dsRNA-induced callose deposition at PD is likely independent of
283 ROS and MPK3/6 signaling, which differs from the immune signaling triggered by fungal and
284 bacterial elicitors (Kadota et al., 2014; Cheval et al., 2020).

285

286 **dsRNA-induced callose deposition is suppressed by viral movement protein**
287 The plant-pathogen arms race causes pathogens to evolve virulent effectors that overcome host
288 defenses. Viral MPs are essential in mediating virus movement during infection. We tested whether
289 viral MPs are involved in the suppression of the dsRNA-induced callose deposition at PD. To address
290 this question, we divided the local TMV infection site into different zones (**Figure 6A**): zone I ahead
291 of infection and without MP, zone II at the virus front where MP facilitates virus movement, zone III
292 behind the infection front, and zone IV, which is the center of the infection site where MP is no longer
293 expressed. *In vivo* detection of dsRNA with GFP-fused dsRNA-binding protein B2 of *Flock house*
294 *virus* (Monsion et al., 2018) shows that zones II-IV accumulate dsRNA in distinct replication
295 complexes that also produce MP (**Figure 6B**). Aniline blue staining demonstrates high PD-associated
296 callose levels within and around the infection site (**Figure 6C**). However, cells in zone II and zone III,
297 where virus cell-to-cell movement is associated with a transient activity of MP in increasing the PD
298 size exclusion limit (SEL) (Oparka et al., 1997), exhibit a marked reduction in PD-associated callose
299 levels as compared to cells in zone I (ahead of infection) and zone IV (center of infection) (**Figure 6,**
300 **C** and **D**). The low level of PD-associated callose in cells at the virus front (zone II) is consistent with
301 the ability of MP to interfere with dsRNA-triggered immunity leading to PD closure.

302

303   To test this hypothesis, we examined whether the expression of MP causes suppression of the
304   poly(I:C)-induced callose deposition at PD in the absence of viral infection. Transgenic *N.*
305   *benthamiana* plants that stably express MP:RFP at PD (**Figure 7, A** and **B**) complement a MP-
306   deficient TMV mutant for movement, thus indicating that the MP:RFP in these plants is functional
307   (**Figure 7C**). Treatment of such plants with poly(I:C) led to a 50% lower induction of callose
308   deposition at PD as compared to WT plants (**Figure 7, D** and **E**). The ability of poly(I:C) treatment to
309   induce callose deposition at PD was also reduced upon transient expression of MP:GFP (**Figure 7, F**
310   and **G**). Importantly, the same effect was observed with MP^{C55}:GFP. This mutant MP lacks 55 amino
311   acids from the C-terminus but still accumulates at PD and is functional in TMV movement (Boyko et
312   al., 2000). By contrast, dysfunctional MP^{P81S} carrying a P to S substitution at amino acid position 81,
313   which fails to target PD and to support virus movement (Boyko et al., 2002), does not interfere with
314   poly(I:C)-induced callose deposition. These experiments show that the TMV MP can significantly
315   interfere with the dsRNA-induced callose deposition at PD, and that this interference requires a MP
316   that can facilitate virus movement. Consistent with the absence of a significant role of MPK3/6
317   signaling in poly(I:C) induced callose deposition, expression of MP:GFP or the MP:GFP mutants did
318   not interfere with flg22 elicitor-triggered MPK activation (**Figure 7H**). Interestingly, MP also reduces
319   PD callose deposition induced by flg22 (**Figure 7I**), suggesting that MP interferes with signaling or
320   signaling target mechanisms shared by both elicitors. To determine if also the MPs of other viruses
321   interfere with the poly(I:C) induction of PD callose deposition, we tested the MPs of ORMV and
322   turnip vein clearing virus (TVCV). The RFP-fused version of these MPs and of the MP of TMV are
323   functional as their transient expression in *N. benthamiana* leaves allowed the intercellular spreading
324   of the co-expressed, MP-deficient TMVΔMΔC-GFP replicon, as can be seen by the development of
325   multiple fluorescent foci (**Figure 8A**). Consistent with function, the different MP:RFP fusion proteins
326   colocalize with PD-associated callose (**Figure 8B**). Importantly, similar to the functional MP:RFP
327   derived from TMV, the functional MP:RFP fusion proteins derived from ORMV and TVCV reduced
328   the levels of PD callose deposition induced by poly(I:C) treatment (**Figure 8C**). Thus, the capacity to
329   interfere with poly(I:C)-induced PD callose deposition may be a widespread function of viral MPs to
330   achieve efficient infections. These observations also further substantiate the importance of antiviral
331   PTI in the inhibition of virus movement for plants to fend off virus infections.
332

Poly(I:C) enters plant cells

334   As viruses replicate and produce dsRNA within cells, poly(I:C)-induced responses may only be
335   relevant to virus infection if poly(I:C) is able to enter cells. To test this, we used B2:GFP as an
336   intracellular dsRNA localization marker and monitored the responses of B2:GFP-transgenic *N.*
337   *benthamiana* plants upon poly(I:C) treatment. Externally applied poly(I:C) may enter cells from all
338   sides and then diffuse into the cytoplasm. Thus, a strong redistribution of B2:GFP similar as in virus-
339   infected cells, where dsRNA production centers within the VRCs, should not be expected. Indeed,

340   imaging GFP fluorescence under normal conditions did not show obvious changes in the distribution

341   of B2:GFP between poly(I:C)-treated and water-treated tissues. Nevertheless, by assigning specific

342   color to low intensity pixels, poly(I:C)-treated tissues clearly showed an accumulation of low intensity

343   signals along the periphery of the cells (**Figure 9**), thus suggesting poly(I:C) uptake by plant cells.

344

345

346   **Discussion**

347

348   **dsRNA-induced callose deposition during virus infection**

349   Accumulation and degradation of callose at PD play an essential role in controlling macromolecular

350   transport between cells (De Storme and Geelen, 2014; Wu et al., 2018). Mutations and conditions that

351   alter the levels of callose at PD strongly affect the conductivity of PD for macromolecular transport

352   (Simpson et al., 2009; Guseman et al., 2010; Vaten et al., 2011; Benitez-Alfonso et al., 2013). A role

353   of callose in plant-virus interactions became apparent by the observation that elevated callose levels in

354   plants silenced for the callose-degrading enzyme restricted the spread of virus infection, thus

355   suggesting that PD callose deposition may be part of early defense responses against virus attack

356   (Beffa et al., 1996). However, how viruses trigger PD callose deposition and yet still maintain their

357   cell-to-cell movement despite of this host defense response remained open. The induction of callose

358   deposition at PD by cell-autonomous replication of an MP-deficient TMV replicon led to the

359   conclusion that virus replication induces "stress" leading to callose deposition at PD (Guenoune-

360   Gelbart et al., 2008), but the nature of the "stress" and the underlying mechanism remained obscure.

361   The finding that viruses induce innate immunity (Kørner et al., 2013) and that dsRNA is a potent

362   PAMP elicitor in plants (Niehl et al., 2016) suggests dsRNA as a potential candidate for the perceived

363   stress signal. Our data shown here that dsRNA-induced immunity is linked to PD callose deposition

364   raise a model that virus replication causes callose deposition and PD closure mediated through a PTI

365   response triggered by viral dsRNA.

366

367   **MP facilitates virus movement by suppressing a dsRNA-induced PTI response**

368   Because virus movement depends on prior replication of the viral genome (Christensen et al., 2009),

369   and given that the virus must continue to replicate to produce progeny, the PTI response is likely

370   triggered immediately in the newly infected cells at the infection front and maintained in cells behind

371   the front. Thus, the perception of dsRNA may target PD for closure throughout the infection site. This

372   mechanism may have evolved to isolate the infected cells from surrounding cells to prevent further

373   spread of infection but also to protect the virus replication and virus progeny production in the

374   infected cells against intercellular defense signaling. At the infection front, the dsRNA-producing

375   virus must nevertheless be able to overcome PD closure in order to spread infection into non-infected

376   cells. Consistently, pioneering studies with TMV showed that the virus moves between cells with the

377   help of virus-encoded MP, that MP targets PD, and that it increases the size exclusion limit (SEL) of

378   PD and thus the permeability of the channels for macromolecular trafficking (Citovsky, 1999).

379   Importantly, using microinjection, MP was shown to gate the PD between cells only at, but not

380   behind, the virus infection front (Oparka et al., 1997). Our observations link this activity to the

381   suppression of a dsRNA- induced response by showing (i) that cells at the virus infection front, where

382   MP increases the PD SEL, have a significantly lower level of callose at PD as compared to other cells

383   and (ii) that the induction of PD callose deposition by dsRNA [poly(I:C)] is significantly reduced by

384   ectopically expressed MP. The ability of MP of TMV to interfere with dsRNA-induced callose

385   deposition seems to reflect an activity shared with other MPs as similar to MP^{TMV} also the expression

386   of MP^{ORMV} or MP^{TVCV} reduced the intensity of PD callose induction by poly(I:C) as compared to the

387   control (absence of the respective MP) (**Figure 8**). These observations suggest a new paradigm for

388   virus movement whereby dsRNA produced by TMV replication in a newly infected cell at the

389   infection front triggers a host PTI response that targets PD for callose deposition and closure in order

390   to restrict the spreading of the virus. To allow the spread of replicated viral genomes into non-infected

391   cells, the viral MP acts as an effector to transiently suppress this dsRNA-induced response (**Figure**

392   **10, A** and **B**). Upon enhancement of the PTI response by external treatment of infected plants with

393   poly(I:C) the virus-encoded MP may become insufficient for efficient suppression, thus leading to the

394   inhibition of virus movement (**Figure 1, A** and **B**).

395

396   The MP is expressed in cells at and also closely behind the infection front (**Figure 6, A** to **C**). The

397   restriction of MP activity and of low callose levels in cells at the infection front indicates that the

398   protein exists in different activity states. Consistently, several studies correlated the activity of MP

399   with its phosphorylation state (Lee and Lucas, 2001). The partial, rather than full, suppression of

400   dsRNA-induced callose deposition by ectopically expressed MP may reflect the different activity

401   states of MP expressed under such conditions.

402

403   The mechanism by which MP suppresses the dsRNA-induced callose deposition at PD remains to be

404   studied. dsRNA sequestration by MP is precluded as MP has no dsRNA binding activity (Citovsky et

405   al., 1990). Electron micrographs indicated that the TMV MP forms fibrillar substructures within PD

406   cavities (Ding et al., 1992; Moore et al., 1992; Heinlein et al., 1998) but it is unknown whether these

407   structures are functional. Several studies support the hypothesis that a callose-degrading beta-1,3-

408   glucanase enzyme activity may regulate virus movement (Iglesias and Meins, 2000; Bucher et al.,

409   2001; Levy et al., 2007), but strong evidence indicating that viruses like TMV indeed operate such

410   activities for virus movement is lacking. More recent observations suggest that the MPs of different

411   viruses interact with the synaptotagmin SYTA for movement (Uchiyama et al., 2014; Levy et al.,

412   2015; Yuan et al., 2018). Synaptotagmins (SYTs) and other Ca^{2+}-sensitive C2 domain-containing

413   proteins, such as the multiple C2 domains and transmembrane region proteins (MCTPs) are proposed

414   to function as membrane-tethering proteins at membrane contact sites (Tilsner et al., 2016; Brault et

415   al., 2019). Notably, the strand of endoplasmic reticulum (desmotubule) that traverses the PD channel

416   between cells is tethered to the adjacent plasma membrane (PM) by MCTPs and SYTs (Brault et al.,

417   2019; Ishikawa et al., 2020). Therefore, it is conceivable that MPs target SYTA to reach PD or even

418   to modify a membrane tethering activity of SYTA within PD in order to alter the cytoplasmic space

419   between the tethered membranes available for macromolecular transport (Pitzalis and Heinlein, 2017).

420   However, while further studies are needed to explore this idea, the results shown here promote the

421   model that the MPs of TMV and also the MPs of ORMV and TVCV facilitate movement by

422   interacting with components of the dsRNA-induced signaling and callose synthesis and turnover

423   pathways to inhibit callose deposition at PD. The MPs may interfere with these pathways in the

424   cytoplasm (**Figure 10A and B**) or at PD. However, earlier studies indicated that the MPs of TMV,

425   TVCV and cauliflower mosaic virus have the capacity to interact with the cell wall protein pectin-

426   methylesterase (PME) which may allow transport of MP through the secretory pathway (Chen et al.,

427   2000). It is conceivable, therefore, that MPs are partially secreted to inhibit the activity of the dsRNA

428   perceiving receptors at the PM. However, whether the MPs of TMV, ORMV and TVCV inhibit PD

429   callose deposition through interaction with PTI signaling components or rather through direct

430   interactions with callose synthesizing or degrading enzymes at PD remains to be investigated. As the

431   MP of TMV suppressed PD callose deposition triggered by either poly(I:C) and flg22, the signaling

432   components, enzymes, or mechanisms affected by MP likely play a role in both poly(I:C)- and flg22-

433   triggered pathways.

434

dsRNA induces antiviral defense through a novel PTI signaling pathway

436   We have shown here that the dsRNA-induced signaling pathway leading to callose deposition at PD

437   involves SERK1, BIK1/PBL1, CML41, Ca^{2+}, and potentially PDLP1/2/3, but neither strong MPK

438   activation or ROS production nor the presence of the major ROS-producing enzymes (RBOHD and

439   RBOHF). Thus, although MPK activation and ROS production are hallmarks of PTI (DeFalco and

440   Zipfel, 2021) and ROS signaling plays a role in PD regulation (Cheval and Faulkner, 2018), dsRNA

441   activates its own specific pathway to regulate PD. Moreover, the lack of ROS production clearly

442   distinguishes virus/dsRNA-induced signaling from the ROS-associated responses induced by other

443   pathogens. Importantly, we found that poly(I:C) treatment triggers BIK1 phosphorylation and that the

444   level of poly(I:C)-induced BIK1 phosphorylation depends on SERK1, thus potentially suggesting the

445   existence of dsRNA-perceiving SERK1-containing receptor complex that signals to BIK1.

446   Alternatively, dsRNA may induce yet non-identified signaling molecules that are signaled through

447   SERK1 and BIK1. The PD-localized CML41 protein was previously shown to participate in flg22-

448   triggered, but not chitin-triggered PD callose deposition (Xu et al., 2017). Thus, although differing in

449   upstream components, dsRNA-induced signaling may target PD-associated regulatory components

450   also regulated by flg22. The absence of ROS signaling in dsRNA-induced PD regulation could reflect

451   this specific elicitor type or a specific location of perception. Bacterial and fungal PAMPs are released

452   in the apoplast and perceived by PRRs at the PM, while viral dsRNA formation and perception may

453   occur at intracellular membranes where viruses replicate. RIG-I-like receptors (RLRs) including RIG-

454   I, MDA5 and LGP2 detect the presence of dsRNA in animals (Tan et al., 2018) and provide examples

455   of dsRNA perception in the cytoplasm. Viral RNAs in animals are also recognized by Toll-like

456   receptors in endosomes following internalization by dendritic cells and macrophages. In analogy, it is

457   known that bacterial PAMP receptor complexes in plants are internalized from the PM to endosomes

458   and that plant receptor-complexes can signal from endosomes. Recognition of viral dsRNA may

459   therefore occur during membrane fusion events between viral RNA-containing vesicles or membrane-

460   associated viral replication complexes (VRCs) (Niehl and Heinlein, 2019). Alternatively, the

461   cytoplasmic dsRNA may be exported into the apoplast to be sensed by the PM-resident PRRs. A

462   precedent for the transport of functional RNA molecules across plant membranes is provided by

463   cross-kingdom RNAi (Huang et al., 2019). For example, dsRNAs sprayed onto plants were shown to

464   inhibit fungal growth in tissues distant from the sprayed tissues by inducing RNAi against essential

465   fungal genes thus suggesting that applied dsRNAs are taken up by plants and that either dsRNAs or

466   derived small RNAs processed within cells are able to reach the fungus in distant tissues (Koch et al.,

467   2016). Moreover, emerging evidence suggest the presence of viral particles, viral proteins, and viral

468   RNA in the apoplast of infected plants (Mohaved et al., 2019; Hu et al., 2021; Wan et al, 2015; Wan

469   and Laliberté, 2015). Moreover, extracellular vesicles that are secreted from plants cells and are

470   present in apoplastic fluid contain various RNA species, including viral RNA (Cai et al., 2018; Cai et

471   al., 2021; Ruf et al., 2022). Poly (I:C) used in this study mimics these potential pathways by

472   apparently being able to enter plant cells upon treatment (**Figure 9**), which is consistent with dsRNA

473   perception in the cytoplasm, or be sensed in the apoplasm, either upon secretion or before cell entry

474   (**Figure 10A** and **B**). Plant viruses like TMV and ORMV undergo early replication stages at punctate,

475   cortical microtubule-associated ER sites in close vicinity of the PM (potentially ER:PM contact sites

476   (Pitzalis and Heinlein, 2017; Huang and Heinlein, 2022)), which may facilitate dsRNA perception

477   through membrane fusion events or dsRNA secretion from the VRCs and activation of PM-localized

478   signaling proteins in the apoplasm (Niehl and Heinlein, 2019). DRB2 and other double-stranded RNA

479   binding proteins (DRBs) were recently shown to accumulate in VRCs and to play a role in virus

480   accumulation (Incarbone et al., 2021) or virus-induced necrosis (Fatyol et al., 2020) and could have an

481   important function in dsRNA sensing. Importantly, dsRNA-induced innate immunity is unaffected by

482   mutations in dsRNA binding DICER-LIKE (DCL) proteins, which excludes these proteins as the

483   dsRNA receptors for PTI and also shows that dsRNA silencing and dsRNA-induced innate immunity

484   require different protein machinery (Niehl et al., 2016). The two different antiviral defense responses

485   are also spatially separated. Inactivating the TMV VSR causes virus silencing but has no effect on

486   virus movement and causes potent antiviral silencing only in cells behind the front engaged in virus

487   replication for the production of virus progeny (Kubota et al., 2003; Vogler et al., 2007). Thus, we

488   propose a model whereby a virus requires MP as viral virulence effector in cells at the infection front
489   to suppress dsRNA-triggered PTI to support virus movement whereas a VSR is required as virulence
490   effector in cells behind the front to suppress dsRNA-induced silencing for producing viral progeny
491   (**Figure 10C**).

492   It will be interesting to dissect how the SERK1-BIK1/PBL1 module signals to CML41 and
493   PDLP1/2/3 to regulate PD callose deposition. It is possible that BIK1/PBL1 may interact with and
494   phosphorylate directly PDLPs in mediating callose deposition at the PD. It has been shown that the
495   plasma membrane-tethered BIK1 regulates PAMP-triggered calcium signals by directly
496   phosphorylating cyclic nucleotide-gated channel 2 and 4 (CNGC2/4), whose activities can be
497   regulated by CAM7 (Tian et al., 2019). Additionally, BIK1 also phosphorylates calcium-permeable
498   channel, hyperOsmolality-induced $[Ca^{2+}]$ increase 1.3 (OSCA1.3) in regulating stomatal immunity
499   (Thor el al., 2020). Our observation that the calcium-chelating EGTA inhibits dsRNA-induced PD
500   callose deposition supports the involvement of the calcium binding protein CML41 and calcium
501   signaling in PD regulation. Therefore, it will be interesting to determine if any calcium channels
502   directly regulated by BIK1/PBL1 and modulated by CML41 may be involved in mediating calcium
503   signaling in plant antiviral immunity. This will help to delineate a genetic and biochemical signaling
504   pathway linking SERKs-RLCKs-calcium channels/CML41-PDLP1/2/3 to calcium signals in
505   regulating PD and plant antiviral immunity. It will also be interesting to determine the role of other
506   SERKs in virus sensing and immunity. It has been shown that SERK3/BAK1 plays a role in antiviral
507   defense (Kørner et al., 2013) but the molecular mechanism remains to be explored. While poly(I:C)-
508   induced ethylene production was not affected in *serk3/bak1* mutants (Niehl et al., 2016), it remains to
509   be tested if SERK3/BAK1 or also SERK2 or SERK4 could play a role in dsRNA sensing leading to
510   PD callose deposition, thus potentially explaining cases of *serk1*-independent dsRNA-induced gene
511   activation (**Figure 2A**) as well as the residual poly(I:C)-induced activation of PD callose deposition in
512   *serk1* mutants (**Figure 3E**).

513   In conclusion, we found that as a plant defense mechanism, dsRNA-induced antiviral PTI targets
514   PD for callose deposition through some shared typical PTI signaling components with distinct
515   features. To counteract this and launch efficient infections, viral MPs could effectively suppress
516   dsRNA-induced callose deposition at PD, thus leading to a new concept of plant-virus interaction
517   arm-race. This study calls upon the identification of the PTI dsRNA receptor, the mechanisms of
518   SERK1-BIK1-calcium channels/CML41-PDLP1/2/3 signaling and PTI suppression by MP, and how
519   dsRNA-induced PTI and RNA silencing are controlled during the spread of infection, all of which
520   present exciting new challenges for additional studies.

521

522

523   **Methods**

524

Plant materials and growth conditions

N. benthamiana and *A. thaliana* plants were grown from seeds in soil. *N. benthamiana* were kept under 16h/8h light/dark periods at +22 °C/+18 °C in a greenhouse equipped with Philips SON-T 400 W HPS Lamps (200-250 μmol/m^2/s). *A. thaliana* plants were kept under 12h/12h light/dark periods at +21°C/+18 °C in a growth chamber equipped with LED lights (160-175 μmol/m^2/s). MP:RFP-transgenic *N. benthamiana* plants were produced by leaf disk transformation (Horsch et al., 1985) using binary plasmid pK7-MP:RFP (Boutant et al., 2010). The plasmid was constructed by inserting the MP coding sequence of TMV into pK7RWG2 using Gateway procedures. *N. benthamiana* plants expressing GFP fused *Flock house virus* B2 protein have been described previously (Monsion et al., 2018) and were provided by Christophe Ritzenthaler (IBMP, CNRS, Strasbourg, France). The Arabidopsis mutants used in this study have been described previously and homozygous seeds were kind provided from different research laboratories. Seeds of the *bik1 pbl1* double mutant (SALK_005291 SAIL_1236_D07) (Zhang et al., 2010) were provided by Cyril Zipfel (University of Zürich, Switzerland). *mpk3-1* (SALK_151594) and *mpk6-2* (SALK_073907) lines were given by Kenichi Tsuda (Max Planck Institute for Plant Breeding research, Cologne, Germany) and, together with seeds of the *mpk3amiRmpk6* (Li et al., 2014) and *serk1-1* (SALK_044330) (Meng et al., 2015b) mutants, also by the author Libo Shan. Seeds for *rbohd* and *rbohf* mutants (Torres et al., 2002) were provided by Christine Faulkner (John Innes Centre, Norwich) and seeds of *CML41* overexpressing and silenced lines (*CML41-OEX-2, CML41-OEX-12, CML41-amiRNA-1* and *CML41-amiRNA-4*) (Xu et al., 2017) were a gift of Matthew Gilliham (University of Adelaide, Australia). Arabidopsis lines transgenic for PD markers mCherry-BDCB1 (Simpson et al., 2009; Benitez-Alfonso et al., 2013) or PdBG2-citrine (Benitez-Alfonso et al., 2013) were provided by Yoselin Benitez-Alfonso (University of Leeds, UK).

Virus inoculation

cDNA constructs for TMV-MP:RFP (Ashby et al., 2006), TMV-GFP (Heinlein et al., 1995), and TMVΔM-GFP (Vogler et al., 2008) have been described previously. *N. benthamiana* plants were mechanically inoculated in the presence of an abrasive (Celite®545) with infectious RNA *in vitro*-transcribed from these constructs. A TMV replicon (TMV-ΔMP-ΔCP-GFP) cloned in a binary vector for agroinfiltration and used for testing virus replication and movement trans-complementation has been described (Borniego et al., 2016). Arabidopsis plants were inoculated with purified ORMV virions (Niehl et al., 2012).

Analysis of virus infection in the presence of elicitors

To test the effect of elicitors on TMV-GFP infection in *N. benthamiana*, plants were inoculated with 200 μl inoculum containing 20 μl of infectious viral RNA transcription mix and 0.5 μg/μl (equals ~1 μM) poly(I:C) (Sigma-Aldrich, USA), or 1 uM flg22 (EZBiolabs, USA or Proteogenix, France), or

15

562   water. Infection sites on the inoculated leaves were imaged using a hand-held camera and UV lamp

563   (BLAK RAY B-100AP; UVP Inc., Upland, California) in the presence of a ruler for size

564   normalization. The areas of infection sites in each leaf were measured with Image J software upon

565   selection of infection site as regions of interest using fluorescence thresholding and the wand tracing

566   tool, and by setting the scale according to the ruler. For testing the effect of poly(I:C) on viral

567   replication, *N. benthamiana* leaves were agro-inoculated with a MP-deficient, cell-autonomous TMV

568   replicon (TMVΔM-ΔC-GFP) (Borniego et al., 2016). After 1 day, the fluorescent leaf patches were

569   gently rubbed with 200 µl of 0.5 µg/µl poly(I:C) in the presence of celite. At 1, 3 and 5 days after this

570   treatment, the GFP-expressing leaf patches were analysed for viral RNA accumulation by quantitative

571   Taqman RT-qPCR using previously described methods (Mansilla et al., 2009; Niehl et al., 2016).

572   To test the effect of elicitors on ORMV infection in Arabidopsis, 4 µl of elicitor solution (10 µg/ml

573   poly(I:C) or 10 µM flg22) or 4 µl PBS were placed on rosette leaves of 3 weeks old Arabidopsis

574   wildtype or mutant Col-0 plants. A volume of 2.5 µl of a 20 ng/µl solution of purified ORMV virions

575   was placed on the same leaves. Subsequently, the leaves were gently rubbed in the presence of celite

576   as abrasive. Immediately after treatment, remaining elicitors, buffers and virions were washed off the

577   leaf surface. Symptoms were analysed at 28 dpi. At the same time young, systemic leaves were

578   sampled for analysis of virus accumulation by quantitative Taqman RT-qPCR using previously

579   described methods (Mansilla et al., 2009; Niehl et al., 2016).

580

581   <u>Analysis of differential gene expression by RT-qPCR</u>

582   *N. Benthamiana* or Arabidopsis Col-0 leaf discs were excised with a cork borer and incubated

583   overnight in 12-well plates containing 600 µl deionized, ultra-pure water. The leaf disks were washed

584   several times with water and then incubated with elicitor (1 µM flg22, 0.5 µg/µl poly(I:C), or water as

585   control) for 3 hours. After washing the discs with deionized, ultra-pure water three times, samples

586   were ground to a fine powder in liquid nitrogen and total RNA was extracted by TRIzol™ reagent

587   according to the protocol of the manufacturer. 2 µg of RNA were reverse transcribed using a reverse

588   transcription kit (GoScript™ Reverse Transcription System, Promega). The abundance of specific

589   transcript was measured by probing 1 µL cDNA by quantitative real-time PCR in a total volume of 10

590   µl containg 5 µL SYBR-green master mix (Roche), 0.5 µM forward and reverse primer and water.

591   qPCR was performed in a Lightcycler480 (Roche) using a temperature regime consisting of 5 minutes

592   at 95℃ followed by 45 cycles at 95℃ for 10 seconds, 60℃ for 15 seconds, and 72℃ for 15 seconds,

593   and ending with a cycle of 95℃ for 5 seconds, 55℃ for 60 seconds, 95℃ for continuous time until

594   final cooling to 40℃ for 30 seconds. The threshold cycle (CT) values were normalized to CT-values

595   obtained for reference genes ACTIN 2 and UBIQUITIN 10 (Czechowski et al., 2005), providing ΔCT

596   values. These were used to calculate the $2^{-\Delta CT}$ values representing relative expression levels, the mean

597   values and standard errors (SE). Each mean value represents the analysis of three independent

598 replicate samples (individual plants treated the same way and harvested at the same time), each

599 measured by three technical replicates. Primers are listed in Table S1.

600

601 <u>Transient expression of proteins by agroinfiltration</u>

602 Binary plasmids for transient expression of RFP and of TMV-derived MP:RFP, MP:GFP,

603 MP^{C55}:GFP, and MP^{P81S}:GFP as well as of MP^{ORMV}:RFP and MP^{TVCV}:RFP were created by Gateway

604 cloning as has been described previously (Brandner et al., 2008; Sambade et al., 2008; Boutant et al.,

605 2010).

606 For transient expression of the fluorescent fusion proteins, cultures of *A. tumefaciens* bacteria (strain

607 GV3101) carrying these plasmids were harvested by centrifugation, resuspended in infiltration

608 medium (10 mM MES, 10 mM MgCl$_2$, 200 μM acetosyringone; pH 5.5) to a final optical density at

609 600 nm (OD$_{600}$) of 0.1 (unless stated differently), and infiltrated into the abaxial side of the leaf using

610 a syringe without a needle. Leaves were observed by confocal microscopy at 48 hours after

611 agroinfiltration.

612 For GFP mobility assays, we used Agrobacteria that were co-transformed with binary vectors for

613 expression of GFP together with the cell-autonomous nuclear protein NLS:RFP (pB7-

614 NLS:M2CP:RFP; this vector was created by recombining pZeo-NLS:MS2CP (Sambade et al., 2008)

615 with expression vector pH7RWG2). The two binary vectors carry different resistance genes and their

616 presence in the same agrobacteria was maintained by appropriate antibiotic co-selection. Before

617 infiltration, the diluted culture (OD$_{600}$ = 0.1) was further diluted 1:1000 or 1:10000 to ensure

618 expression of both proteins in only few cells of the leaf. 24 hours after infiltration, the agroinfiltrated

619 leaves were detached and analyzed by confocal microscopy, revealing about 10-15 single cell

620 transformation events with both markers. The levels of cytoplasmic GFP and nuclear NLS:RFP

621 differed between the transformed cells but cells expressing only GFP or only NLS:GFP were not

622 observed, which excludes the occurrence of transformation events in which only one of the T-DNAs

623 was transferred. Subsequently, leaf disks with the single cell transformation events were excised and

624 incubated in 0.5 μg/μl poly(I:C) or water for 48 hours. Finally, each of the transformation events was

625 evaluated for GFP movement by confocal microscopy by counting the radial cell layers into which

626 GFP has moved away from the infiltrated cell (marked by red fluorescent nucleus).

627 For movement trans-complementation assays, *N. benthamiana* leaves were infiltrated with

628 *Agrobacterium* cultures (OD$_{600 nm}$ = 0.3) for the expression of either MP^{TMV}:mRFP MP^{ORMV}:mRFP,

629 MP^{TVCV}:mRFP or of free mRFP together with a highly diluted *Agrobacterium* culture for infection of

630 single cells with TMVΔMPΔCP-GFP (OD$_{600 nm}$ = 1 x 10^{-5}). Fluorescent infection sites indicating

631 complementation of the MP-deficient virus were imaged with a Nikon D80 camera at 5 dpi under

632 UV illumination. For the movement trans-complementation assay with MP:RFP-transgenic *N.*

633 *benthamiana* plants, leaves were inoculated with infectious RNA *in vitro*-transcribed from pTMVΔM-

634 GFP (Vogler et al., 2008) and infection sites were observed at 7 dpi.

635

Callose staining

636 Callose staining

637 Leaf disks were excised with a cork borer and placed into wells of 12-well culture plates containing 1

638 ml water and incubated overnight under conditions at which the plants were raised. The leaf discs

639 were washed several times with water before use. For callose staining, individual leaf disks were

640 placed on microscope slides and covered with a coverslip fixed with tape. If not otherwise stated, 200

641 µl of a 1% aniline blue solution (in 50 mM potassium phosphate buffer, pH 8.0) containing either 0.5

642 µg/µl poly(I:C), 50 ng/µl dsRNA^{phi6} or 1 µm flg22 were soaked into the space between the glass slide

643 and coverslip. The glass slide with the sample was evacuated for 1-2 minutes (< 0.8 pa) in a vacuum

644 desiccator followed by slow release of the pressure. Aniline blue fluorescence was imaged 30 minutes

645 after dsRNA or control treatment using a Zeiss LSM 780 confocal laser scanning microscope with

646 ZEN 2.3 software (Carl Zeiss, Jean, Germany) and using a 405 nm diode laser for excitation and

647 filtering the emission at 475-525 nm. 8-bit Images acquired with a 40× 1.3 N.A. Plan Neofluar

648 objective with oil immersion were analyzed with ImageJ software (http://rsbweb.nih. gov/ij/) using

649 the plug-in *calloseQuant*, which after setting few parameters localizes fluorescent callose spots and

650 quantifies callose fluorescence intensity of each spot automatically (Huang et al., 2022). This plugin is

651 available at https://raw.githubusercontent.com/mutterer/callose/main/calloseQuant_.ijm. Callose spots

652 were measured in 1-3 images taken from each leaf disk. If not otherwise mentioned, three leaf discs

653 from three different plants were evaluated for each genotype or condition. To control for normal

654 poly(I:C) treatment and callose staining conditions, samples of Arabidopsis mutants were always

655 analyzed in parallel to samples from the Col-0 wild-type. Similarly, samples from agroinfiltrated

656 MP:GFP/RFP-expressing *N. benthamiana* leaves were compared with samples from agroinfiltrated

657 GFP/RFP-expressing control leaves. The distribution of pooled fluorescence intensities obtained for

658 the specific genotype or treatment condition is shown in boxplots or column diagrams. Regions of

659 interest (ROIs) selected by *calloseQuant* were verified visually before measurement. ROIs that were

660 not at the plant cell walls or showed no clear signal above the background signal were deleted.

661 Moreover, individual fluorescence intensities that occurred as outliers from the general distribution of

662 fluorescence intensities (<1%) in the sample were excluded from analysis.

663

Analysis of MPK activation

664 Analysis of MPK activation

665 Leaf disks from 4-week-old *A. thaliana* or *N. benthamiana* plants were elicited with 1 µM flg22 or 0.5

666 µg/µl (equals ~1 µM) poly(I:C). As a control, leaf discs were treated with water or treated with PBS.

667 Elicitor and control treatment was performed by addition of the elicitor or the controls to leaf disks

668 acclimated overnight in ultrapure water. After addition of the elicitor, leaf disks were vacuum

669 infiltrated for 10 min. Samples were taken after an additional 20 min of incubation. MPK

670 phosphorylation was determined using protein extracts obtained from elicitor or control-treated leaf

671 disks using immunoblots probed with antibodies against phosphor-p44/42 ERK (Cell Signaling

672 Technology, Beverly, MA, USA; Ozyme S4370S) and horseradish peroxidase (HRP)-labelled

673 secondary antibodies for luminescence detection (SuperSignal™ West Femto Maximum Sensitivity

674 Substrate, ThermoFisher, France).

675

676 Analysis of ROS production

677 Leaf discs excised from 4-week-old *A. thaliana* or *N. benthamiana* plants were incubated overnight in

678 96-well plates with 600 μL of deionized, ultra-pure water. The next day deionized, ultra-pure water

679 was replaced with 100 μL reaction solution containing 50 μM luminol and 10 μg/mL horseradish

680 peroxidase (Sigma, USA) together with or without 1 μM flg22 or 0.5μg/μl poly(I:C). Luminescence

681 was determined with a luminometer (BMG LABTECH, FLUOstar®Omega) at 1.5 minute intervals

682 for a period of 40 minutes. Mean values obtained for 10 leaf discs per treatment were expressed as

683 mean relative light units (RLU).

684

685 Seedling growth inhibition assay

686 Seeds were surface-sterilized and grown vertically at 22°C under 12h/12h light/dark periods in square

687 petri-dishes on half-strength Murashige and Skoog (MS) basal medium (pH 5.8) containing 0.5 g/L

688 MES and 0.8% agar. 7 days old seedlings were transferred into liquid half-strength Murashige and

689 Skoog (MS) medium with or without 500 ng/μl (equals ~1 μM) poly(I:C) or 1 μM flg22. The effect of

690 treatment on seedling growth was documented on photographs 12 days after treatment and measured

691 with a ruler.

692

693 Protoplast transient expression and BIK1 mobility shift assays

694 Arabidopsis protoplasts (about 40,000 cells) isolated from wildtype Col-0 or *serk1-1* were transfected

695 with HA-epitope-tagged BIK1 (pHBT-35S::BIK1-HA) or co-transfected with pHBT-35S::BIK1-HA

696 and pHBT-35S::SERK1-FLAG. Protoplast isolation and the transient expression assay were done as

697 described previously (He et al., 2007). Also the BIK1 and SERK1 constructs have already been

698 described (Lu et al., 2010; Meng et al., 2015a). The transfected protoplasts were incubated at room

699 temperature overnight. After stimulation with flg22 (1 μM) or poly(I:C) (0.5 μg/ul) for 20 minutes,

700 the protoplasts were collected by centrifugation and lysed by vortexing in 100 μl co-IP buffer (150

701 mM NaCl, 50 mM Tris-HCl, pH7.5, 5 mM EDTA, 0.5% Triton, 1 × protease inhibitor cocktail.

702 Before use, 2.5 μl 0.4 M DTT, 2 μl 1 M NaF and 2 μl 1 M Na_3VO_3 were added per 1 ml IP buffer). A

703 final concentration of 1 μM K-252a inhibitor (Sigma-Aldrich, 05288) was added 1 hour before

704 poly(I:C) (0.5 μg/ul) treatment. Lysed protoplasts were treated with calf intestinal phosphatase (CIP)

705 (New England Biolabs) for 60 minutes at 37°C (1 unit per μg of total protein). BIK1 was detected in

706 Western blots assays using HA-HRP antibody (Invitrogen, 26183-HRP)) and its phosphorylation was

707 quantified by calculating the ratio between the intensity of the shifted upper band of phosphorylated

708 BIK1 (pBIK1) and the sum of the intensities of both shifted and non-shifted bands (pBIK1 + BIK1)

709 (no treatment set to 0.0). The BIK1 mobility shift assays have been described previously (Lu et al.,

710 2010; Ma et al., 2020). SERK1-FLAG was detected in Western blot assays using monoclonal anti-

711 FLAG (Sigma-Aldrich, F1804).

712

713 <u>Imaging</u>

714 Microscopical imaging was performed with a Zeiss LSM 780 confocal laser scanning microscope

715 equipped with ZEN 2.3 software (Carl Zeiss, Jean, Germany). Excitation / emission wavelengths were

716 405 nm/475-525 nm for aniline blue, 488 nm / 500-525 nm for GFP, and 561 nm/560-610 nm for

717 RFP.

718

728

729 **Author Contributions**

730 Conceptualization: MH

731 Methodology: CH, JM, EB, YY, MR, ARS, LEG, LS, MH

732 Investigation: CH, ARS, LEG, YY, MR, MH

733 Visualization: CH, ARS, LEG, YY, LS, MH

734 Funding acquisition: LS, MH

735 Project administration: MH

736 Supervision: LS, MH

737 Writing - original draft: MH

738 Writing – review & editing: CH, ARS, JM, LS, MH

739

740 **Competing Interests**

741 Authors declare that they have no competing interests

742

743 **Data and materials availability**

744 All data are available in the main text or the supplementary materials.

745

746 **Supplementary Materials**

747 Table S1

748 Figure S1

749

750 **References**

751

752 Alexopoulou, L., Holt, A.C., Medzhitov, R., and Flavell, R.A. (2001). Recognition of double-stranded

753 RNA and activation of NF-kappaB by Toll-like receptor 3. Nature 413, 732-738.

754 Amari, K., Boutant, E., Hofmann, C., Schmitt-Keichinger, C., Fernandez-Calvino, L., Didier, P.,

755 Lerich, A., Mutterer, J., Thomas, C.L., Heinlein, M., Mély, Y., Maule, A.J., and Ritzenthaler, C.

756 (2010). A family of plasmodesmal proteins with receptor-like properties for plant viral movement

757 proteins. PLoS Pathog 6, e1001119.

758 Ashby, J., Boutant, E., Seemanpillai, M., Groner, A., Sambade, A., Ritzenthaler, C., and Heinlein, M.

759 (2006). *Tobacco mosaic virus* movement protein functions as a structural microtubule-associated

760 protein. J Virol 80, 8329-8344.

761 Beffa, R.S., Hofer, R.M., Thomas, M., and Meins, F., Jr. (1996). Decreased susceptibility to viral

762 disease of [beta]-1,3-glucanase-deficient plants generated by antisense transformation. Plant Cell 8,

763 1001-1011.

764 Benitez-Alfonso, Y., Faulkner, C., Pendle, A., Miyashima, S., Helariutta, Y., and Maule, A. (2013).

765 Symplastic intercellular connectivity regulates lateral root patterning. Dev Cell 26, 136-147.

766 Borniego, M.B., Karlin, D., Pena, E.J., Robles Luna, G., and Garcia, M.L. (2016). Bioinformatic and

767 mutational analysis of ophiovirus movement proteins, belonging to the 30K superfamily. Virology

768 498, 172-180.

769 Boutant, E., Didier, P., Niehl, A., Mely, Y., Ritzenthaler, C., and Heinlein, M. (2010). Fluorescent

770 protein recruitment assay for demonstration and analysis of in vivo protein interactions in plant cells

771 and its application to *Tobacco mosaic virus* movement protein. Plant J 62, 171-177.

772 Boyko, V., van der Laak, J., Ferralli, J., Suslova, E., Kwon, M.-O., and Heinlein, M. (2000). Cellular

773 targets of functional and dysfunctional mutants of *Tobacco mosaic virus* movement protein fused to

774 GFP. J. Virol. 74, 11339-11346.

775 Boyko, V., Ashby, J.A., Suslova, E., Ferralli, J., Sterthaus, O., Deom, C.M., and Heinlein, M. (2002).

776 Intramolecular complementing mutations in *tobacco mosaic virus* movement protein confirm a role

777 for microtubule association in viral RNA transport. J Virol 76, 3974-3980.

778 Brandner, K., Sambade, A., Boutant, E., Didier, P., Mély, Y., Ritzenthaler, C., and Heinlein, M.

779 (2008). *Tobacco mosaic virus* movement protein interacts with green fluorescent protein-tagged

780 microtubule end-binding protein 1. Plant Physiol 147, 611-623.

781 Brault, M.L., Petit, J.D., Immel, F., Nicolas, W.J., Glavier, M., Brocard, L., Gaston, A., Fouche, M.,

782 Hawkins, T.J., Crowet, J.M., Grison, M.S., Germain, V., Rocher, M., Kraner, M., Alva, V., Claverol,

783   S., Paterlini, A., Helariutta, Y., Deleu, M., Lins, L., Tilsner, J., and Bayer, E.M. (2019). Multiple C2

784   domains and transmembrane region proteins (MCTPs) tether membranes at plasmodesmata. EMBO

785   Rep 20, e47182.

786   Bucher, G.L., Tarina, C., Heinlein, M., Di Serio, F., Meins Jr., F., and Iglesias, V.A. (2001). Local

787   expression of enzymatically active class 1 beta-1,3-glucanase enhances symptoms of TMV infection

788   in tobacco. Plant J. 28, 361-369.

789   Cai, Q., Qiao, L., Wang, M., He, B., Lin, F.-M., Palmquist, J., Huang, S.-D. and Jin, H. (2018). Plants

790   send small RNAs in extracellular vesicles to fungal pathogen to silence virulence genes. Science 360,

791   1126.

792   Cai, Q., He, B., Wang, S., Fletcher, S., Niu, D., Mitter, N., Birch, P.R.J., Jin, H. (2021). Message in a

793   bubble: shuttling small RNAs and proteins between cells and interacting organisms using extracellular

794   vesicles. Annu Rev Plant Biol 72, 497-524.

795   Caillaud, M.C., Wirthmueller, L., Sklenar, J., Findlay, K., Piquerez, S.J., Jones, A.M., Robatzek, S.,

796   Jones, J.D., and Faulkner, C. (2014). The plasmodesmal protein PDLP1 localises to haustoria-

797   associated membranes during downy mildew infection and regulates callose deposition. PLoS Pathog

798   10, e1004496.

799   Castro, B., Citterico, M., Kimura, S., Stevens, D.M., Wrzaczek, M., and Coaker, G. (2021). Stress-

800   induced reactive oxygen species compartmentalization, perception and signalling. Nat Plants 7, 403-

801   412.

802   Chen, M.H., Shen, J., Hind, G., Handa, A.K., and Citovsky, V. (2000). Interaction between the

803   tobacco mosaic virus movement protein and host cell pectin methylesterases is required for viral cell-

804   to-cell movement. EMBO J 19, 913-920.

805   Cheval, C., and Faulkner, C. (2018). Plasmodesmal regulation during plant-pathogen interactions.

806   New Phytol 217, 62-67.

807   Cheval, C., Samwald, S., Johnston, M.G., de Keijzer, J., Breakspear, A., Liu, X., Bellandi, A.,

808   Kadota, Y., Zipfel, C., and Faulkner, C. (2020). Chitin perception in plasmodesmata characterizes

809   submembrane immune-signaling specificity in plants. Proc Natl Acad Sci U S A 117, 9621-9629.

810   Christensen, N., Tilsner, J., Bell, K., Hammann, P., Parton, R., Lacomme, C., and Oparka, K. (2009).

811   The 5' cap of *Tobacco mosaic virus* (TMV) is required for virion attachment to the actin/endoplasmic

812   reticulum network during early infection. Traffic 10, 536-551.

813   Citovsky, V. (1999). *Tobacco mosaic virus*: a pioneer of cell-to-cell movement. Philos Trans R Soc

814   Lond B Biol Sci 354, 637-643.

815   Citovsky, V., Knorr, D., Schuster, G., and Zambryski, P. (1990). The P30 movement protein of

816   *Tobacco mosaic virus* is a single-strand nucleic acid binding protein. Cell 60, 637-647.

817   Csorba, T., Kontra, L., and Burgyan, J. (2015). Viral silencing suppressors: Tools forged to fine-tune

818   host-pathogen coexistence. Virology 479-480C, 85-103.

819   Czechowski, T., Stitt, M., Altmann, T., Udvardi, M.K., and Scheible, W.R. (2005). Genome-wide
820   identification and testing of superior reference genes for transcript normalization in Arabidopsis. Plant
821   Physiol 139, 5-17.

822   De Storme, N., and Geelen, D. (2014). Callose homeostasis at plasmodesmata: molecular regulators
823   and developmental relevance. Front Plant Sci 5, 138.

824   DeFalco, T.A., and Zipfel, C. (2021). Molecular mechanisms of early plant pattern-triggered immune
825   signaling. Mol Cell 81, 3449-3467.

826   Ding, B., Haudenshield, J.S., Hull, R.J., Wolf, S., Beachy, R.N., and Lucas, W.J. (1992). Secondary
827   plasmodesmata are specific sites of localization of the *Tobacco mosaic virus* movement protein in
828   transgenic tobacco plants. Plant Cell 4, 915-928.

829   Ding, S.W., and Voinnet, O. (2007). Antiviral immunity directed by small RNAs. Cell 130, 413-426.

830   Dolja, V.V., Krupovic, M., and Koonin, E.V. (2020). Deep roots and splendid boughs of the global
831   plant virome. Annu Rev Phytopathol 58, 23-53.

832   Fatyol, K., Fekete, K.A., and Ludman, M. (2020). Double-stranded-RNA-binding protein 2
833   participates in antiviral defense. J Virol 94, e00017-20.

834   Faulkner, C., Petutschnig, E., Benitez-Alfonso, Y., Beck, M., Robatzek, S., Lipka, V., and Maule, A.J.
835   (2013). LYM2-dependent chitin perception limits molecular flux via plasmodesmata. Proc Natl Acad
836   Sci U S A 110, 9166-9170.

837   Guenoune-Gelbart, D., Elbaum, M., Sagi, G., Levy, A., and Epel, B.L. (2008). *Tobacco mosaic virus*
838   (TMV) replicase and movement protein function synergistically in facilitating TMV spread by lateral
839   diffusion in the plasmodesmal desmotubule of *Nicotiana benthamiana*. Mol Plant Microbe Interact
840   21, 335-345.

841   Guseman, J.M., Lee, J.S., Bogenschutz, N.L., Peterson, K.M., Virata, R.E., Xie, B., Kanaoka, M.M.,
842   Hong, Z., and Torii, K.U. (2010). Dysregulation of cell-to-cell connectivity and stomatal patterning
843   by loss-of-function mutation in Arabidopsis *chorus* (glucan synthase-like 8). Development 137, 1731-
844   1741.

845   He, P., Shan, L., and Sheen, J. (2007). The use of protoplasts to study innate immune responses.
846   Methods Mol Biol 354, 1-9.

847   Heinlein, M. (2015). Plant virus replication and movement. Virology 479-480, 657-671.

848   Heinlein, M., Epel, B.L., Padgett, H.S., and Beachy, R.N. (1995). Interaction of tobamovirus
849   movement proteins with the plant cytoskeleton. Science 270, 1983-1985.

850   Heinlein, M., Wood, M.R., Thiel, T., and Beachy, R.N. (1998). Targeting and modification of
851   prokaryotic cell-cell junctions by *Tobacco mosaic virus* cell-to-cell movement protein. Plant J 14,
852   345-351.

853   Holdaway-Clarke, T.L., Walker, N.A., Hepler, P.K., and Overall, R.L. (2000). Physiological
854   elevations in cytoplasmic free calcium by cold or ion injection result in transient closure of higher
855   plant plasmodesmata. Planta 210, 329-335.

856 Horsch, A.B., Fry, J.E., Hoffmann, N.L., Eichholtz, D., Rogers, S.G., and Fraley, R.T. (1985). A
857 simple and general method for transferring genes into plants. Science 227, 1229-1231.

858 Hu, S., Yin, Y., Chen, B., Lin, Q., Tian, Y., Song, X., Peng, J., Zheng, H., Rao, S., Wu, G., Mo, X.,
859 Yan, F., Chen, J., and Lu, Y. (2021). Identification of viral particles in the apoplast of *Nicotiana*
860 *benthamiana* leaves infected by potato virus X. Mol Plant Pathol 22, 456-464.

861 Huang, C., and Heinlein, M. (2022). Function of plasmodesmata in the interaction of plants with
862 microbes and viruses. Methods Mol Biol 2457, 23-54.

863 Huang, C., Mutterer, J., and Heinlein, M. (2022). I*n vivo* aniline blue staining and semi-automated
864 quantification of callose deposition at plasmodesmata Methods Mol Biol 2457, 151-165.

865 Huang, C.Y., Wang, H., Hu, P., Hamby, R., and Jin, H. (2019) Small RNAs – Big players in plant-
866 microbe interactions. Cell Host Microbe 26, 173-182.

867 Iglesias, V.A., and Meins, F., Jr. (2000). Movement of plant viruses is delayed in a β-1,3-glucanase-
868 deficient mutant showing a reduced plasmodesmatal size exclusion limit and enhanced callose
869 deposition. Plant J. 21, 157-166.

870 Incarbone, M., Clavel, M., Monsion, B., Kuhn, L., Scheer, H., Vantard, E., Poignavent, V., Dunoyer,
871 P., Genschik, P., and Ritzenthaler, C. (2021). Immunocapture of dsRNA-bound proteins provides
872 insight into *Tobacco rattle virus* replication complexes and reveals Arabidopsis DRB2 to be a wide-
873 spectrum antiviral effector. Plant Cell 33, 3402-3420.

874 Ishikawa, K., Tamura, K., Fukao, Y., and Shimada, T. (2020). Structural and functional relationships
875 between plasmodesmata and plant endoplasmic reticulum-plasma membrane contact sites consisting
876 of three synaptotagmins. New Phytol 226, 798-808.

877 Jones, R.A.C. (2021). Global plant virus disease pandemics and epidemics. Plants (Basel) 10, 233.

878 Jones, R.A.C., and Naidu, R.A. (2019). Global dimensions of plant virus diseases: Current status and
879 future perspectives. Annu Rev Virol 6, 387-409.

880 Kadota, Y., Sklenar, J., Derbyshire, P., Stransfeld, L., Asai, S., Ntoukakis, V., Jones, J.D., Shirasu, K.,
881 Menke, F., Jones, A., and Zipfel, C. (2014). Direct regulation of the NADPH oxidase RBOHD by the
882 PRR-associated kinase BIK1 during plant immunity. Mol Cell 54, 43-55.

883 Koch, A., Biedenkopf, D., Furch, A., Weber, L., Rossbach, O., Abdellatef, E., Linicus, L.,
884 Johannsmeier, J., Jelonek, L., Goesmann, A., Cardoza, V., Mcmillan, J., Mentzel, T. and Kogel, K.-H.
885 (2016). An RNAi-based con- trol of *Fusarium graminearum* infections through spraying of long
886 dsRNAs involves a plant passage and is controlled by the fungal silencing machinery. PLoS Pathog
887 12, e1005901.

888 Kørner, C.J., Klauser, D., Niehl, A., Dominguez-Ferreras, A., Chinchilla, D., Boller, T., Heinlein, M.,
889 and Hann, D.R. (2013). The immunity regulator BAK1 contributes to resistance against diverse RNA
890 viruses. Mol Plant Microbe Interact 26, 1271-1280.

891 Kubota, K., Tsuda, S., Tamai, A., and Meshi, T. (2003). *Tomato mosaic virus* replication protein
892 suppresses virus-targeted posttranscriptional gene silencing. J Virol 77, 11016-11026.

893   Lee, J.Y., and Lucas, W.J. (2001). Phosphorylation of viral movement proteins--regulation of cell-to-

894   cell trafficking. Trends Microbiol 9, 5-8.

895   Lee, J.Y., Wang, X., Cui, W., Sager, R., Modla, S., Czymmek, K., Zybaliov, B., van Wijk, K., Zhang,

896   C., Lu, H., and Lakshmanan, V. (2011). A plasmodesmata-localized protein mediates crosstalk

897   between cell-to-cell communication and innate immunity in Arabidopsis. Plant Cell 23, 3353-3373.

898   Levy, A., Zheng, J.Y., and Lazarowitz, S.G. (2015). Synaptotagmin SYTA forms ER-plasma

899   membrane junctions that are recruited to plasmodesmata for plant virus movement. Curr Biol 25,

900   2018-2025.

901   Levy, A., Erlanger, M., Rosenthal, M., and Epel, B.L. (2007). A plasmodesmata-associated beta-1,3-

902   glucanase in Arabidopsis. Plant J 49, 669-682.

903   Li, F., Cheng, C., Cui, F., de Oliveira, M.V., Yu, X., Meng, X., Intorne, A.C., Babilonia, K., Li, M.,

904   Li, B., Chen, S., Ma, X., Xiao, S., Zheng, Y., Fei, Z., Metz, R.P., Johnson, C.D., Koiwa, H., Sun, W.,

905   Li, Z., de Souza Filho, G.A., Shan, L., and He, P. (2014). Modulation of RNA polymerase II

906   phosphorylation downstream of pathogen perception orchestrates plant immunity. Cell Host Microbe

907   16, 748-758.

908   Lim, G.H., Shine, M.B., de Lorenzo, L., Yu, K., Cui, W., Navarre, D., Hunt, A.G., Lee, J.Y.,

909   Kachroo, A., and Kachroo, P. (2016). Plasmodesmata localizing proteins regulate transport and

910   signaling during systemic acquired immunity in plants. Cell Host Microbe 19, 541-549.

911   Liu, Z., Wu, Y., Yang, F., Zhang, Y., Chen, S., Xie, Q., Tian, X., and Zhou, J.M. (2013). BIK1

912   interacts with PEPRs to mediate ethylene-induced immunity. Proc Natl Acad Sci U S A 110, 6205-

913   6210.

914   Lu, D., Wu, S., Gao, X., Zhang, Y., Shan, L., and He, P. (2010). A receptor-like cytoplasmic kinase,

915   BIK1, associates with a flagellin receptor complex to initiate plant innate immunity. Proc Natl Acad

916   Sci U S A 107, 496-501.

917   Ma, X., Claus, L.A.N., Leslie, M.E., Tao, K., Wu, Z., Liu, J., Yu, X., Li, B., Zhou, J., Savatin, D.V.,

918   Peng, J., Tyler, B.M., Heese, A., Russinova, E., He, P., and Shan, L. (2020). Ligand-induced

919   monoubiquitination of BIK1 regulates plant immunity. Nature 581, 199-203.

920   Mansilla, C., Sanchez, F., Padgett, H.S., Pogue, G.P., and Ponz, F. (2009). Chimeras between *Oilseed*

921   *rape mosaic virus* and *Tobacco mosaic virus* highlight the relevant role of the tobamoviral RdRp as

922   pathogenicity determinant in several hosts. Mol Plant Pathol 10, 59-68.

923   Meng, X., Shan, L., and He, P. (2015a). Stack heterotrimeric G proteins and MAPK cascades on a

924   RACK. Mol Plant 8, 1691-1693.

925   Meng, X., Chen, X., Mang, H., Liu, C., Yu, X., Gao, X., Torii, K.U., He, P., and Shan, L. (2015b).

926   Differential function of Arabidopsis SERK family receptor-like kinases in stomatal patterning. Curr

927   Biol 25, 2361-2372.

928   Mittler, R. (2017). ROS are good. Trends Plant Sci 22, 11-19.

929 Movahed, N., Cabanillas, D.G., Wan, J., Vali, H., Laliberte, J.F., and Zheng, H. (2019). Turnip
930 mosaic virus components are released into the extracellular space by vesicles in infected leaves. Plant
931 Physiol 180, 1375-1388.
932
933 Monsion, B., Incarbone, M., Hleibieh, K., Poignavent, V., Ghannam, A., Dunoyer, P., Daeffler, L.,
934 Tilsner, J., and Ritzenthaler, C. (2018). Efficient detection of long dsRNA in vitro and in vivo using
935 the dsRNA binding domain from FHV B2 protein. Front Plant Sci 9, 70.
936 Moore, P.J., Fenczik, C.A., Deom, C.M., and Beachy, R.N. (1992). Developmental changes in
937 plasmodesmata in transgenic tobacco expressing the movement protein of Tobacco mosaic virus.
938 Protoplasma 170, 115-127.
939 Niehl, A., and Heinlein, M. (2019). Perception of double-stranded RNA in plant antiviral immunity.
940 Mole Plant Pathol 20, 1203-1210.
941 Niehl, A., Wyrsch, I., Boller, T., and Heinlein, M. (2016). Double-stranded RNAs induce a pattern-
942 triggered immune signaling pathway in plants. New Phytol 211, 1008-1019.
943 Niehl, A., Soininen, M., Poranen, M.M., and Heinlein, M. (2018). Synthetic biology approach for
944 plant protection using dsRNA. Plant Biotechnol J 16, 1679-1687.
945 Niehl, A., Amari, K., Gereige, D., Brandner, K., Mély, Y., and Heinlein, M. (2012). Control of
946 Tobacco mosaic virus movement protein fate by CELL-DIVISION-CYCLE protein 48 (CDC48).
947 Plant Physiol 160, 2093-2108.
948 Nuhse, T.S., Bottrill, A.R., Jones, A.M., and Peck, S.C. (2007). Quantitative phosphoproteomic
949 analysis of plasma membrane proteins reveals regulatory mechanisms of plant innate immune
950 responses. Plant J 51, 931-940.
951 Oparka, K.J., Prior, D.A.M., Santa Cruz, S., Padgett, H.S., and Beachy, R.N. (1997). Gating of
952 epidermal plasmodesmata is restricted to the leading edge of expanding infection sites of Tobacco
953 mosaic virus. Plant J. 12, 781-789.
954 Pitzalis, N., and Heinlein, M. (2017). The roles of membranes and associated cytoskeleton in plant
955 virus replication and cell-to-cell movement. J Exp Bot 69, 117-132.
956 Ruf, A., Oberkofler, L., Robatzek, S., and Weiberg, A. (2022). Spotlight on plant RNA-containing
957 extracellular vesicles. Curr Opin Plant Biol 69, 102272.
958 Sambade, A., Brandner, K., Hofmann, C., Seemanpillai, M., Mutterer, J., and Heinlein, M. (2008).
959 Transport of TMV movement protein particles associated with the targeting of RNA to
960 plasmodesmata. Traffic 9, 2073-2088.
961 Simpson, C., Thomas, C., Findlay, K., Bayer, E., and Maule, A.J. (2009). An Arabidopsis GPI-anchor
962 plasmodesmal neck protein with callose binding activity and potential to regulate cell-to-cell
963 trafficking. Plant Cell 21, 581-594.
964 Tan, X., Sun, L., Chen, J., and Chen, Z.J. (2018). Detection of Microbial infections through innate
965 immune sensing of nucleic acids. Annu Rev Microbiol 72, 447-478.

966   Thomas, C.L., Bayer, E.M., Ritzenthaler, C., Fernandez-Calvino, L., and Maule, A.J. (2008). Specific
967   targeting of a plasmodesmal protein affecting cell-to-cell communication. PLoS Biol 6, e7.

968   Thor, K., Jiang, S., Michard, E., George, J., Scherzer, S., Huang, S., Dindas, J., Derbyshire, P., Leitao,
969   N., DeFalco, T.A., Koster, P., Hunter, K., Kimura, S., Gronnier, J., Stransfeld, L., Kadota, Y.,
970   Bucherl, C.A., Charpentier, M., Wrzaczek, M., MacLean, D., Oldroyd, G.E.D., Menke, F.L.H.,
971   Roelfsema, M.R.G., Hedrich, R., Feijo, J., and Zipfel, C. (2020). The calcium-permeable channel
972   OSCA1.3 regulates plant stomatal immunity. Nature 585, 569-573.

973   Tian, W., Hou, C., Ren, Z., Wang, C., Zhao, F., Dahlbeck, D., Hu, S., Zhang, L., Niu, Q., Li, L.,
974   Staskawicz, B.J., and Luan, S. (2019). A calmodulin-gated calcium channel links pathogen patterns to
975   plant immunity. Nature 572, 131-135.

976   Tilsner, J., Nicolas, W., Rosado, A., and Bayer, E.M. (2016). Staying tight: Plasmodesmal membrane
977   contact sites and the control of cell-to-cell connectivity in plants. Annu Rev Plant Biol 67, 337-364.

978   Torres, M.A., Dangl, J.L., and Jones, J.D. (2002). Arabidopsis gp91phox homologues AtrbohD and
979   AtrbohF are required for accumulation of reactive oxygen intermediates in the plant defense response.
980   Proc Natl Acad Sci U S A 99, 517-522.

981   Tucker, E.B., and Boss, W.F. (1996). Mastoparan induced intracellular Ca^{2+} fluxes may regulate cell-
982   to-cell communication in plants. Plant Physiol. 111, 459-467.

983   Uchiyama, A., Shimada-Beltran, H., Levy, A., Zheng, J.Y., Javia, P.A., and Lazarowitz, S.G. (2014).
984   The Arabidopsis synaptotagmin SYTA regulates the cell-to-cell movement of diverse plant viruses.
985   Front Plant Sci 5, 584.

986   Vatén, A., Dettmer, J., Wu, S., Stierhof, Y.D., Miyashima, S., Yadav, S.R., Roberts, C.J., Campilho,
987   A., Bulone, V., Lichtenberger, R., Lehesranta, S., Mahonen, A.P., Kim, J.Y., Jokitalo, E., Sauer, N.,
988   Scheres, B., Nakajima, K., Carlsbecker, A., Gallagher, K.L., and Helariutta, Y. (2011). Callose
989   biosynthesis regulates symplastic trafficking during root development. Dev Cell 21, 1144-1155.

990   Vogler, H., Kwon, M.O., Dang, V., Sambade, A., Fasler, M., Ashby, J., and Heinlein, M. (2008).
991   *Tobacco mosaic virus* movement protein enhances the spread of RNA silencing. PLoS Pathog 4,
992   e1000038.

993   Vogler, H., Akbergenov, R., Shivaprasad, P.V., Dang, V., Fasler, M., Kwon, M.O., Zhanybekova, S.,
994   Hohn, T., and Heinlein, M. (2007). Modification of small RNAs associated with suppression of RNA
995   silencing by tobamovirus replicase protein. J Virol 81, 10379-10388.

996   Wan, J., Cabanillas, D.G., Zheng, H. and Laliberté, J.-F. (2015). Turnip mosaic virus moves
997   systemically through both phloem and xylem as membrane-associated complexes. Plant Physiol 167,
998   1374-1388.

999   Wan, J. and Laliberté, J.-F. (2015). Membrane-associated virus replication complexes locate to plant
1000   conducting tubes. Plant Signal Behav 10, e1042639–e1042639.

1001   Wang, X., Sager, R., Cui, W., Zhang, C., Lu, H., and Lee, J.Y. (2013). Salicylic acid regulates
1002   plasmodesmata closure during innate immune responses in Arabidopsis. Plant Cell 25, 2315-2329.

1003   Wu, S.W., Kumar, R., Iswanto, A.B.B., and Kim, J.Y. (2018). Callose balancing at plasmodesmata. J

1004   Exp Bot 69, 5325-5339.

1005   Xu, B., Cheval, C., Laohavisit, A., Hocking, B., Chiasson, D., Olsson, T.S.G., Shirasu, K., Faulkner,

1006   C., and Gilliham, M. (2017). A calmodulin-like protein regulates plasmodesmal closure during

1007   bacterial immune responses. New Phytol 215, 77-84.

1008   Yuan, C., Lazarowitz, S.G., and Citovsky, V. (2018). The plasmodesmal localization signal of TMV

1009   MP is recognized by plant synaptotagmin SYTA. mBio 9, e01314-18.

1010   Zhang, J., Li, W., Xiang, T., Liu, Z., Laluk, K., Ding, X., Zou, Y., Gao, M., Zhang, X., Chen, S.,

1011   Mengiste, T., Zhang, Y., and Zhou, J.M. (2010). Receptor-like cytoplasmic kinases integrate signaling

1012   from multiple plant immune receptors and are targeted by a Pseudomonas syringae effector. Cell Host

1013   Microbe 7, 290-301.

1014

1015

1016

1017

1018   **Figure Legends**

1019

1020   **Figure 1. Poly(I:C) treatment causes inhibition of virus movement in *N. benthamiana*.** (**A**) TMV-

1021   GFP infection sites in *N. benthamiana* leaves at 7 days post inoculation (dpi) with the virus together

1022   with either water (control), 0.5 µg/µl (≈1 µM) poly(I:C), or 1 µM flg22. Scale bar, 1 cm. (**B**) Sizes of

1023   individual infection sites measured in 10 leaf samples collected from three plants per treatment. Two-

1024   tailed Mann-Whitney test; ****, p <0.0001; ***, p <0.001; **, p <0.01. The experiment was

1025   performed three times with similar results. (**C**) TMV replication in *N. benthamiana* is not influenced

1026   by poly(I:C). A cell-autonomous, MP-deficient TMV replicon (TMVΔMΔC-GFP) expressed in cells

1027   of agroinoculated leaves produces the same number of RNA genome copies in the presence and

1028   absence of treatment with 0.5 µM poly(I:C), as determined by Taqman RT-qPCR. Poly(I:C) and

1029   control treatments were applied 1 day after agroinoculation and results obtained at indicated days after

1030   this treatment (dpt) are shown. The data represent means of three biological replicates (with SD) per

1031   time point and treatment. Two-tailed Mann-Whitney test. ns, not significant. (**D**) and (**E**) Treatment of

1032   *N. benthamiana* with poly(I:C) or flg22 induces increased callose deposition at PD within 30 minutes

1033   in a dose-specific manner. (**D**) Callose fluorescence at PD upon aniline blue staining. Scale bar, 10

1034   µm. (**E**) Relative callose content in individual PD (blue dots, n > 100) as determined in three leaf

1035   discs per treatment. Two-tailed Mann-Whitney test; ****, p = <0.0001. (**F**) Callose deposition at PD

1036   in *N. benthamiana* leaf epidermal tissue upon treatment with 50 ng/µl biological dsRNA (dsRNA[Phi6]).

1037   Relative callose content in individual PD (blue dots, n > 100) as determined in three leaf discs per

1038   treatment. Two-tailed Mann-Whitney test; ****, p = <0.0001. (**G-I**) GFP mobility assay in *N.*

1039   *benthamiana*. Leaf disks expressing GFP together with cell-autonomous NLS:RFP one day after

1040   agroinfiltration were treated with water or 0.5 μg/μl poly(I:C) and imaged 48 hours later. (**G**)

1041   Example of GFP movement from an epidermal cell marked by cell-autonomous NLS:RFP into

1042   adjacent cells. Transiently expressed GFP shows a nucleocytoplasmic distribution (yellow arrow) and

1043   its movement from the expressing epidermal cell (co-expressed NLS:RFP in the nucleus, in red) is

1044   evident by appearance of green fluorescence in the nuclei and cytoplasm of adjacent cells (white

1045   arrowheads). Cells into which GFP moved are indicated by the red dashed line in the merged image.

1046   Scale bar, 50 μm. (**H** and **I**) Quantification of GFP movement between epidermal cells in leaf disks

1047   exposed to 0.5 μg/μl poly(I:C) or water (control) (29 transformation events were analyzed for each

1048   treatment). (**H**) Stacked column diagram showing the relative frequency of transformation events

1049   associated with either no GFP movement (dark grey), GFP movement into one adjacent cell layer

1050   (medium grey), or GFP movement into two adjacent cell layers (light grey). (**I**) Average intercellular

1051   movement (total number of cell layers into which GFP has moved divided by the number of evaluated

1052   transformation events). Two-tailed Mann-Whitney test; ****, p = <0.0001. A repetition of the GFP

1053   mobility assay provided similar results. (**J**) Low level of MPK activation by poly(I:C) relative to flg22

1054   after 30 minutes. Concentrations (conc.) are in ng/μl for poly(I:C) and in nM for flg22. The

1055   experiment was performed three times with similar results. (**K**) Poly(I:C) induces innate immunity

1056   marker genes, but suppresses expression of *BRI1*, in *N. benthamiana*. Mean value and SD of gene

1057   expression values obtained by RT-qPCR with three biological replicates (blue dots) harvested three

1058   hours after treatment.

1059

1060   **Figure 2. Poly(I:C)-induced signaling in Arabidopsis depends on BIK1/PBL1. (A)** and (**B**)

1061   Transcriptional regulation of Arabidopsis genes three hours after treatment with 0.5 μg/μl poly(I:C).

1062   For each gene, the mean value and the SD of gene expression values obtained by RT-qPCR analysis

1063   of three biological replicates (blue dots) is shown. (**A**) Poly(I:C) induces innate immunity marker

1064   genes in *A. thaliana* Col-0 wildtype. (**B**) Absence of poly(I:C)-induced *PR5* expression in the *serk1-1*

1065   mutant. (**C**) Poly(I:C) treatment causes callose deposition at PD in *A. thaliana* Col-0. Images were

1066   taken 30 minutes after treatment. Inlays show enlargements of the areas within the dashed boxes.

1067   Scale bar, 20 μm. Relative callose content in individual PD (blue dots, n > 100) as determined in three

1068   leaf discs from three plants per treatment. Two-tailed Mann-Whitney test; ****, p = <0.0001. (**D**)

1069   Callose deposition at PD in *A. thaliana* Col-0 leaf epidermal tissue 30 minutes after treatment with 50

1070   ng/μl of biological dsRNA (dsRNA^Phi6). Inlays show enlargements of the areas within the dashed

1071   boxes. Scale bar, 20 μm. Relative callose content in individual PD (blue dots, n > 100) as determined

1072   in three leaf discs per treatment. Two-tailed Mann-Whitney test; ****, p = <0.0001. (**E**) and (**F**)

1073   Poly(I:C)-induced callose spots are localized to PD as shown by co-localization with PD markers

1074   mCherry-PDCB1 (**E**) and PdBG2-citrine (**F**). Inlays show enlargements of the areas within the dashed

1075   boxes. Scale bar, 10 μm. (**G**) poly(I:C)-induced callose deposition at PD is inhibited in the *bik1 pbl1*

1076   mutant Images were taken 30 minutes after treatment and the WT control of the same experiments is

29

1077   shown in (**C**). Inlays show enlargements of the areas within the dashed boxes. Scale bar, 20 μm.

1078   Relative callose content in individual PD (blue dots) as determined in three leaf discs per treatment.

1079   Two-tailed Mann-Whitney test; ns, non-significant. (**H**) Poly(I:C)-induced MPK activation is reduced

1080   in the *bik1 pbl1* mutant. Immunoblot detection of phosphorylated MPK. Samples were harvested 30

1081   minutes after treatment with 0.5 μg/μl poly(I:C), 1 μM flg22, or water. "*bik1*" stands for *bik1 pbl1*.

1082   CBB, Coomassie brilliant blue-stained gel showing staining of ribulose-bisphosphate-carboxylase

1083   (Rubisco) as gel loading control. (**I**) *bik1 pbl1* plants do not show significant seedling root growth

1084   inhibition in the presence of poly(I:C) as compared to WT Col-0 plants. Seedlings were kept for 12

1085   days in 0.5 μg/μl poly(I:C) or water. Scale bar, 1 cm. Quantification of poly(I:C)-induced root growth

1086   inhibition in *A. thaliana* WT Col-0 and *bik1 pbl1* seedlings. Analysis of 6-7 seedlings (blue dots) per

1087   condition. Two-tailed Mann-Whitney test; ****, $p < 0.0001$; ns, non-significant.

1088

1089   **Figure 3. Poly(I:C) causes BIK1 phosphorylation and PD callose deposition in a SERK1-**

1090   **dependent manner.** (**A**) to (**C**) Analysis if BIK1 phosphorylation in poly(I:C)-treated *A. thaliana*

1091   Col-0 protoplasts. (**A**) Poly(I:C) treatment induces BIK1 phosphorylation as shown by a protein

1092   mobility shift detected by Western blot analysis. Protoplasts expressing BIK1-HA were non-treated

1093   (mock) or treated with 1 μM flg22 or 0.5 μg/μl poly(I:C), lysed after 20 minutes and treated or non-

1094   treated with calf intestine phosphatase (CIP) for 60 before Western blot analysis using HA-HRP

1095   antibody. BIK1 band intensities were quantified using Image Lab (Bio-Rad). Quantification of BIK1

1096   phosphorylation (upper panel) calculated as ratio of intensity of the upper band (phosphorylated

1097   BIK1, pBIK1) to the sum intensities of shifted and non-shifted bands (pBIK1 + BIK1) (no treatment

1098   set to 0.0). CCB, Coomassie brilliant blue staining of Rubisco as gel loading control (lower panel).

1099   (**B**) Poly(I:C)-induced BIK1 phosphorylation is blocked by 1 μM of the kinase inhibitor K-252a

1100   added 1 hour before poly(I:C) treatment. Rubisco detection by CBB staining is shown as gel loading

1101   control (lower panel). Experimental conditions and quantification of BIK1 phosphorylation as in (**A**).

1102   (**C**) SERK1 enhances poly(I:C)-induced BIK1 phosphorylation. Protoplasts from WT Col-0 or *serk1-*

1103   *1* mutants were transfected with BIK1-HA together with or without SERK1-FLAG and followed by

1104   treatment with or without 0.5 μg/μl poly(I:C). Phosphorylated BIK1 band intensities were quantified

1105   as in (**A**). The middle panel shows SERK1-FLAG expression. Rubisco detection by CBB staining is

1106   shown as gel loading control (lower panel). (**D**) and (**E**) Poly(I:C)-induced PD callose deposition

1107   depends on SERK1. (**D**) Callose fluorescence at PD seen upon aniline blue staining of epidermal cells

1108   of WT Col-0 plants and *serk1-1* mutants treated with water (control) or 0.5 μg/μl poly(I:C). Inlays

1109   show enlargements of the areas within the dashed boxes. Scale bar, 10 μm. (**E**) Relative callose

1110   content (fluorescence intensity) in individual PD (blue dots, $n > 100$) as determined in three leaf discs

1111   taken from three plants per treatment. Two-tailed Mann-Whitney test; ****, $p = < 0.0001$. The

1112   increase in PD callose levels in poly(I:C)-treated samples relative to water control-treated samples is

1113   shown in percent (%). Although the callose intensity data distributions between poly(I:C)-treated and

1114 control-treated samples are significantly different in both WT Col-0 and *serk1*, the comparison of the

1115 callose intensity median levels indicate a drastic inhibition of the poly(I:C)-induced PD callose

1116 deposition response in *serk1* as compared to the WT.

1117

1118 **Figure 4. poly(I:C)-induced PD callose deposition is ROS- and MPK3/6 cascade-independent**

1119 **but requires PDLP1/2/3 and CML41.** (**A**) and (**B**) Unlike flg22, poly(I:C) treatment does not induce

1120 any ROS production in Arabidopsis (**A**) or *N. benthamiana* (**B**). RLU, relative luminescence units.

1121 Mean values (black dots) and error bars (SD) obtained for each time point for 10 replicates (leaf

1122 disks) per treatment. (**C**) Poly(I:C)-induced callose deposition at PD is not affected in *rbohd* or *rbohf*

1123 mutants. Relative callose content in individual PD (blue dots, n > 100) 30 minutes after treatment with

1124 0.5 µg/µl poly(I:C) or water and determined in three leaf discs from three plants per treatment. Two-

1125 tailed Mann-Whitney test; ****, p = <0.0001. (**D**) Poly(I:C)-induced callose deposition at PD is not

1126 affected in *mpk3* and *mpk6* single mutants, and neither in a *mpk3* mutant in which *MPK6* is silenced

1127 by an artificial miRNA (*mpk3 amiRmpk6*). Relative callose content in individual PD (blue dots, n >

1128 100) 30 minutes after treatment with 0.5 µg/µl poly(I:C) or water and determined in three leaf discs

1129 from three plants per treatment. Two-tailed Mann-Whitney test; ****, p = <0.0001. (**E**) Poly(I:C)-

1130 induced callose deposition at PD is independent of PDLP5 but depends on the redundantly acting

1131 PDLP1, PDLP2, and PDLP3. Relative callose content in individual PD (blue dots, n > 100) 30

1132 minutes after treatment with 0.5 µg/µl poly(I:C) or water and determined in three leaf discs from three

1133 plants per treatment. Two-tailed Mann-Whitney test; ****, p = <0.0001; ns, non-significant. (**F**) and

1134 (**G**) Poly(I:C)-induced callose deposition at PD depends on CML41. (**F**) PD callose deposition levels

1135 in poly(I:C)-treated and control-treated leaf disks of two *CML41*-overexpressing lines (OEX2 and

1136 OEX12) and of two lines in which the expression of *CML41* is reduced by expression of artificial

1137 miRNA (amiRNA1 and amiRNA4). As compared to the WT (Col-0) and the *CML41*-overexpressing

1138 lines, the inducibility of PD callose deposition by poly(I:C) is strongly decreased in the amiRNA

1139 lines. Relative callose content in individual PD (blue dots, n > 100) 30 minutes after treatment with

1140 0.5 µg/µl poly(I:C) or water and determined in three leaf discs from three plants per treatment. Two-

1141 tailed Mann-Whitney test; ****, p = <0.0001. According to the Mann-Whitney test the distribution of

1142 individual PD callose intensities is different between all control- and poly(I:C)-treated samples.

1143 However, unlike in WT Col-0 and *CML41*-overexpressing lines, the median PD callose intensity

1144 levels are not increased upon poly(I:C)-treatment in amiRNA lines thus indicating a deficiency in the

1145 induction of PD callose deposition upon poly(I:C) treatment in these lines. (**G**) Relative levels of

1146 *CML41* expression in plants of the OEX2, OEX12, amiRNA1 and amiRNA4 lines in comparison to

1147 WT (Col-0), as determined by RT-qPCR. Mean value and standard error of gene expression values

1148 obtained by RT-qPCR with 3-6 biological replicates (blue dots). (**H**) poly(I:C)-induced callose

1149 deposition is reduced in the presence of EGTA. Relative callose content in individual PD (blue dots, n

31

1150   > 100) as determined in three leaf discs per treatment. Two-tailed Mann-Whitney test; ****, p =

1151   <0.0001.

1152

1153   **Figure 5. BIK1/PBL1 and CML41 are required for antiviral defense** (**A**) and (**B**) Disease

1154   symptoms (**A**) and viral RNA accumulation (**B**) at 28 dpi in wild-type plants and mutants

1155   inoculated with ORMV in the presence and absence of 0.5 µg/µl poly(I:C). Unlike in wild-

1156   type plants (Col-0) the antiviral effect of poly(I:C) treatment is lost in *bik1 pbl1* mutants and

1157   *CML41-amiRNA-1* expressing plants. Viral RNA accumulation (**B**) is depicted for 6

1158   biological replicates per condition. Mean values and standard errors are shown. (**C**) and (**D**)

1159   BIK1 and CML41 inhibit virus movement. (**C**) Representative symptom phenotypes at 21 dpi

1160   of Arabidopsis Col-0 plants, *bik1 pbl1* mutant plants and plants transgenic for *CML41-*

1161   *amiRNA-1* that were locally inoculated with ORMV and from which the inoculated leaves

1162   were removed at the indicated times in hours (h) and days (d). Whereas systemic leaves of

1163   Col-0 plants show symptoms on plants that carried the inoculated leaves for 3 or more days

1164   following inoculation, the systemic leaves of the *bik1 pbl1* mutant and of the CML41-

1165   amiRNA-expressing plants show symptoms already if the inoculated leaves were present for

1166   only 24 hours. (**D**) Immunoblot analysis of the youngest systemic leaves at 21 dpi using

1167   antibodies against viral coat protein (CP) (Youcai mosaic virus antibody, AS-0527, DSMZ,

1168   Braunschweig, Germany). The pattern of CP expression in the systemic leaves confirms that

1169   in WT Col-0 plants the virus needs between 24 h and 3 d to exit the inoculated leaves and

1170   move systemically, whereas the time needed for systemic movement is reduced to less than

1171   24 h in the *bik1 pbl1* mutant and of the CML41-amiRNA expressing plants, thus indicating a

1172   role of BIK1 and CML41 in restricting virus movement.

1173

1174   **Figure 6. Viral MP expression correlates with a suppression of PD-associated callose levels. (A)**

1175   Local site of infection by TMV-MP:RFP (at 4 dpi) in *N. benthamiana*. Different zones ahead of

1176   infection (zone 1), at the infection front (zone II), behind the infection front (zone III) and in the

1177   center of infection (zone IV) are indicated. Scale bar, 200 µm. **(B)** Viral dsRNA accumulation in the

1178   different zones of local TMV infection. Inlay images show magnifications of image areas framed by a

1179   dashed line. Scale bar, 20 µm. The MP of TMV is tagged with RFP (MP:RFP) and the accumulating

1180   dsRNA is imaged through binding of the *Flock house virus* B2 protein fused to GFP (B2:GFP). In

1181   cells of zone I (non-infected cells ahead of infection) B2:GFP shows a nucleo-cytoplasmic

1182   distribution, which is the typical distribution of this protein in the absence of dsRNA (Monsion et al.,

1183   2018). In cells at the virus front (zone II), B2:GFP co-localizes to MP:RFP to spots at the cell wall

1184   (likely at PD) indicating the localization of early virus-replication complexes (VRCs) engaged in virus

1185 replication and virus movement. In zone III, the VRCs have grown in size and accumulate high

1186 amounts of dsRNA consistent with high levels of virus replication to produce virus progeny. In zone

1187 IV, the MP is no longer expressed but residual MP:RFP is still seen in PD. The B2:GFP-tagged VRCs

1188 now appear rounded. (**C**) Pattern of MP:RFP and callose accumulation in the different zones. Inlays

1189 show magnifications of the image areas highlighted by dashed boxes. Scale bar, 40 µm. In zone II,

1190 where MP localizes to PD to facilitate virus movement, and to some extend also still in zone III, the

1191 PD-associated callose levels are decreased as compared to the other zones. (**D**) Quantification of PD

1192 callose in the different zones. The number of analyzed PD is shown in brackets. Two-tailed Mann-

1193 Whitney test; ****, $p < 0.0001$; ns, $p > 0.05$.

1194

1195 **Figure 7. Suppression of poly(I:C)-induced immunity by MP.** (**A-E**) Inhibition of dsRNA-induced

1196 callose deposition in MP:RFP-transgenic *N. benthamiana* plants. (**A-C**) MP:RFP is functional. (**A**)

1197 Transgenically expressed MP:RFP localizes to distinct locations at the cell wall. Scale bar, 10 µm. (**B**)

1198 The MP:RFP localizes to PD as revealed by callose staining with aniline blue. Scale bar, 10 µm. (**C**)

1199 The stably expressed MP:RFP in this line is functional and complements infection upon inoculation

1200 with *in vitro* transcribed infectious RNA of the MP-deficient TMVΔMΔC-GFP (Vogler et al., 2008),

1201 as can be seen by the occurrence of distinct GFP fluorescent infection sites at 7 dpi. (**D**) and (**E**)

1202 Inhibition of dsRNA-induced callose deposition in MP:RFP-transgenic plants. (**D**) Leaf epidermal

1203 cells of non-transgenic (WT) and MP:RFP-transgenic plants *N. benthamiana* stained with aniline

1204 blue. Inlay images show magnifications of image areas framed by a dashed line. Scale bar, 10 µm.

1205 Treatment of leaf tissues with 0.5 µg/µl poly(I:C) for 30 minutes causes a stronger increase in the

1206 level of PD-associated callose in WT plants than in MP:RFP-transgenic plants. (**E**) Quantification of

1207 callose in leaf epidermal cells upon aniline blue staining. Relative callose content in individual PD

1208 (blue dots, $n > 100$) as determined in three leaf discs from three plants per treatment. Two-tailed

1209 Mann-Whitney test; ****, $p < 0.0001$. (**F**) and (**G**) Inhibition of poly(I:C)-induced PD callose

1210 deposition by transiently expressed MP:GFP. Leaf disks excised from the GFP, MP:GFP, MP[P81S]:GFP

1211 or MP[C55]:GFP-expressing leaves 48h after agroinfiltration were incubated for one day in water, then

1212 transferred into aniline blue solution with and without 0.5 µg/µl poly(I:C) and imaged after 30

1213 minutes. (**F**) Images of leaf epidermal cells stained for callose with aniline blue (callose) and

1214 corresponding images of the same cell area with GFP fluorescence are shown. The ability of MP:GFP

1215 to reduce the poly(I:C) induction of callose deposition at PD is inhibited by a single amino acid

1216 exchange mutation in MP (P81S) previously shown to affect its ability to efficiently target PD and to

1217 function in virus movement. Functional MP with a C-terminal deletion of 55 amino acids (C55) that

1218 targets PD also inhibits poly(I:C)-induced callose deposition like wildtype MP. (**G**) Quantification of

1219 PD-associated callose levels in leaf epidermal cells upon aniline blue staining. Leaf disks from three

1220 plants per condition were analyzed. Two-tailed Mann-Whitney test; ****, $p < 0.0001$. (**H**) Western

1221 blot showing that the expression of wild type or mutant MP:GFP does not interfere with flg22-

33

1222   induced MPK activation. Ponc., Ponceau S-stained Western blot membrane. (**I**) Inhibition of flg22-

1223   and poly(I:C)-induced PD callose deposition by MP:RFP as compared to RFP. Leaf disks excised

1224   from the RFP or MP:RFP-expressing leaves 48 hours after agroinfiltration were incubated for one day

1225   in water, then transferred into aniline blue solution with and without 0.5 µg/µl poly(I:C) and imaged

1226   after 30 minutes. Six leaf disks from two plants were evaluated for each condition. ****, $p < 0.0001$.

1227

1228   **Figure 8. Inhibition of poly(I:C)-induced callose deposition by MPs of different viruses.** (**A**)

1229   Different MPs are functional. Unlike free RFP, RFP fusions to the MPs of TMV (MP^{TMV}:RFP),

1230   ORMV (MP^{ORMV}:RFP), and TVCV (MP^{TVCV}:RFP) complement the movement function of MP-

1231   deficient TMVΔM-GFP in *N. benthamiana*. Leaves were co-infiltrated with agrobacteria containing

1232   the respective RFP or MP:RFP-encoding plasmids together with highly diluted agrobacteria (OD$_{600\ nm}$

1233 $= 1 \times 10^{-5}$) for agro-inoculation with TMVΔMPΔCP-GFP. Pictures were taken at 5 dpi. Scale bar, 1

1234   cm. (B) MP^{TMV}:RFP, MP^{ORMV}:RFP, and MP^{TVCV}:RFP localize to PD as shown by the presence of

1235   callose. MP-expressing leaves were stained with aniline blue and imaged after 30 minutes. Inlay

1236   images show magnifications of image areas framed by a dashed line. Scale bar, 20 µm. (C)

1237   Expression of either MP^{TMV}:RFP, MP^{ORMV}:RFP, or MP^{TVCV}:RFP strongly reduces the induction of PD

1238   callose deposition in the presence of poly(I:C). Leaf disks excised from the RFP (control) or MP:RFP-

1239   expressing leaves 48h after agroinfiltration were incubated for one day in water, then transferred into

1240   aniline blue solution with and without 0.5 µg/µl poly(I:C) and imaged after 30 minutes. For each

1241   treatment, three images of three leaf disks taken from three plants were analyzed for PD-associated

1242   callose levels. RFP data are combined data from the 27 leaf disks that were used as RFP control in the

1243   individual agroinfiltration experiments. The increase in poly(I:C)-induced PD-callose levels seen in

1244   the presence of poly(I:C) as compared to the water-treated control is shown in percent (%). Two-

1245   tailed Mann-Whitney test; ****, $p = <0.0001$; ***, $p = 0.0002$.

1246

1247   **Figure 9**. **Poly(I:C) enters plant cells. (A)** B2:GFP-transgenic *N. benthamiana* leaf tissue treated

1248   with water (control) or 0.5 µg/µl poly(I:C) and imaged with ImageJ "green" (left) and "6 shades"

1249   (right) color look-up tables (LUT). The "6 shades" LUT assigns 6 colors to specific ranges of pixel

1250   intensity values and low intensity pixels are shown in red color. As compared to the control treatment,

1251   the poly(I:C) treatment results in an enrichment of red color pixels in the periphery of the cells.

1252   Highlighted regions of interest (ROI) are further analyzed in **(C)** and **(D)**. Scale bar, 50 µm. **(B)**

1253   Histograms showing the number of pixels for each of the 65536 tonal values stored in the 16-bit "6

1254   shades" LUT images. As compared to the control image histogram, the poly(I:C) image histogram

1255   shows an increased number of "red" pixel values. **(C)** and **(D)** Surface plot and histogram analysis of

1256   the ROIs shown in **(A)**. As compared to the surface plots of the control image ROIs, the surface plots

1257   of ROIs within the poly(I:C) image indicate a strong accumulation of B2:GFP along the periphery of

1258   the cells. This is also indicated by the corresponding histograms indicating the increased amount of

1259   red, low intensity B2:GFP pixels in the poly(I:C) ROIs as compared to the control ROIs. These

1260   observations have been confirmed by analyzing 8 images per treatment.

1261

1262   **Figure 10. Virus infection facilitated by virus-encoded effector proteins.** (**A**) and (**B**) Suppression

1263   of PTI by MP. (**A**) Perception of dsRNA produced in cortical ER-associated VRCs at the PM by an

1264   unknown cytoplasmic or membrane-associated pathogen recognition receptor (PRR) and the SERK1

1265   co-receptor (with potential contribution by one or more other co-receptors) triggers a signaling

1266   pathway leading to callose deposition and PD closure. dsRNA produced during infection may require

1267   secretion into the apoplasm to allow perception at the PM (dashed blue lines and arrows). Externally

1268   applied poly(I:C) may be perceived from the apoplasm or secreted upon initial uptake by the cells

1269   (dashed gray lines and arrows). (**B**) MP suppresses dsRNA-triggered callose deposition and allows

1270   intercellular spread of the viral ribonucleoprotein complex (vRNP). The MP may interact with

1271   intracellular PTI signaling as indicated or interact with callose synthesizing or degrading enzymes at

1272   PD. The MP may also be secreted to inhibit dsRNA perception at the PM. (**C**) dsRNA triggers PTI

1273   and antiviral RNA silencing and both responses are suppressed by viral effector proteins to support

1274   virus propagation. Whereas MP acts in cells at the virus front to facilitate virus movement by blocking

1275   a dsRNA-induced callose defense response at PD, the VSR blocks dsRNA-induced antiviral RNA

1276   silencing in the center of infection sites to support virus replication and production of virus progeny.

1277   A local infection site of TMV encoding MP fused to GFP (TMV-MP:GFP, 7 dpi) in *N. benthamiana*

1278   is shown. Scale bar, 1 mm.

1279

1280   **Supplemental Data**

1281

1282   **Table S1:** Primers used for RT-qPCR.

1283

1284   **Figure S1:** Development of TMV-GFP infection sites in *N. benthamiana* treated with water,

1285   poly(I:C), or flg22. Poly(I:C) and, to some extent, also flg22 treatment delays virus movement.

1286   Infection sites in leaves treated with poly(I:C) are smaller, and the rate by which these infection sites

1287   increase their size is lower than in infection sites in leaves treated with either water (control) or flg22

1288   (supports **Figure 1A** and **B**).

1289

1290

1291
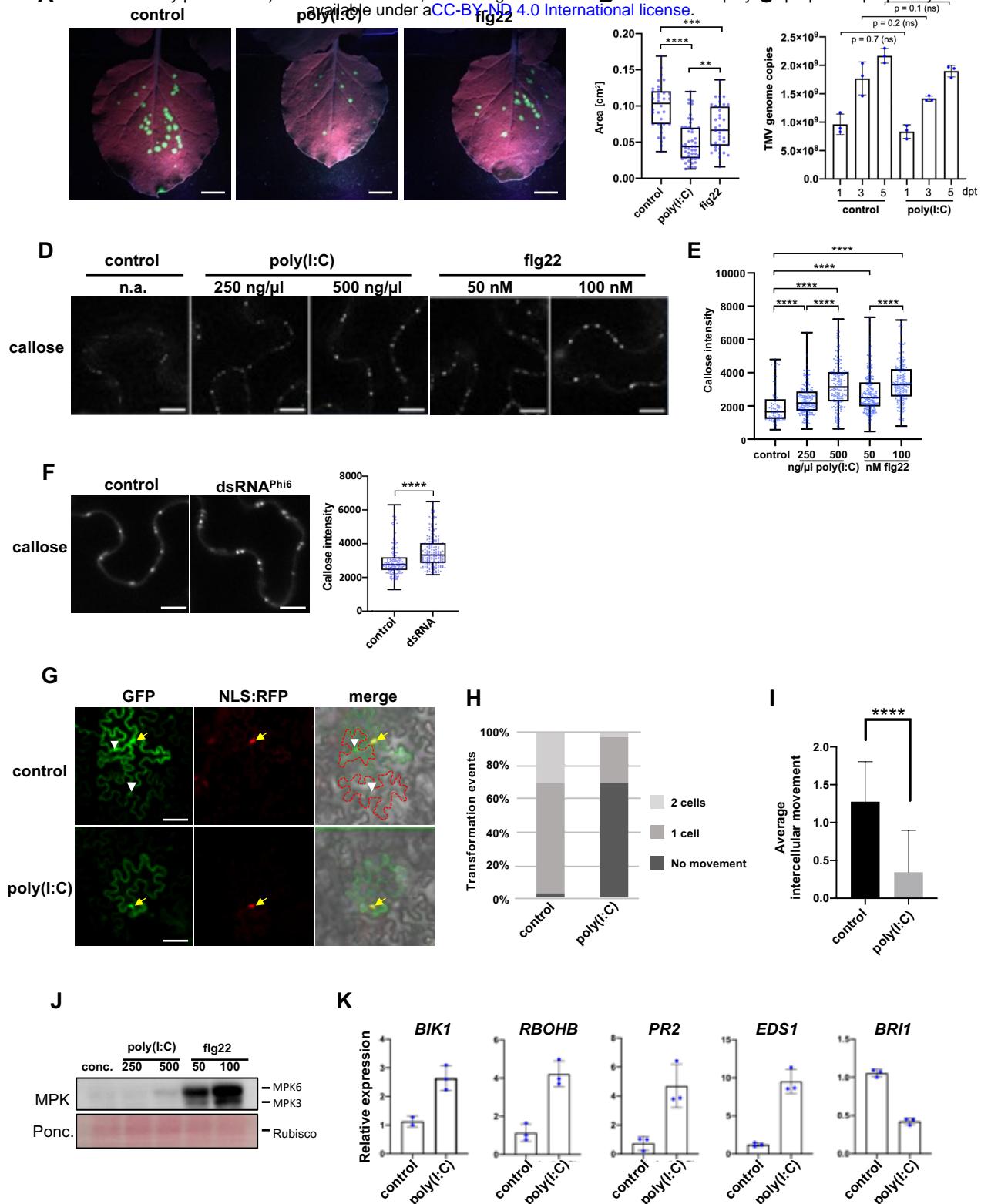
Figure 1. Poly(I:C) treatment causes inhibition of virus movement in *N. benthamiana*. (**A**) TMV-GFP infection sites in *N. benthamiana* leaves at 7 days post inoculation (dpi) with the virus together with either water (control), 0.5 μg/μl (≈1 μM) poly(I:C), or 1 μM flg22. Scale bar, 1 cm. (**B**) Sizes of individual infection sites measured in 10 leaf samples collected from three plants per treatment. Two-tailed Mann-Whitney test; ****, p <0.0001; ***, p <0.001; **, p <0.01. The experiment was performed three times with similar results. (**C**) TMV replication in *N. benthamiana* is not influenced by poly(I:C). A cell-autonomous, MP-deficient TMV replicon (TMVΔMΔC-GFP) expressed in cells of agroinoculated leaves produces the same number of RNA genome copies in the presence and absence of treatment with 0.5 μM poly(I:C), as determined by Taqman RT-qPCR. Poly(I:C) and control treatments were applied 1 day after agroinoculation and results obtained at indicated days after this treatment (dpt) are shown. The data represent means of three biological replicates (with SD) per time point and treatment. Two-tailed Mann-Whitney test. ns, not significant. (**D**) and (**E**) Treatment of *N.*

manner. (**D**) Callose fluorescence at PD upon poly(I:C) or flg22 treatment. Scale bar, 4 μm. (**E**) Relative callose content in individual PD (blue dots, n > 100) as determined in three leaf discs per treatment. Two-tailed Mann-Whitney test; ****, p = <0.0001. (**F**) Callose deposition at PD in *N. benthamiana* leaf epidermal tissue 30 minutes after treatment with 50 ng/μl biological dsRNA (dsRNA^{Phi6}). Relative callose content in individual PD (blue dots, n > 100) as determined in three leaf discs per treatment. Two-tailed Mann-Whitney test; ****, p = <0.0001. (**G-I**) GFP mobility assay in *N. benthamiana*. Leaf disks expressing GFP together with cell-autonomous NLS:RFP one day after agroinfiltration were treated with water or 0.5 μg/μl poly(I:C) and imaged 48 hours later. (**G**) Example of GFP movement from an epidermal cell marked by cell-autonomous NLS:RFP into adjacent cells. Transiently expressed GFP shows a nucleocytoplasmic distribution (yellow arrow) and its movement from the expressing epidermal cell (co-expressed NLS:RFP in the nucleus, in red) is evident by appearance of green fluorescence in the nuclei and cytoplasm of adjacent cells (white arrowheads). Cells into which GFP moved are indicated by the red dashed line in the merged image. Scale bar, 50 μm. (**H** and **I**) Quantification of GFP movement between epidermal cells in leaf disks exposed to 0.5 μg/μl poly(I:C) or water (control) (29 transformation events were analyzed for each treatment). (**H**) Stacked column diagram showing the relative frequency of transformation events associated with either no GFP movement (dark grey), GFP movement into one adjacent cell layer (medium grey), or GFP movement into two adjacent cell layers (light grey). (**I**) Average intercellular movement (total number of cell layers into which GFP has moved divided by the number of evaluated transformation events). Two-tailed Mann-Whitney test; ****, p = <0.0001. A repetition of the GFP mobility assay provided similar results. (**J**) Low level of MPK activation by poly(I:C) relative to flg22 after 30 minutes. Concentrations (conc.) are in ng/μl for poly(I:C) and in nM for flg22. The experiment was performed three times with similar results. (**K**) Poly(I:C) induces innate immunity marker genes, but suppresses expression of *BRI1*, in *N. benthamiana*. Mean value and SD of gene expression values obtained by RT-qPCR with three biological replicates (blue dots) harvested three hours after treatment.
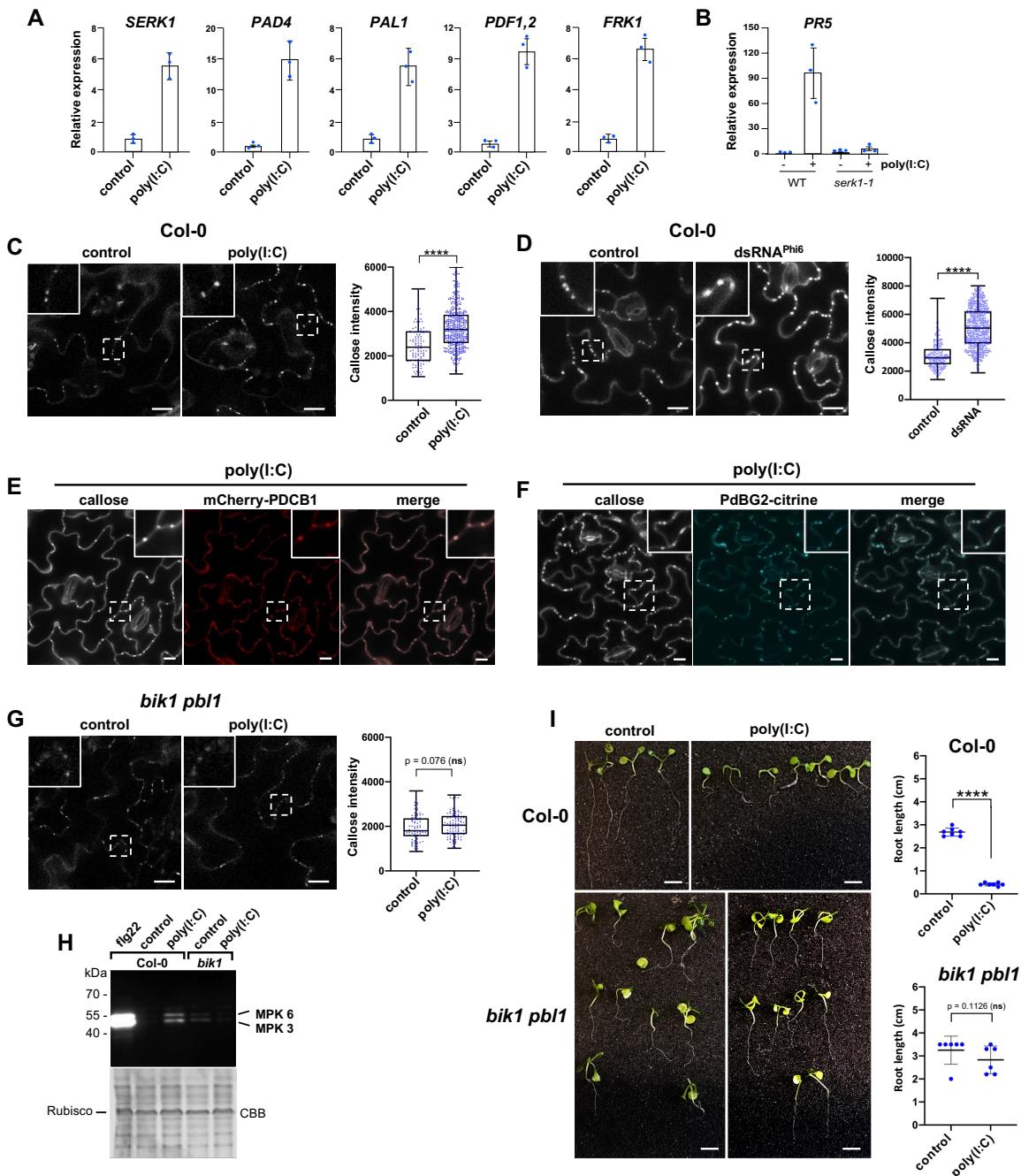
Figure 2. Poly(I:C)-induced signaling in Arabidopsis depends on BIK1/PBL1. (A) and (**B**) Transcriptional regulation of Arabidopsis genes three hours after treatment with 0.5 µg/µl poly(I:C). For each gene, the mean value and the SD of gene expression values obtained by RT-qPCR analysis of three biological replicates (blue dots) is shown. (**A**) Poly(I:C) induces innate immunity marker genes in *A. thaliana* Col-0 wildtype. (**B**) Absence of poly(I:C)-induced *PR5* expression in the *serk1-1* mutant. (**C**) Poly(I:C) treatment causes callose deposition at PD in *A. thaliana* Col-0. Images were taken 30 minutes after treatment. Inlays show enlargements of the areas within the dashed boxes. Scale bar, 20 µm. Relative callose content in individual PD (blue dots, n > 100) as determined in three leaf discs from three plants per treatment. Two-tailed Mann-Whitney test; ****, p = <0.0001. (**D**) Callose deposition at PD in *A. thaliana* Col-0 leaf epidermal tissue 30 minutes after treatment with 50 ng/µl of biological dsRNA (dsRNA^{Phi6}). Inlays show enlargements of the areas within the dashed boxes. Scale bar, 20 µm. Relative callose content in individual PD (blue dots, n > 100) as determined in three leaf discs per treatment. Two-tailed Mann-Whitney test; ****, p = <0.0001. (**E**) and (**F**) Poly(I:C)-induced callose spots are localized to PD as shown by co-localization with PD markers mCherry-PDCB1 (**E**) and PdBG2-citrine (**F**). Inlays show enlargements of the areas within the dashed boxes. Scale bar, 10 µm. (**G**) poly(I:C)-induced callose deposition in PD is inhibited in the *bik1 pbl1* mutant. Images were taken 30 minutes after treatment and the WT control of the same experiments is shown in (**C**). Inlays show enlargements of the areas within the dashed boxes. Scale bar, 20 µm. Relative callose content in individual PD (blue dots) as determined in three leaf discs per treatment. Two-tailed Mann-Whitney test; ns, non-significant. (**H**) Poly(I:C)-induced MPK activation is reduced in the *bik1 pbl1* mutant. Immunoblot detection of phosphorylated MPK. Samples were harvested 30 minutes after treatment with 0.5 µg/µl poly(I:C), 1 µM flg22, or water. "*bik1*" stands for *bik1 pbl1*.

CBB, Coomassie brilliant blue-stained gel showing staining of ribulose-bisphosphate-carboxylase (Rubisco) as gel loading control. (**I**) *bik1 pbl1* plants do not show significant seedling root growth inhibition in the presence of poly(I:C) as compared to WT Col-0 plants. Seedlings were kept for 12 days in 0.5 µg/µl poly(I:C) or water. Scale bar, 1 cm. Quantification of poly(I:C)-induced root growth inhibition in *A. thaliana* WT Col-0 and *bik1 pbl1* seedlings. Analysis of 6-7 seedlings (blue dots) per condition. Two-tailed Mann-Whitney test; ****, $p < 0.0001$; ns, non-significant.
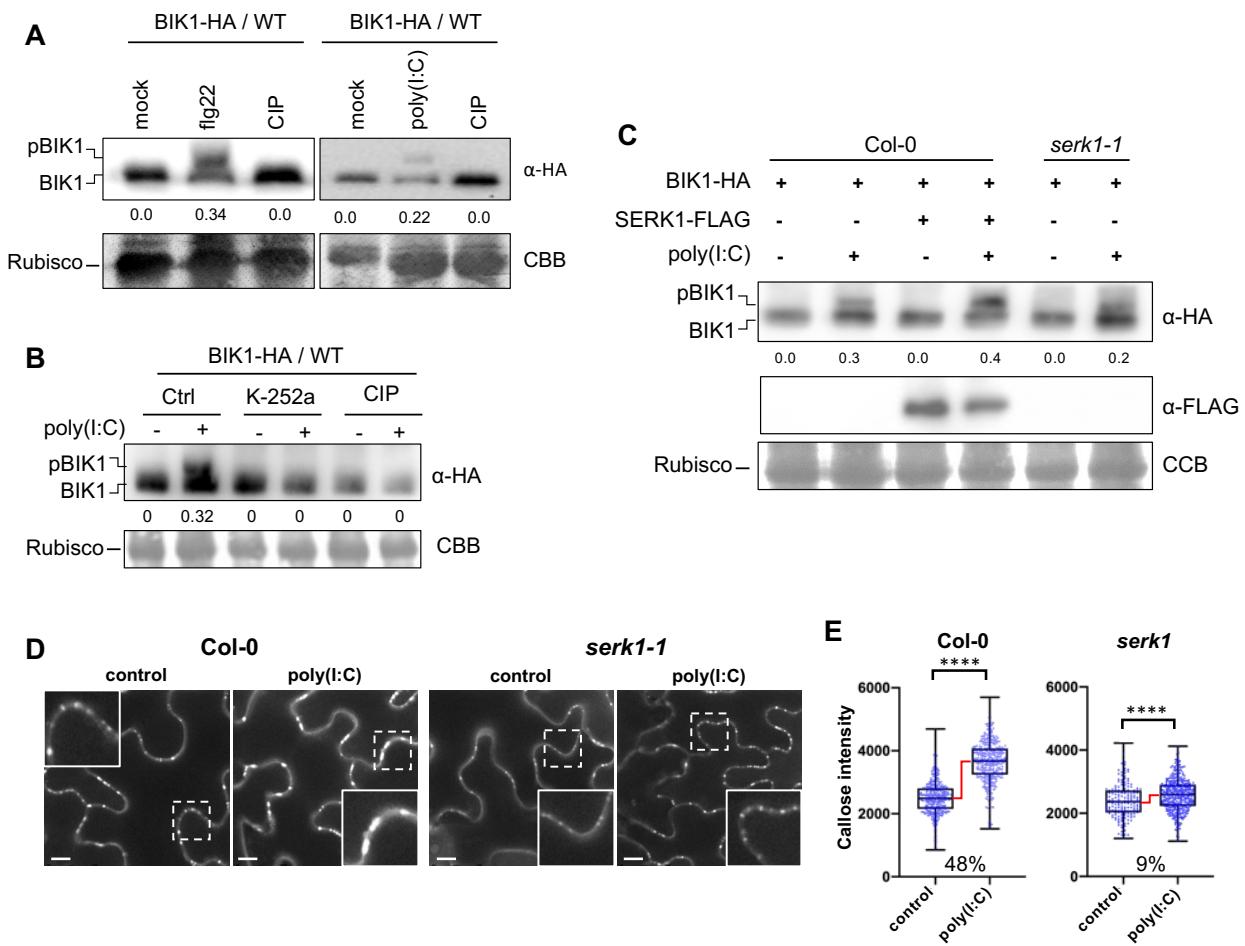
Figure 3. Poly(I:C) causes BIK1 phosphorylation and PD callose deposition in a SERK1-dependent manner. (**A**) to (**C**) Analysis if BIK1 phosphorylation in poly(I:C)-treated *A. thaliana* Col-0 protoplasts. (**A**) Poly(I:C) treatment induces BIK1 phosphorylation as shown by a protein mobility shift detected by Western blot analysis. Protoplasts expressing BIK1-HA were non-treated (mock) or treated with 1 μM flg22 or 0.5 μg/μl poly(I:C), lysed after 20 minutes and treated or non-treated with calf intestine phosphatase (CIP) for 60 before Western blot analysis using HA-HRP antibody. BIK1 band intensities were quantified using Image Lab (Bio-Rad). Quantification of BIK1 phosphorylation (upper panel) calculated as ratio of intensity of the upper band (phosphorylated BIK1, pBIK1) to the sum intensities of shifted and non-shifted bands (pBIK1 + BIK1) (no treatment set to 0.0). CCB, Coomassie brilliant blue staining of Rubisco as gel loading control (lower panel). (**B**) Poly(I:C)-induced BIK1 phosphorylation is blocked by 1 μM of the kinase inhibitor K-252a added 1 hour before poly(I:C) treatment. Rubisco detection by CBB staining is shown as gel loading control (lower panel). Experimental conditions and quantification of BIK1 phosphorylation as in (**A**). (**C**) SERK1 enhances poly(I:C)-induced BIK1 phosphorylation. Protoplasts from WT Col-0 or *serk1-1* mutants were transfected with BIK1-HA together with or without SERK1-FLAG and followed by treatment with or without 0.5 μg/μl poly(I:C). Phosphorylated BIK1 band intensities were quantified as in (**A**). The middle panel shows SERK1-FLAG expression. Rubisco detection by CBB staining is shown as gel loading control (lower panel). (**D**) and (**E**) Poly(I:C)-induced PD callose deposition depends on SERK1. (**D**) Callose fluorescence at PD seen upon aniline blue staining of epidermal cells of WT Col-0 plants and *serk1-1* mutants treated with water (control) or 0.5 μg/μl poly(I:C). Inlays show enlargements of the areas within the dashed boxes. Scale bar, 10 μm. (**E**) Relative callose content (fluorescence intensity) in individual PD (blue dots, n > 100) as determined in three leaf discs taken from three plants per treatment. Two-tailed Mann-Whitney test; ****, p = < 0.0001. The increase in PD callose levels in poly(I:C)-treated samples relative to water control-treated samples is shown in percent (%). Although the callose intensity data distributions between poly(I:C)-treated and control-treated samples are significantly different in both WT Col-0 and *serk1*, the comparison of the callose intensity median levels indicate a drastic inhibition of the poly(I:C)-induced PD callose deposition response in *serk1* as compared to the WT.
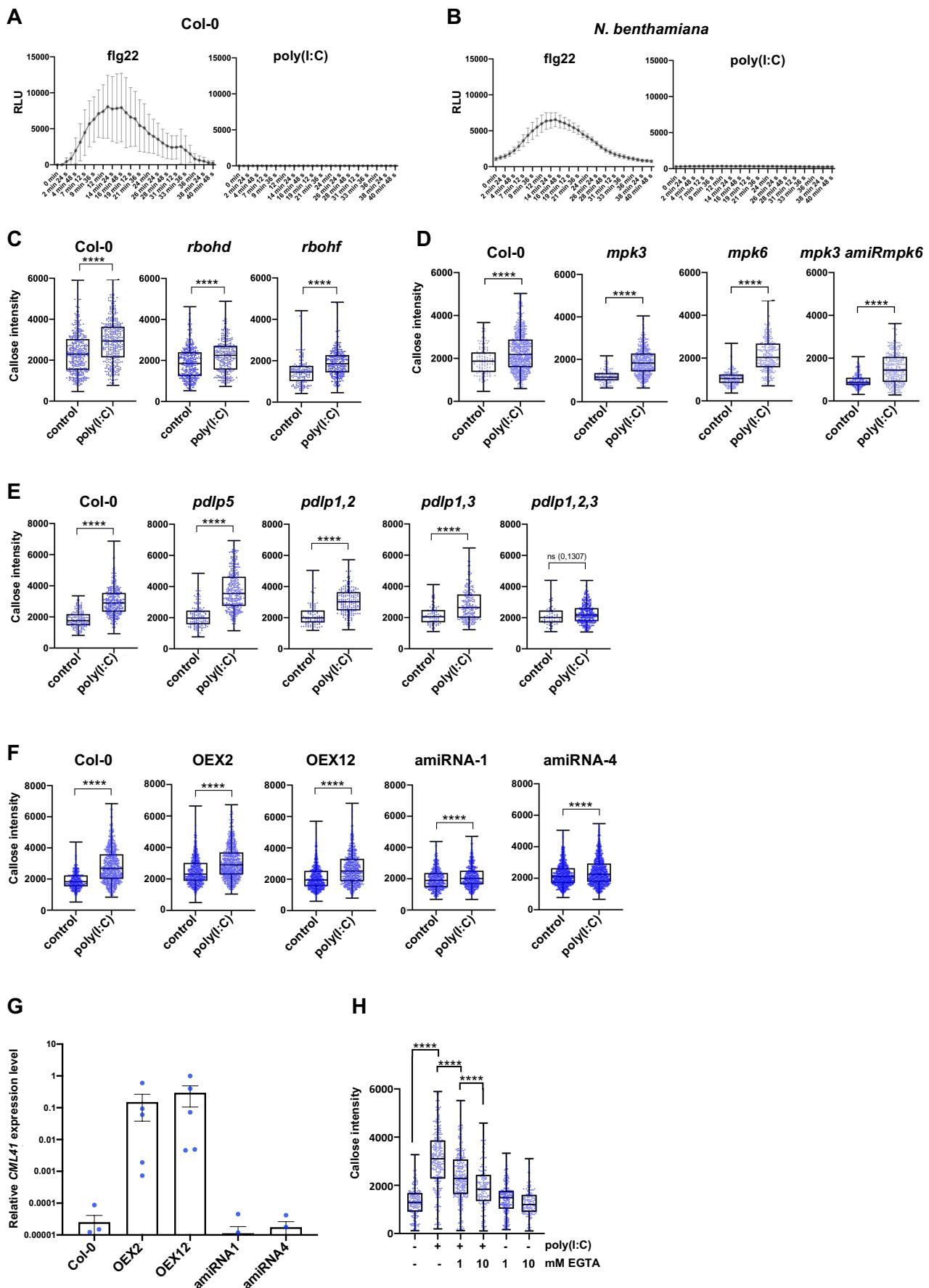
Figure 4. poly(I:C)-induced PD callose deposition is ROS- and MPK3/6 cascade-independent but requires PDLP1/2/3 and CML41. (**A**) and (**B**) Unlike treatment with 1 μM flg22, the treatment with 0.5 μg/μl poly(I:C) does not induce any ROS production in Arabidopsis (**A**) or *N. benthamiana* (**B**). RLU, relative luminescence units. Mean values (black dots) and error bars (SD) obtained for each time point for 10 replicates (leaf disks) per treatment. (**C**) Poly(I:C)-induced callose deposition at PD is not affected in *rbohd* or *rbohf* mutants. Relative callose content in individual PD (blue dots, n > 100) 30 minutes after treatment with 0.5 μg/μl poly(I:C) or water and determined in three leaf discs from three

plants per treatment. Two-tailed Mann-Whitney test; ****, p = <0.0001. (**D**) Poly(I:C)-induced callose deposition at PD is not affected in *mpk3* and *mpk6* single mutants, and neither in a *mpk3* mutant in which *MPK6* is silenced by an artificial miRNA (*mpk3 amiRmpk6*). Relative callose content in individual PD (blue dots, n > 100) 30 minutes after treatment with 0.5 µg/µl poly(I:C) or water and determined in three leaf discs from three plants per treatment. Two-tailed Mann-Whitney test; ****, p = <0.0001. (**E**) poly(I:C)-induced callose deposition at PD is independent of PDLP5 but depends on the redundantly acting PDLP1, PDLP2, and PDLP3. Relative callose content in individual PD (blue dots, n > 100) 30 minutes after treatment with 0.5 µg/µl poly(I:C) or water and determined in three leaf discs from three plants per treatment. Two-tailed Mann-Whitney test; ****, p = <0.0001; ns, non-significant. (**F**) and (**G**) Poly(I:C)-induced callose deposition at PD depends on CML41. (**F**) PD callose deposition levels in poly(I:C)-treated and control-treated leaf disks of two *CML41*-overexpressing lines (OEX2 and OEX12) and of two lines in which the expression of *CML41* is reduced by expression of artificial miRNA (amiRNA1 and amiRNA4). As compared to the WT (Col-0) and the *CML41*-overexpressing lines, the inducibility of PD callose deposition by poly(I:C) is strongly decreased in the amiRNA lines. Relative callose content in individual PD (blue dots, n > 100) 30 minutes after treatment with 0.5 µg/µl poly(I:C) or water and determined in three leaf discs from three plants per treatment. Two-tailed Mann-Whitney test; ****, p = <0.0001. According to the Mann-Whitney test the distribution of individual PD callose intensities is different between all control- and poly(I:C)-treated samples. However, unlike in WT Col-0 and *CML41*-overexpressing lines, the median PD callose intensity levels are not increased upon poly(I:C)-treatment in amiRNA lines thus indicating a deficiency in the induction of PD callose deposition upon poly(I:C) treatment in these lines. (**G**) Relative levels of *CML41* expression in plants of the OEX2, OEX12, amiRNA1 and amiRNA4 lines in comparison to WT (Col-0), as determined by RT-qPCR. Mean value and standard error of gene expression values obtained by RT-qPCR with 3-6 biological replicates (blue dots). (**H**) poly(I:C)-induced callose deposition is reduced in the presence of EGTA. Relative callose content in individual PD (blue dots, n > 100) as determined in three leaf discs per treatment. Two-tailed Mann-Whitney test; ****, p = <0.0001.
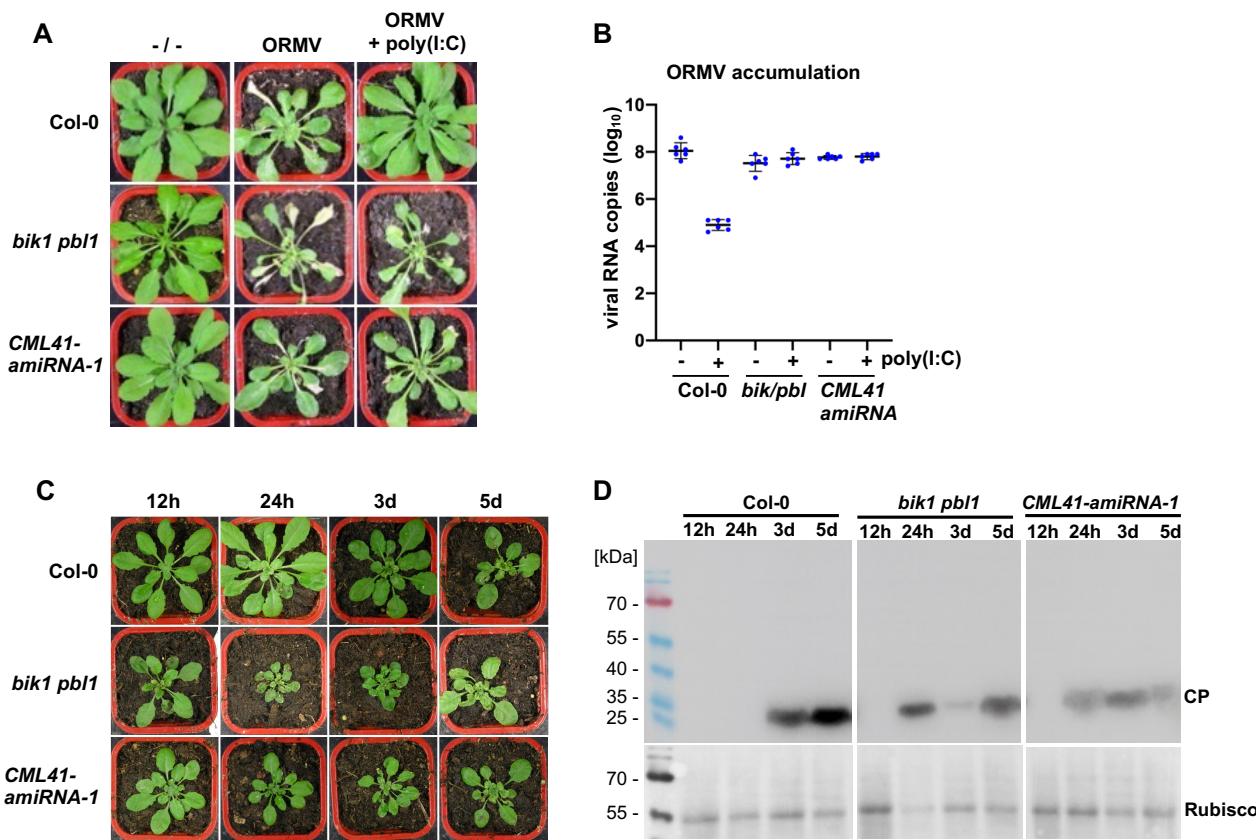
Figure 5. BIK1/PBL1 and CML41 are required for antiviral defense (**A**) and (**B**) Disease symptoms (**A**) and viral RNA accumulation (**B**) at 28 dpi in wild-type plants and mutants inoculated with ORMV in the presence and absence of 0.5 µg/µl poly(I:C). Unlike in wild-type plants (Col-0) the antiviral effect of poly(I:C) treatment is lost in *bik1 pbl1* mutants and *CML41-amiRNA-1* expressing plants. Viral RNA accumulation (**B**) is depicted for 6 biological replicates per condition. Mean values and standard errors are shown. (**C**) and (**D**) BIK1 and CML41 inhibit virus movement. (**C**) Representative symptom phenotypes at 21 dpi of Arabidopsis Col-0 plants, *bik1 pbl1* mutant plants and plants transgenic for *CML41-amiRNA-1* that were locally inoculated with ORMV and from which the inoculated leaves were removed at the indicated times in hours (h) and days (d). Whereas systemic leaves of Col-0 plants show symptoms on plants that carried the inoculated leaves for 3 or more days following inoculation, the systemic leaves of the *bik1 pbl1* mutant and of the CML41-amiRNA-expressing plants show symptoms already if the inoculated leaves were present for only 24 hours. (**D**) Immunoblot analysis of the youngest systemic leaves at 21 dpi using antibodies against viral coat protein (CP) (*Youcai mosaic virus* antibody, AS-0527, DSMZ, Braunschweig, Germany). The pattern of CP expression in the systemic leaves confirms that in WT Col-0 plants the virus needs between 24 h and 3 d to exit the inoculated leaves and move systemically, whereas the time needed for systemic movement is reduced to less than 24 h in the *bik1 pbl1* mutant and of the CML41-amiRNA expressing plants, thus indicating a role of BIK1 and CML41 in restricting virus movement.
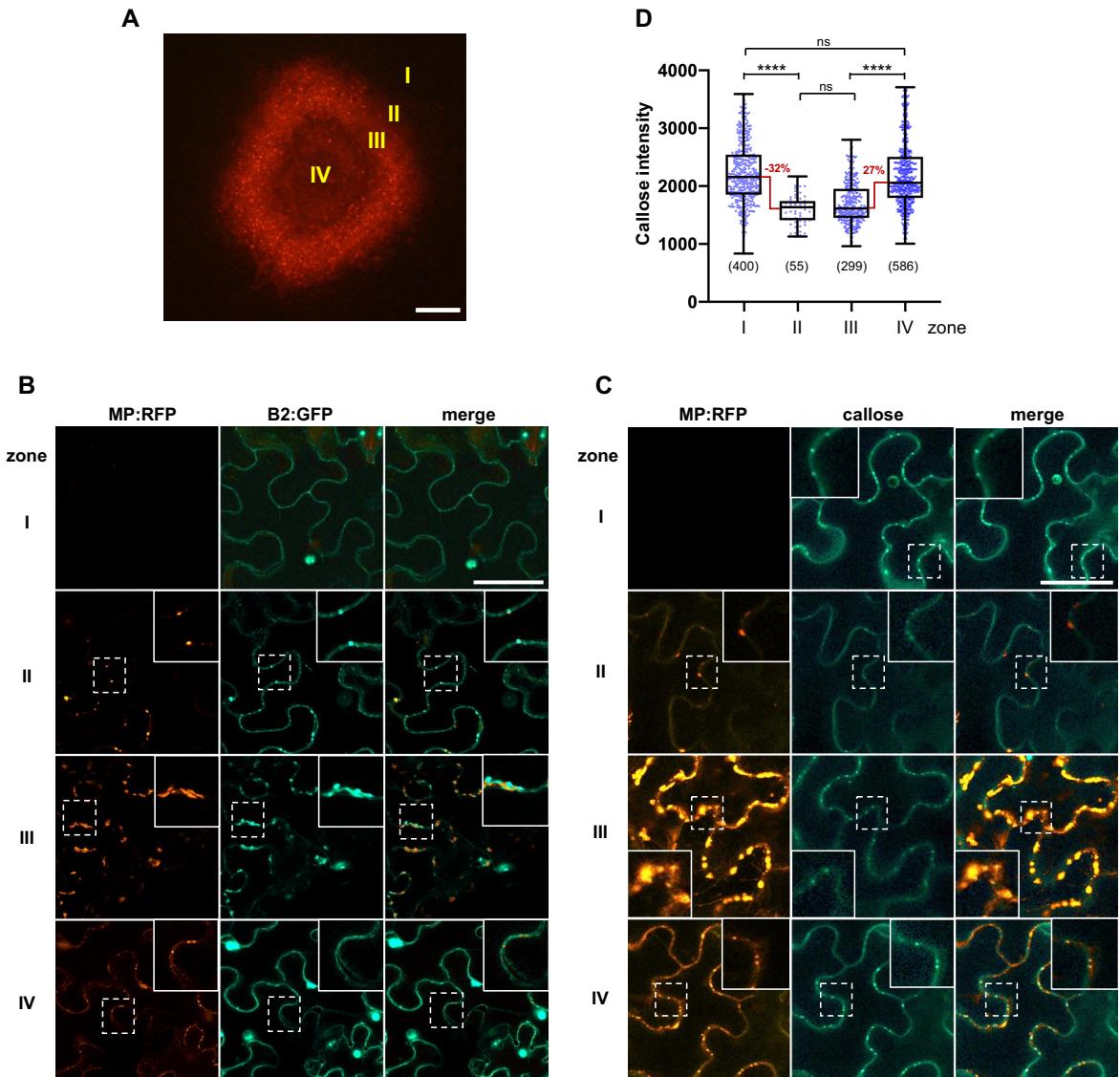
Figure 6. Viral MP expression correlates with a suppression of PD-associated callose levels. (A) Local site of infection by TMV-MP:RFP (at 4 dpi) in *N. benthamiana*. Different zones ahead of infection (zone 1), at the infection front (zone II), behind the infection front (zone III) and in the center of infection (zone IV) are indicated. Scale bar, 200 μm. **(B)** Viral dsRNA accumulation in the different zones of local TMV infection. Inlay images show magnifications of image areas framed by a dashed line. Scale bar, 20 μm. The MP of TMV is tagged with RFP (MP:RFP) and the accumulating dsRNA is imaged through binding of the *Flock house virus* B2 protein fused to GFP (B2:GFP). In cells of zone I (non-infected cells ahead of infection) B2:GFP shows a nucleo-cytoplasmic distribution, which is the typical distribution of this protein in the absence of dsRNA (Monsion et al., 2018). In cells at the virus front (zone II), B2:GFP co-localizes to MP:RFP to spots at the cell wall (likely at PD) indicating the localization of early virus-replication complexes (VRCs) engaged in virus replication and virus movement. In zone III, the VRCs have grown in size and accumulate high amounts of dsRNA consistent with high levels of virus replication to produce virus progeny. In zone IV, the MP is no longer expressed but residual MP:RFP is still seen in PD. The B2:GFP-tagged VRCs now appear rounded. **(C)** Pattern of MP:RFP and callose accumulation in the different zones. Inlays show magnifications of the image areas highlighted by dashed boxes. Scale bar, 40 μm. In zone II, where MP localizes to PD to facilitate virus movement, and to some extend also still in zone III, the PD-associated callose levels are decreased as compared to the other zones. **(D)** Quantification of PD callose in the different zones. The number of analyzed PD is shown in brackets. Two-tailed Mann-Whitney test; ****, p < 0.0001; ns, p > 0.05.
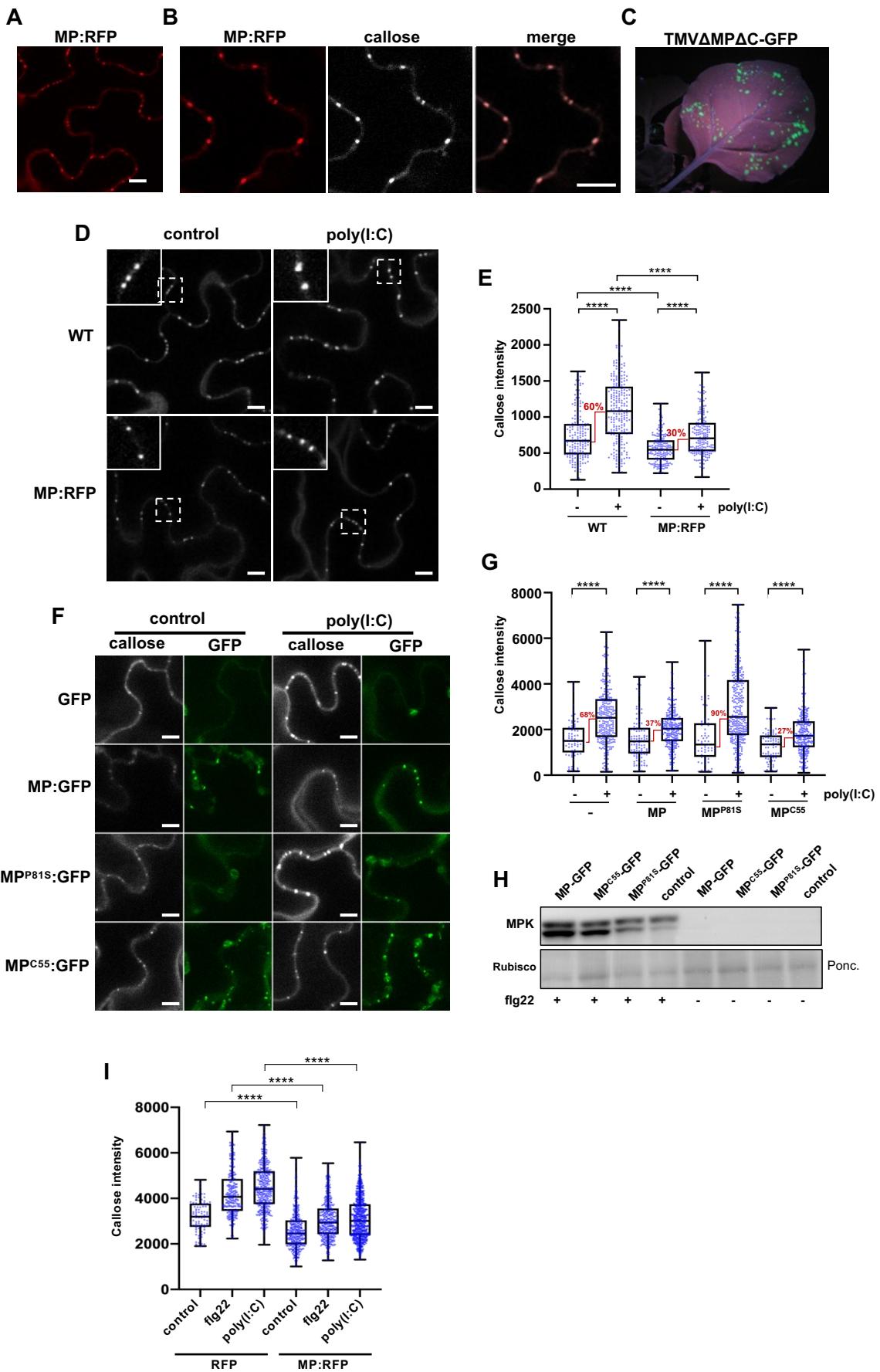
Figure 7. Suppression of poly(I:C)-induced immunity by MP. (**A-E**) Inhibition of dsRNA-induced callose deposition in MP:RFP-transgenic *N. benthamiana* plants. (**A-C**) MP:RFP is functional. (**A**) Transgenically expressed MP:RFP localizes to distinct locations at the cell wall. Scale bar, 10 μm. (**B**) The MP:RFP localizes to PD as revealed by callose

staining with aniline blue. Scale bar, 10 μm. (**C**) The stably expressed MP:RFP in this line is functional and complements infection upon inoculation with *in vitro* transcribed infectious RNA of the MP-deficient TMVΔMΔC-GFP (Vogler et al., 2008), as can be seen by the occurrence of distinct GFP fluorescent infection sites at 7 dpi. (**D**) and (**E**) Inhibition of dsRNA-induced callose deposition in MP:RFP-transgenic plants. (**D**) Leaf epidermal cells of non-transgenic (WT) and MP:RFP-transgenic plants *N. benthamiana* stained with aniline blue. Inlay images show magnifications of image areas framed by a dashed line. Scale bar, 10 μm. Treatment of leaf tissues with 0.5 μg/μl poly(I:C) for 30 minutes causes a stronger increase in the level of PD-associated callose in WT plants than in MP:RFP-transgenic plants. (**E**) Quantification of callose in leaf epidermal cells upon aniline blue staining. Relative callose content in individual PD (blue dots, n > 100) as determined in three leaf discs from three plants per treatment. Two-tailed Mann-Whitney test; ****, $p < 0.0001$. (**F**) and (**G**) Inhibition of poly(I:C)-induced PD callose deposition by transiently expressed MP:GFP. Leaf disks excised from the GFP, MP:GFP, MP^{P81S}:GFP or MP^{C55}:GFP-expressing leaves 48h after agroinfiltration were incubated for one day in water, then transferred into aniline blue solution with and without 0.5 μg/μl poly(I:C) and imaged after 30 minutes. (**F**) Images of leaf epidermal cells stained for callose with aniline blue (callose) and corresponding images of the same cell area with GFP fluorescence are shown. The ability of MP:GFP to reduce the poly(I:C) induction of callose deposition at PD is inhibited by a single amino acid exchange mutation in MP (P81S) previously shown to affect its ability to efficiently target PD and to function in virus movement. Functional MP with a C-terminal deletion of 55 amino acids (C55) that targets PD also inhibits poly(I:C)-induced callose deposition like wildtype MP. (**G**) Quantification of PD-associated callose levels in leaf epidermal cells upon aniline blue staining. Leaf disks from three plants per condition were analyzed. Two-tailed Mann-Whitney test; ****, $p < 0.0001$. (**H**) Western blot showing that the expression of wild type or mutant MP:GFP does not interfere with flg22-induced MPK activation. Ponc., Ponceau S-stained Western blot membrane. (**I**) Inhibition of flg22- and poly(I:C)-induced PD callose deposition by MP:RFP as compared to RFP. Leaf disks excised from the RFP or MP:RFP-expressing leaves 48h after agroinfiltration were incubated for one day in water, then transferred into aniline blue solution with and without 0.5 μg/μl poly(I:C) and imaged after 30 minutes. Six leaf disks from two plants were evaluated for each condition. ****, $p < 0.0001$.
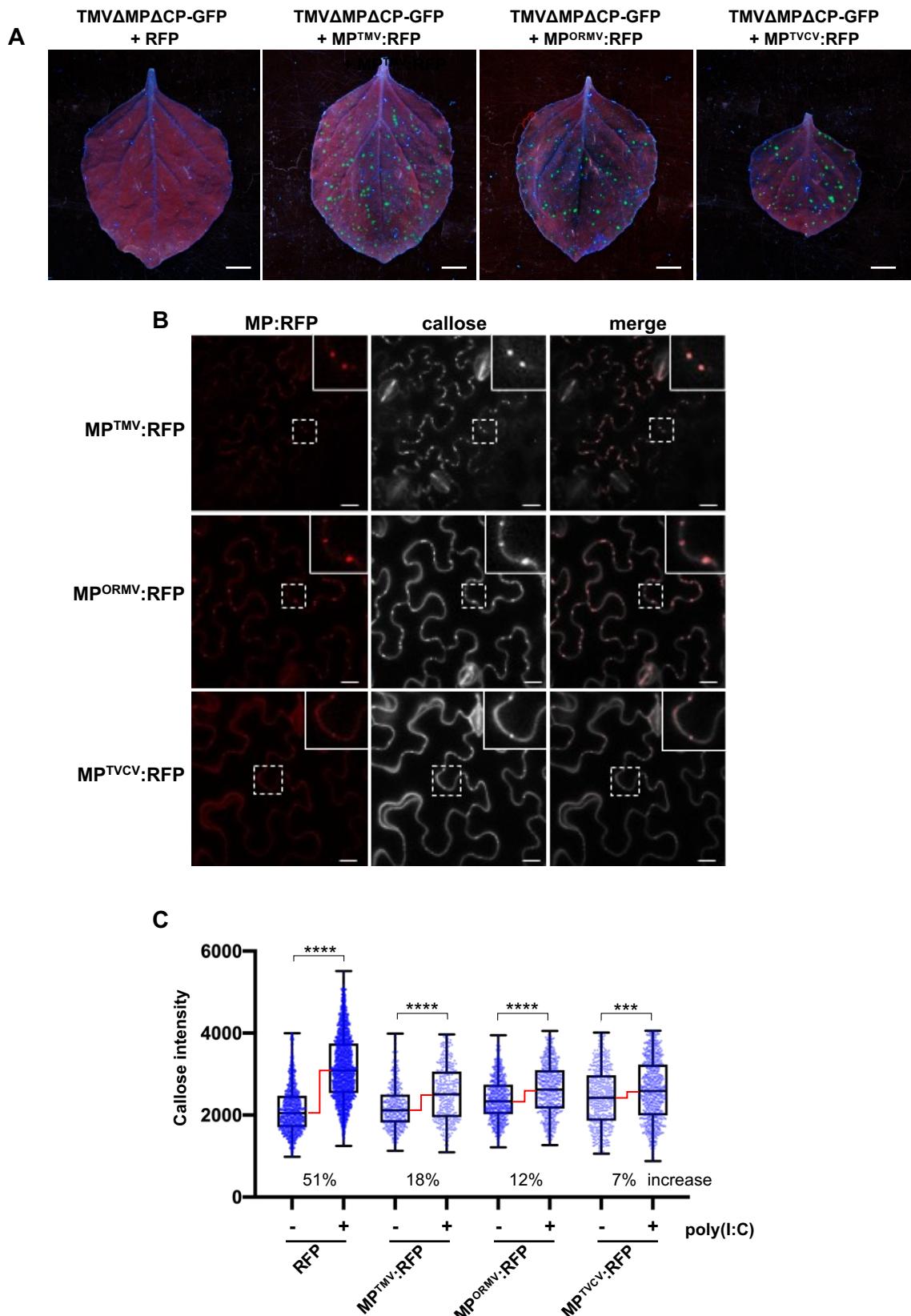
Figure 8. Inhibition of poly(I:C)-induced callose deposition by MPs of different viruses. (**A**) Different MPs are functional. Unlike free RFP, RFP fusions to the MPs of TMV (MP^{TMV}:RFP), ORMV (MP^{ORMV}:RFP), and TVCV (MP^{TVCV}:RFP) complement the movement function of MP-deficient TMVΔM-GFP in *N. benthamiana*. Leaves were co-infiltrated with agrobacteria containing the respective RFP or MP:RFP-encoding plasmids together with highly diluted agrobacteria (OD$_{600\ nm}$ = 1 x 10^{-5}) for agro-inoculation with TMVΔMP-GFP. Pictures were taken at 5 dpi. Scale bar, 1 cm. (**B**) MP^{TMV}:RFP, MP^{ORMV}:RFP, and MP^{TVCV}:RFP localize to PD as shown by the presence of callose. MP-expressing leaves were stained with aniline blue and imaged after 30 minutes. Inlay images show magnifications of image areas framed by a dashed line. Scale bar, 20 μm. (**C**) Expression of either MP^{TMV}:RFP, MP^{ORMV}:RFP, or MP^{TVCV}:RFP strongly

reduces the induction of PD callose deposition in the presence of poly(I:C). Leaf disks excised from the RFP (control) or MP:RFP-expressing leaves 48h after agroinfiltration were incubated for one day in water, then transferred into aniline blue solution with and without 0.5 µg/µl poly(I:C) and imaged after 30 minutes. For each treatment, three images of three leaf disks taken from three plants were analyzed for PD-associated callose levels. RFP data are combined data from the 27 leaf disks that were used as RFP control in the individual agroinfiltration experiments. The increase in poly(I:C)-induced PD-callose levels seen in the presence of poly(I:C) as compared to the water-treated control is shown in percent (%). Two-tailed Mann-Whitney test; ****, $p = <0.0001$; ***, $p = 0.0002$.
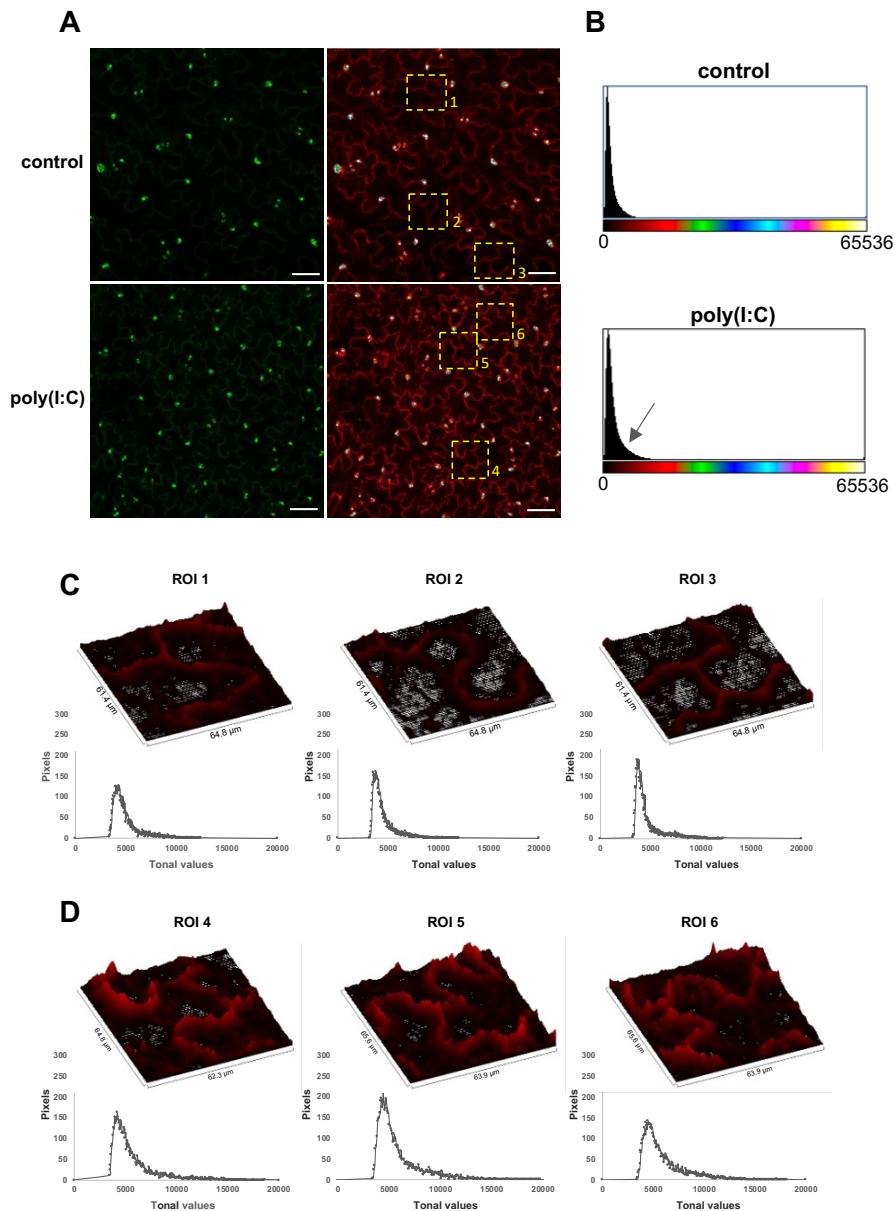
Figure 9. **Poly(I:C) enters plant cells. (A)** B2:GFP-transgenic *N. benthamiana* leaf tissue treated with water (control) or 0.5 µg/µl poly(I:C) and imaged with ImageJ "green" (left) and "6 shades" (right) color look-up tables (LUT). The "6 shades" LUT assigns 6 colors to specific ranges of pixel intensity values and low intensity pixels are shown in red color. As compared to the control treatment, the poly(I:C) treatment results in an enrichment of red color pixels in the periphery of the cells. Highlighted regions of interest (ROI) are further analyzed in **(C)** and **(D)**. Scale bar, 50 µm. **(B)** Histograms showing the number of pixels for each of the 65536 tonal values stored in the 16-bit "6 shades" LUT images. As compared to the control image histogram, the poly(I:C) image histogram shows an increased number of "red" pixel values. **(C)** and **(D)** Surface plot and histogram analysis of the ROIs shown in **(A)**. As compared to the surface plots of the control image ROIs, the surface plots of ROIs within the poly(I:C) image indicate a strong accumulation of B2:GFP along the periphery of the cells. This is also indicated by the corresponding histograms indicating the increased amount of red, low intensity B2:GFP pixels in the poly(I:C) ROIs as compared to the control ROIs. These observations have been confirmed by analyzing 8 images per treatment.
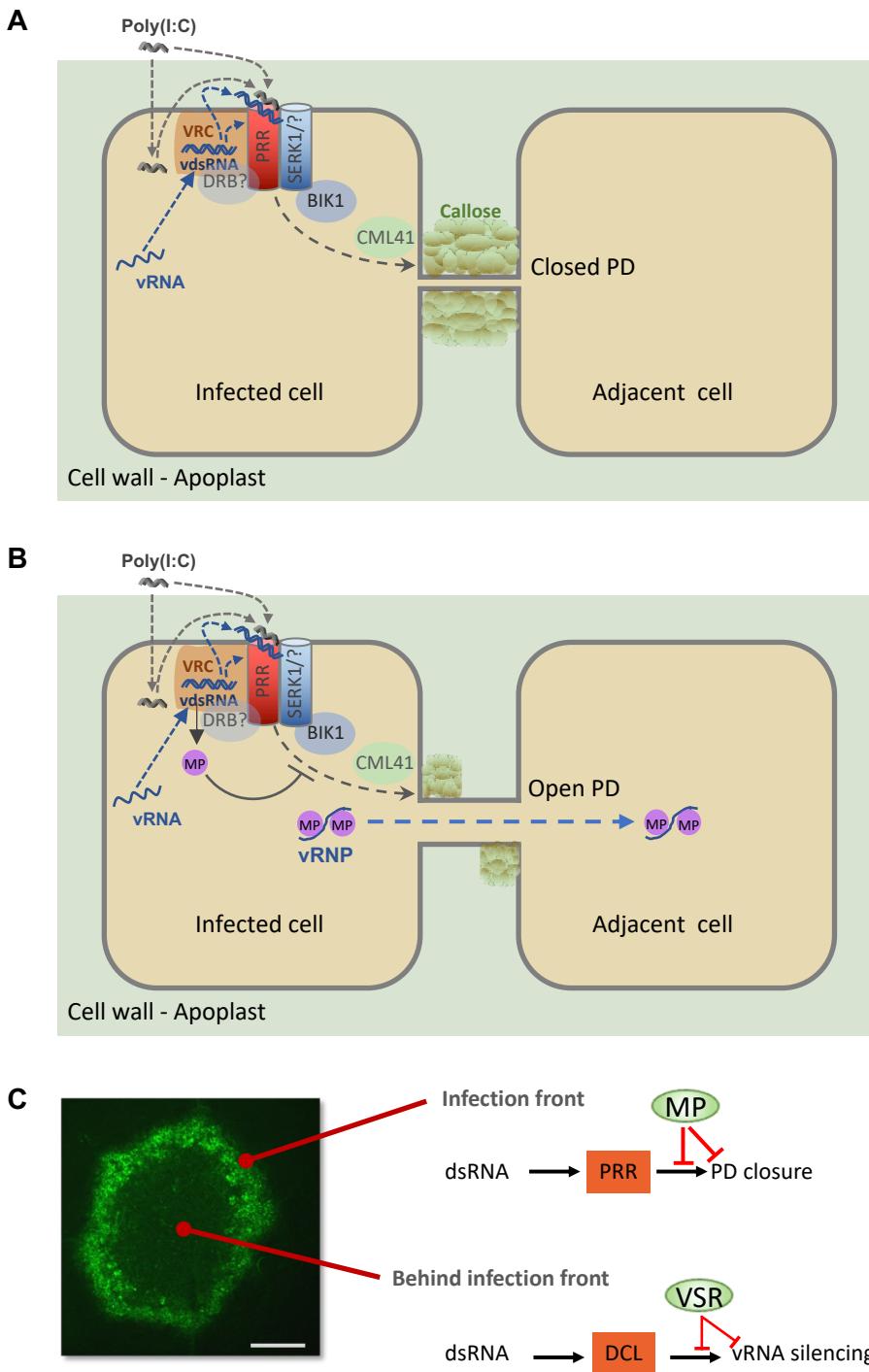
Figure 10. Virus infection facilitated by virus-encoded effector proteins. (**A**) and (**B**) Suppression of PTI by MP. (**A**) Perception of dsRNA produced in cortical ER-associated VRCs at the PM by an unknown cytoplasmic or membrane-associated pathogen recognition receptor (PRR) and the SERK1 co-receptor (with potential contribution by one or more other co-receptors) triggers a signaling pathway leading to callose deposition and PD closure. dsRNA produced during infection may require secretion into the apoplast to allow perception at the PM (dashed blue lines and arrows). Externally applied poly(I:C) may be perceived from the apoplasm or secreted upon initial uptake by the cells (dashed gray lines and arrows). (**B**) MP suppresses dsRNA-triggered callose deposition and allows intercellular spread of the viral ribonucleoprotein complex (vRNP). The MP may interact with intracellular PTI signaling as indicated or interact with callose synthesizing or degrading enzymes at PD. The MP may also be secreted to inhibit dsRNA perception at the PM. (**C**) dsRNA triggers PTI and antiviral RNA silencing and both responses are suppressed by viral effector proteins to support virus propagation. Whereas MP acts in cells at the virus front to facilitate virus movement by blocking a dsRNA-induced callose defense response at PD, the VSR blocks dsRNA-induced antiviral RNA silencing in the center of infection sites to support virus replication and production of virus progeny. A local infection site of TMV encoding MP fused to GFP (TMV-MP:GFP, 7 dpi) in *N. benthamiana* is shown. Scale bar, 1 mm.

Parsed Citations

Alexopoulou, L., Holt, A.C., Medzhitov, R., and Flavell, R.A. (2001). Recognition of double-stranded RNA and activation of NF-kappaB by Toll-like receptor 3. Nature 413, 732-738.
  Google Scholar: Author Only Title Only Author and Title

Amari, K., Boutant, E., Hofmann, C., Schmitt-Keichinger, C., Fernandez-Calvino, L., Didier, P., Lerich, A, Mutterer, J., Thomas, C.L., Heinlein, M., Mély, Y., Maule, A.J., and Ritzenthaler, C. (2010). A family of plasmodesmal proteins with receptor-like properties for plant viral movement proteins. PLoS Pathog 6, e1001119.
  Google Scholar: Author Only Title Only Author and Title

Ashby, J., Boutant, E., Seemanpillai, M., Groner, A, Sambade, A, Ritzenthaler, C., and Heinlein, M. (2006). Tobacco mosaic virus movement protein functions as a structural microtubule-associated protein. J Virol 80, 8329-8344.
  Google Scholar: Author Only Title Only Author and Title

Beffa, R.S., Hofer, R.M., Thomas, M., and Meins, F., Jr. (1996). Decreased susceptibility to viral disease of [beta]-1,3-glucanase-deficient plants generated by antisense transformation. Plant Cell 8, 1001-1011.
  Google Scholar: Author Only Title Only Author and Title

Benitez-Alfonso, Y., Faulkner, C., Pendle, A, Miyashima, S., Helariutta, Y., and Maule, A. (2013). Symplastic intercellular connectivity regulates lateral root patterning. Dev Cell 26, 136-147.
  Google Scholar: Author Only Title Only Author and Title

Borniego, M.B., Karlin, D., Pena, E.J., Robles Luna, G., and Garcia, M.L. (2016). Bioinformatic and mutational analysis of ophiovirus movement proteins, belonging to the 30K superfamily. Virology 498, 172-180.
  Google Scholar: Author Only Title Only Author and Title

Boutant, E., Didier, P., Niehl, A, Mely, Y., Ritzenthaler, C., and Heinlein, M. (2010). Fluorescent protein recruitment assay for demonstration and analysis of in vivo protein interactions in plant cells and its application to Tobacco mosaic virus movement protein. Plant J 62, 171-177.
  Google Scholar: Author Only Title Only Author and Title

Boyko, V., van der Laak, J., Ferralli, J., Suslova, E., Kwon, M.-O., and Heinlein, M. (2000). Cellular targets of functional and dysfunctional mutants of Tobacco mosaic virus movement protein fused to GFP. J. Virol. 74, 11339-11346.
  Google Scholar: Author Only Title Only Author and Title

Boyko, V., Ashby, J.A, Suslova, E., Ferralli, J., Sterthaus, O., Deom, C.M., and Heinlein, M. (2002). Intramolecular complementing mutations in tobacco mosaic virus movement protein confirm a role for microtubule association in viral RNA transport. J Virol 76, 3974-3980.
  Google Scholar: Author Only Title Only Author and Title

Brandner, K., Sambade, A, Boutant, E., Didier, P., Mély, Y., Ritzenthaler, C., and Heinlein, M. (2008). Tobacco mosaic virus movement protein interacts with green fluorescent protein-tagged microtubule end-binding protein 1. Plant Physiol 147, 611-623.
  Google Scholar: Author Only Title Only Author and Title

Brault, M.L., Petit, J.D., Immel, F., Nicolas, W.J., Glavier, M., Brocard, L., Gaston, A, Fouche, M., Hawkins, T.J., Crowet, J.M., Grison, M.S., Germain, V., Rocher, M., Kraner, M., Alva, V., Claverol, S., Paterlini, A, Helariutta, Y., Deleu, M., Lins, L., Tilsner, J., and Bayer, E.M. (2019). Multiple C2 domains and transmembrane region proteins (MCTPs) tether membranes at plasmodesmata. EMBO Rep 20, e47182.
  Google Scholar: Author Only Title Only Author and Title

Bucher, G.L., Tarina, C., Heinlein, M., Di Serio, F., Meins Jr., F., and Iglesias, V.A (2001). Local expression of enzymatically active class 1 beta-1,3-glucanase enhances symptoms of TMV infection in tobacco. Plant J. 28, 361-369.
  Google Scholar: Author Only Title Only Author and Title

Cai, Q., Qiao, L., Wang, M., He, B., Lin, F.-M., Palmquist, J., Huang, S.-D. and Jin, H. (2018). Plants send small RNAs in extracellular vesicles to fungal pathogen to silence virulence genes. Science 360, 1126.
  Google Scholar: Author Only Title Only Author and Title

Cai, Q., He, B., Wang, S., Fletcher, S., Niu, D., Mitter, N., Birch, P.R.J., Jin, H. (2021). Message in a bubble: shuttling small RNAs and proteins between cells and interacting organisms using extracellular vesicles. Annu Rev Plant Biol 72, 497-524.
  Google Scholar: Author Only Title Only Author and Title

Caillaud, M.C., Wirthmueller, L., Sklenar, J., Findlay, K., Piquerez, S.J., Jones, A.M., Robatzek, S., Jones, J.D., and Faulkner, C. (2014). The plasmodesmal protein PDLP1 localises to haustoria-associated membranes during downy mildew infection and regulates callose deposition. PLoS Pathog 10, e1004496.
  Google Scholar: Author Only Title Only Author and Title

Castro, B., Citterico, M., Kimura, S., Stevens, D.M., Wrzaczek, M., and Coaker, G. (2021). Stress-induced reactive oxygen species compartmentalization, perception and signalling. Nat Plants 7, 403-412.

Google Scholar: Author Only Title Only Author and Title

Chen, M.H., Shen, J., Hind, G., Handa, A.K., and Citovsky, V. (2000). Interaction between the tobacco mosaic virus movement protein and host cell pectin methylesterases is required for viral cell-to-cell movement. EMBO J 19, 913-920.
  Google Scholar: Author Only Title Only Author and Title

Cheval, C., and Faulkner, C. (2018). Plasmodesmal regulation during plant-pathogen interactions. New Phytol 217, 62-67.
  Google Scholar: Author Only Title Only Author and Title

Cheval, C., Samwald, S., Johnston, M.G., de Keijzer, J., Breakspear, A, Liu, X., Bellandi, A, Kadota, Y., Zipfel, C., and Faulkner, C. (2020). Chitin perception in plasmodesmata characterizes submembrane immune-signaling specificity in plants. Proc Natl Acad Sci U S A 117, 9621-9629.
  Google Scholar: Author Only Title Only Author and Title

Christensen, N., Tilsner, J., Bell, K., Hammann, P., Parton, R., Lacomme, C., and Oparka, K. (2009). The 5' cap of Tobacco mosaic virus (TMV) is required for virion attachment to the actin/endoplasmic reticulum network during early infection. Traffic 10, 536-551.
  Google Scholar: Author Only Title Only Author and Title

Citovsky, V. (1999). Tobacco mosaic virus: a pioneer of cell-to-cell movement. Philos Trans R Soc Lond B Biol Sci 354, 637-643.
  Google Scholar: Author Only Title Only Author and Title

Citovsky, V., Knorr, D., Schuster, G., and Zambryski, P. (1990). The P30 movement protein of Tobacco mosaic virus is a single-strand nucleic acid binding protein. Cell 60, 637-647.
  Google Scholar: Author Only Title Only Author and Title

Csorba, T., Kontra, L., and Burgyan, J. (2015). Viral silencing suppressors: Tools forged to fine-tune host-pathogen coexistence. Virology 479-480C, 85-103.
  Google Scholar: Author Only Title Only Author and Title

Czechowski, T., Stitt, M., Altmann, T., Udvardi, M.K., and Scheible, W.R. (2005). Genome-wide identification and testing of superior reference genes for transcript normalization in Arabidopsis. Plant Physiol 139, 5-17.
  Google Scholar: Author Only Title Only Author and Title

De Storme, N., and Geelen, D. (2014). Callose homeostasis at plasmodesmata: molecular regulators and developmental relevance. Front Plant Sci 5, 138.
  Google Scholar: Author Only Title Only Author and Title

DeFalco, T.A, and Zipfel, C. (2021). Molecular mechanisms of early plant pattern-triggered immune signaling. Mol Cell 81, 3449-3467.
  Google Scholar: Author Only Title Only Author and Title

Ding, B., Haudenshield, J.S., Hull, R.J., Wolf, S., Beachy, R.N., and Lucas, W.J. (1992). Secondary plasmodesmata are specific sites of localization of the Tobacco mosaic virus movement protein in transgenic tobacco plants. Plant Cell 4, 915-928.
  Google Scholar: Author Only Title Only Author and Title

Ding, S.W., and Voinnet, O. (2007). Antiviral immunity directed by small RNAs. Cell 130, 413-426.
  Google Scholar: Author Only Title Only Author and Title

Dolja, V.V., Krupovic, M., and Koonin, E.V. (2020). Deep roots and splendid boughs of the global plant virome. Annu Rev Phytopathol 58, 23-53.
  Google Scholar: Author Only Title Only Author and Title

Fatyol, K., Fekete, K.A, and Ludman, M. (2020). Double-stranded-RNA-binding protein 2 participates in antiviral defense. J Virol 94, e00017-20.
  Google Scholar: Author Only Title Only Author and Title

Faulkner, C., Petutschnig, E., Benitez-Alfonso, Y., Beck, M., Robatzek, S., Lipka, V., and Maule, A.J. (2013). LYM2-dependent chitin perception limits molecular flux via plasmodesmata. Proc Natl Acad Sci U S A 110, 9166-9170.
  Google Scholar: Author Only Title Only Author and Title

Guenoune-Gelbart, D., Elbaum, M., Sagi, G., Levy, A, and Epel, B.L. (2008). Tobacco mosaic virus (TMV) replicase and movement protein function synergistically in facilitating TMV spread by lateral diffusion in the plasmodesmal desmotubule of Nicotiana benthamiana. Mol Plant Microbe Interact 21, 335-345.
  Google Scholar: Author Only Title Only Author and Title

Guseman, J.M., Lee, J.S., Bogenschutz, N.L., Peterson, K.M., Virata, R.E., Xie, B., Kanaoka, M.M., Hong, Z, and Torii, K.U. (2010). Dysregulation of cell-to-cell connectivity and stomatal patterning by loss-of-function mutation in Arabidopsis chorus (glucan synthase-like 8). Development 137, 1731-1741.
  Google Scholar: Author Only Title Only Author and Title

He, P., Shan, L., and Sheen, J. (2007). The use of protoplasts to study innate immune responses. Methods Mol Biol 354, 1-9.
Google Scholar: Author Only Title Only Author and Title

Heinlein, M. (2015). Plant virus replication and movement. Virology 479-480, 657-671.
Google Scholar: Author Only Title Only Author and Title

Heinlein, M., Epel, B.L., Padgett, H.S., and Beachy, R.N. (1995). Interaction of tobamovirus movement proteins with the plant cytoskeleton. Science 270, 1983-1985.
Google Scholar: Author Only Title Only Author and Title

Heinlein, M., Wood, M.R., Thiel, T., and Beachy, R.N. (1998). Targeting and modification of prokaryotic cell-cell junctions by Tobacco mosaic virus cell-to-cell movement protein. Plant J 14, 345-351.
Google Scholar: Author Only Title Only Author and Title

Holdaway-Clarke, T.L., Walker, N.A, Hepler, P.K., and Overall, R.L. (2000). Physiological elevations in cytoplasmic free calcium by cold or ion injection result in transient closure of higher plant plasmodesmata. Planta 210, 329-335.
Google Scholar: Author Only Title Only Author and Title

Horsch, A.B., Fry, J.E., Hoffmann, N.L., Eichholtz, D., Rogers, S.G., and Fraley, R.T. (1985). A simple and general method for transferring genes into plants. Science 227, 1229-1231.
Google Scholar: Author Only Title Only Author and Title

Hu, S., Yin, Y., Chen, B., Lin, Q., Tian, Y., Song, X., Peng, J., Zheng, H., Rao, S., Wu, G., Mo, X., Yan, F., Chen, J., and Lu, Y. (2021). Identification of viral particles in the apoplast of Nicotiana benthamiana leaves infected by potato virus X. Mol Plant Pathol 22, 456-464.
Google Scholar: Author Only Title Only Author and Title

Huang, C., and Heinlein, M. (2022). Function of plasmodesmata in the interaction of plants with microbes and viruses. Methods Mol Biol 2457, 23-54.
Google Scholar: Author Only Title Only Author and Title

Huang, C., Mutterer, J., and Heinlein, M. (2022). In vivo aniline blue staining and semi-automated quantification of callose deposition at plasmodesmata Methods Mol Biol 2457, 151-165.
Google Scholar: Author Only Title Only Author and Title

Huang, C.Y., Wang, H., Hu, P., Hamby, R., and Jin, H. (2019) Small RNAs – Big players in plant-microbe interactions. Cell Host Microbe 26, 173-182.
Google Scholar: Author Only Title Only Author and Title

Iglesias, V.A, and Meins, F., Jr. (2000). Movement of plant viruses is delayed in a β-1,3-glucanase-deficient mutant showing a reduced plasmodesmatal size exclusion limit and enhanced callose deposition. Plant J. 21, 157-166.
Google Scholar: Author Only Title Only Author and Title

Incarbone, M., Clavel, M., Monsion, B., Kuhn, L., Scheer, H., Vantard, E., Poignavent, V., Dunoyer, P., Genschik, P., and Ritzenthaler, C. (2021). Immunocapture of dsRNA-bound proteins provides insight into Tobacco rattle virus replication complexes and reveals Arabidopsis DRB2 to be a wide-spectrum antiviral effector. Plant Cell 33, 3402-3420.
Google Scholar: Author Only Title Only Author and Title

Ishikawa, K., Tamura, K., Fukao, Y., and Shimada, T. (2020). Structural and functional relationships between plasmodesmata and plant endoplasmic reticulum-plasma membrane contact sites consisting of three synaptotagmins. New Phytol 226, 798-808.
Google Scholar: Author Only Title Only Author and Title

Jones, R.AC. (2021). Global plant virus disease pandemics and epidemics. Plants (Basel) 10, 233.
Google Scholar: Author Only Title Only Author and Title

Jones, R.AC., and Naidu, R.A (2019). Global dimensions of plant virus diseases: Current status and future perspectives. Annu Rev Virol 6, 387-409.
Google Scholar: Author Only Title Only Author and Title

Kadota, Y., Sklenar, J., Derbyshire, P., Stransfeld, L., Asai, S., Ntoukakis, V., Jones, J.D., Shirasu, K., Menke, F., Jones, A., and Zipfel, C. (2014). Direct regulation of the NADPH oxidase RBOHD by the PRR-associated kinase BIK1 during plant immunity. Mol Cell 54, 43-55.
Google Scholar: Author Only Title Only Author and Title

Koch, A, Biedenkopf, D., Furch, A, Weber, L., Rossbach, O., Abdellatef, E., Linicus, L., Johannsmeier, J., Jelonek, L., Goesmann, A, Cardoza, V., Mcmillan, J., Mentzel, T. and Kogel, K.-H. (2016). An RNAi-based con- trol of Fusarium graminearum infections through spraying of long dsRNAs involves a plant passage and is controlled by the fungal silencing machinery. PLoS Pathog 12, e1005901.
Google Scholar: Author Only Title Only Author and Title

Kørner, C.J., Klauser, D., Niehl, A., Dominguez-Ferreras, A., Chinchilla, D., Boller, T., Heinlein, M., and Hann, D.R. (2013). The immunity regulator BAK1 contributes to resistance against diverse RNA viruses. Mol Plant Microbe Interact 26, 1271-1280.
Google Scholar: Author Only Title Only Author and Title

Kubota, K., Tsuda, S., Tamai, A., and Meshi, T. (2003). Tomato mosaic virus replication protein suppresses virus-targeted posttranscriptional gene silencing. J Virol 77, 11016-11026.
Google Scholar: Author Only Title Only Author and Title

Lee, J.Y., and Lucas, W.J. (2001). Phosphorylation of viral movement proteins--regulation of cell-to-cell trafficking. Trends Microbiol 9, 5-8.
Google Scholar: Author Only Title Only Author and Title

Lee, J.Y., Wang, X., Cui, W., Sager, R., Modla, S., Czymmek, K., Zybaliov, B., van Wijk, K., Zhang, C., Lu, H., and Lakshmanan, V. (2011). A plasmodesmata-localized protein mediates crosstalk between cell-to-cell communication and innate immunity in Arabidopsis. Plant Cell 23, 3353-3373.
Google Scholar: Author Only Title Only Author and Title

Levy, A., Zheng, J.Y., and Lazarowitz, S.G. (2015). Synaptotagmin SYTA forms ER-plasma membrane junctions that are recruited to plasmodesmata for plant virus movement. Curr Biol 25, 2018-2025.
Google Scholar: Author Only Title Only Author and Title

Levy, A., Erlanger, M., Rosenthal, M., and Epel, B.L. (2007). A plasmodesmata-associated beta-1,3-glucanase in Arabidopsis. Plant J 49, 669-682.
Google Scholar: Author Only Title Only Author and Title

Li, F., Cheng, C., Cui, F., de Oliveira, M.V., Yu, X., Meng, X., Intorne, A.C., Babilonia, K., Li, M., Li, B., Chen, S., Ma, X., Xiao, S., Zheng, Y., Fei, Z., Metz, R.P., Johnson, C.D., Koiwa, H., Sun, W., Li, Z., de Souza Filho, G.A., Shan, L., and He, P. (2014). Modulation of RNA polymerase II phosphorylation downstream of pathogen perception orchestrates plant immunity. Cell Host Microbe 16, 748-758.
Google Scholar: Author Only Title Only Author and Title

Lim, G.H., Shine, M.B., de Lorenzo, L., Yu, K., Cui, W., Navarre, D., Hunt, A.G., Lee, J.Y., Kachroo, A., and Kachroo, P. (2016). Plasmodesmata localizing proteins regulate transport and signaling during systemic acquired immunity in plants. Cell Host Microbe 19, 541-549.
Google Scholar: Author Only Title Only Author and Title

Liu, Z., Wu, Y., Yang, F., Zhang, Y., Chen, S., Xie, Q., Tian, X., and Zhou, J.M. (2013). BIK1 interacts with PEPRs to mediate ethylene-induced immunity. Proc Natl Acad Sci U S A 110, 6205-6210.
Google Scholar: Author Only Title Only Author and Title

Lu, D., Wu, S., Gao, X., Zhang, Y., Shan, L., and He, P. (2010). A receptor-like cytoplasmic kinase, BIK1, associates with a flagellin receptor complex to initiate plant innate immunity. Proc Natl Acad Sci U S A 107, 496-501.
Google Scholar: Author Only Title Only Author and Title

Ma, X., Claus, L.A.N., Leslie, M.E., Tao, K., Wu, Z., Liu, J., Yu, X., Li, B., Zhou, J., Savatin, D.V., Peng, J., Tyler, B.M., Heese, A., Russinova, E., He, P., and Shan, L. (2020). Ligand-induced monoubiquitination of BIK1 regulates plant immunity. Nature 581, 199-203.
Google Scholar: Author Only Title Only Author and Title

Mansilla, C., Sanchez, F., Padgett, H.S., Pogue, G.P., and Ponz, F. (2009). Chimeras between Oilseed rape mosaic virus and Tobacco mosaic virus highlight the relevant role of the tobamoviral RdRp as pathogenicity determinant in several hosts. Mol Plant Pathol 10, 59-68.
Google Scholar: Author Only Title Only Author and Title

Meng, X., Shan, L., and He, P. (2015a). Stack heterotrimeric G proteins and MAPK cascades on a RACK. Mol Plant 8, 1691-1693.
Google Scholar: Author Only Title Only Author and Title

Meng, X., Chen, X., Mang, H., Liu, C., Yu, X., Gao, X., Torii, K.U., He, P., and Shan, L. (2015b). Differential function of Arabidopsis SERK family receptor-like kinases in stomatal patterning. Curr Biol 25, 2361-2372.
Google Scholar: Author Only Title Only Author and Title

Mittler, R. (2017). ROS are good. Trends Plant Sci 22, 11-19.
Google Scholar: Author Only Title Only Author and Title

Movahed, N., Cabanillas, D.G., Wan, J., Vali, H., Laliberte, J.F., and Zheng, H. (2019). Turnip mosaic virus components are released into the extracellular space by vesicles in infected leaves. Plant Physiol 180, 1375-1388.
Google Scholar: Author Only Title Only Author and Title

Monsion, B., Incarbone, M., Hleibieh, K., Poignavent, V., Ghannam, A., Dunoyer, P., Daeffler, L., Tilsner, J., and Ritzenthaler, C. (2018). Efficient detection of long dsRNA in vitro and in vivo using the dsRNA binding domain from FHV B2 protein. Front Plant

Sci 9, 70.
  Google Scholar: Author Only Title Only Author and Title

Moore, P.J., Fenczik, C.A., Deom, C.M., and Beachy, R.N. (1992). Developmental changes in plasmodesmata in transgenic tobacco expressing the movement protein of Tobacco mosaic virus. Protoplasma 170, 115-127.
  Google Scholar: Author Only Title Only Author and Title

Niehl, A., and Heinlein, M. (2019). Perception of double-stranded RNA in plant antiviral immunity. Mole Plant Pathol 20, 1203-1210.
  Google Scholar: Author Only Title Only Author and Title

Niehl, A., Wyrsch, I., Boller, T., and Heinlein, M. (2016). Double-stranded RNAs induce a pattern-triggered immune signaling pathway in plants. New Phytol 211, 1008-1019.
  Google Scholar: Author Only Title Only Author and Title

Niehl, A., Soininen, M., Poranen, M.M., and Heinlein, M. (2018). Synthetic biology approach for plant protection using dsRNA. Plant Biotechnol J 16, 1679-1687.
  Google Scholar: Author Only Title Only Author and Title

Niehl, A., Amari, K., Gereige, D., Brandner, K., Mély, Y., and Heinlein, M. (2012). Control of Tobacco mosaic virus movement protein fate by CELL-DIVISION-CYCLE protein 48 (CDC48). Plant Physiol 160, 2093-2108.
  Google Scholar: Author Only Title Only Author and Title

Nuhse, T.S., Bottrill, A.R., Jones, A.M., and Peck, S.C. (2007). Quantitative phosphoproteomic analysis of plasma membrane proteins reveals regulatory mechanisms of plant innate immune responses. Plant J 51, 931-940.
  Google Scholar: Author Only Title Only Author and Title

Oparka, K.J., Prior, D.AM., Santa Cruz, S., Padgett, H.S., and Beachy, R.N. (1997). Gating of epidermal plasmodesmata is restricted to the leading edge of expanding infection sites of Tobacco mosaic virus. Plant J. 12, 781-789.
  Google Scholar: Author Only Title Only Author and Title

Pitzalis, N., and Heinlein, M. (2017). The roles of membranes and associated cytoskeleton in plant virus replication and cell-to-cell movement. J Exp Bot 69, 117-132.
  Google Scholar: Author Only Title Only Author and Title

Ruf, A., Oberkofler, L., Robatzek, S., and Weiberg, A. (2022). Spotlight on plant RNA-containing extracellular vesicles. Curr Opin Plant Biol 69, 102272.
  Google Scholar: Author Only Title Only Author and Title

Sambade, A., Brandner, K., Hofmann, C., Seemanpillai, M., Mutterer, J., and Heinlein, M. (2008). Transport of TMV movement protein particles associated with the targeting of RNA to plasmodesmata. Traffic 9, 2073-2088.
  Google Scholar: Author Only Title Only Author and Title

Simpson, C., Thomas, C., Findlay, K., Bayer, E., and Maule, A.J. (2009). An Arabidopsis GPI-anchor plasmodesmal neck protein with callose binding activity and potential to regulate cell-to-cell trafficking. Plant Cell 21, 581-594.
  Google Scholar: Author Only Title Only Author and Title

Tan, X., Sun, L., Chen, J., and Chen, Z.J. (2018). Detection of Microbial infections through innate immune sensing of nucleic acids. Annu Rev Microbiol 72, 447-478.
  Google Scholar: Author Only Title Only Author and Title

Thomas, C.L., Bayer, E.M., Ritzenthaler, C., Fernandez-Calvino, L., and Maule, A.J. (2008). Specific targeting of a plasmodesmal protein affecting cell-to-cell communication. PLoS Biol 6, e7.
  Google Scholar: Author Only Title Only Author and Title

Thor, K., Jiang, S., Michard, E., George, J., Scherzer, S., Huang, S., Dindas, J., Derbyshire, P., Leitao, N., DeFalco, T.A., Koster, P., Hunter, K., Kimura, S., Gronnier, J., Stransfeld, L., Kadota, Y., Bucherl, C.A., Charpentier, M., Wrzaczek, M., MacLean, D., Oldroyd, G.E.D., Menke, F.L.H., Roelfsema, M.R.G., Hedrich, R., Feijo, J., and Zipfel, C. (2020). The calcium-permeable channel OSCA1.3 regulates plant stomatal immunity. Nature 585, 569-573.
  Google Scholar: Author Only Title Only Author and Title

Tian, W., Hou, C., Ren, Z., Wang, C., Zhao, F., Dahlbeck, D., Hu, S., Zhang, L., Niu, Q., Li, L., Staskawicz, B.J., and Luan, S. (2019). A calmodulin-gated calcium channel links pathogen patterns to plant immunity. Nature 572, 131-135.
  Google Scholar: Author Only Title Only Author and Title

Tilsner, J., Nicolas, W., Rosado, A., and Bayer, E.M. (2016). Staying tight: Plasmodesmal membrane contact sites and the control of cell-to-cell connectivity in plants. Annu Rev Plant Biol 67, 337-364.
  Google Scholar: Author Only Title Only Author and Title

Torres, M.A., Dangl, J.L., and Jones, J.D. (2002). Arabidopsis gp91phox homologues AtrbohD and AtrbohF are required for accumulation of reactive oxygen intermediates in the plant defense response. Proc Natl Acad Sci U S A 99, 517-522.

Google Scholar: Author Only Title Only Author and Title

Tucker, E.B., and Boss, W.F. (1996). Mastoparan induced intracellular Ca2+ fluxes may regulate cell-to-cell communication in plants. Plant Physiol. 111, 459-467.
Google Scholar: Author Only Title Only Author and Title

Uchiyama, A, Shimada-Beltran, H., Levy, A, Zheng, J.Y., Javia, P.A., and Lazarowitz, S.G. (2014). The Arabidopsis synaptotagmin SYTA regulates the cell-to-cell movement of diverse plant viruses. Front Plant Sci 5, 584.
Google Scholar: Author Only Title Only Author and Title

Vatén, A, Dettmer, J., Wu, S., Stierhof, Y.D., Miyashima, S., Yadav, S.R., Roberts, C.J., Campilho, A, Bulone, V., Lichtenberger, R., Lehesranta, S., Mahonen, A.P., Kim, J.Y., Jokitalo, E., Sauer, N., Scheres, B., Nakajima, K., Carlsbecker, A, Gallagher, K.L., and Helariutta, Y. (2011). Callose biosynthesis regulates symplastic trafficking during root development. Dev Cell 21, 1144-1155.
Google Scholar: Author Only Title Only Author and Title

Vogler, H., Kwon, M.O., Dang, V., Sambade, A, Fasler, M., Ashby, J., and Heinlein, M. (2008). Tobacco mosaic virus movement protein enhances the spread of RNA silencing. PLoS Pathog 4, e1000038.
Google Scholar: Author Only Title Only Author and Title

Vogler, H., Akbergenov, R., Shivaprasad, P.V., Dang, V., Fasler, M., Kwon, M.O., Zhanybekova, S., Hohn, T., and Heinlein, M. (2007). Modification of small RNAs associated with suppression of RNA silencing by tobamovirus replicase protein. J Virol 81, 10379-10388.
Google Scholar: Author Only Title Only Author and Title

Wan, J., Cabanillas, D.G., Zheng, H. and Laliberté, J.-F. (2015). Turnip mosaic virus moves systemically through both phloem and xylem as membrane-associated complexes. Plant Physiol 167, 1374-1388.
Google Scholar: Author Only Title Only Author and Title

Wan, J. and Laliberté, J.-F. (2015). Membrane-associated virus replication complexes locate to plant conducting tubes. Plant Signal Behav 10, e1042639–e1042639.
Google Scholar: Author Only Title Only Author and Title

Wang, X., Sager, R., Cui, W., Zhang, C., Lu, H., and Lee, J.Y. (2013). Salicylic acid regulates plasmodesmata closure during innate immune responses in Arabidopsis. Plant Cell 25, 2315-2329.
Google Scholar: Author Only Title Only Author and Title

Wu, S.W., Kumar, R., Iswanto, A.B.B., and Kim, J.Y. (2018). Callose balancing at plasmodesmata. J Exp Bot 69, 5325-5339.
Google Scholar: Author Only Title Only Author and Title

Xu, B., Cheval, C., Laohavisit, A, Hocking, B., Chiasson, D., Olsson, T.S.G., Shirasu, K., Faulkner, C., and Gilliham, M. (2017). A calmodulin-like protein regulates plasmodesmal closure during bacterial immune responses. New Phytol 215, 77-84.
Google Scholar: Author Only Title Only Author and Title

Yuan, C., Lazarowitz, S.G., and Citovsky, V. (2018). The plasmodesmal localization signal of TMV MP is recognized by plant synaptotagmin SYTA. mBio 9, e01314-18.
Google Scholar: Author Only Title Only Author and Title

Zhang, J., Li, W., Xiang, T., Liu, Z, Laluk, K., Ding, X., Zou, Y., Gao, M., Zhang, X., Chen, S., Mengiste, T., Zhang, Y., and Zhou, J.M. (2010). Receptor-like cytoplasmic kinases integrate signaling from multiple plant immune receptors and are targeted by a Pseudomonas syringae effector. Cell Host Microbe 7, 290-301.
Google Scholar: Author Only Title Only Author and Title